

**experimentation for  
students of engineering**

# **Volume 2 Applied Mechanics**

**C.R. Webb and A.R. Luxmoore**



PAISLEY COLLEGE  
OF TECHNOLOGY  
LIBRARY

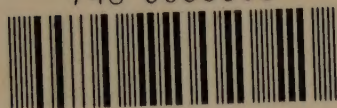
Author WEBB, C.R.

Title Experimentation for  
students of engineer-  
ing Vol. 2

Book No. 41089

Shelf Mark 621.01

748 0066308



PAISLEY COLLEGE

\*

LIBRARY

WITHDRAWN  
FROM STOCK

~~10 NOV 88~~

16 . 7 . 90

3 SEPT 91

23 NOV 1994

17 FEB 1995

02 DEC 1997

28 JAN 2002

ISSUED FOR THE STANDARD LOAN PERIOD





Experimentation for Students of Engineering

---

Volume II

Applied Mechanics

---

McGraw-Hill  
London and New York

Experimentation for Students of Engineering

Volume I

**Experimental Method and Measurement**

Volume II

**Applied Mechanics**

Volume III

**Thermodynamics, Fluid Mechanics, and Heat Transfer**

# EXPERIMENTATION FOR STUDENTS OF ENGINEERING

*Edited by*

**L. Maunder,**  
Ph.D., Sc.D., C.Eng., F.I.Mech.E.  
*Professor of Mechanical  
Engineering, University of  
Newcastle upon Tyne*

**S. D. Probert,**  
M.A., D.Phil., C.Eng., M.I.Mech.E.,  
A.F.R.Ae.S., A.Inst.P., M.Inst.F.  
*Lecturer in Mechanical Engineering,  
University College of Swansea*

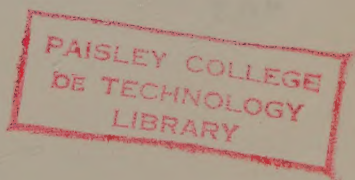
---

## ***Volume II*** ***Applied Mechanics***

---

**C. R. Webb,** J.P., Ph.D., C.Eng., F.I.Mech.E., M.Inst.M.C.  
*Reader in Mechanical Engineering, Queen Mary College, London*

**A. R. Luxmoore,** M.Sc.  
*Lecturer in Civil Engineering, University College of Swansea*



**Heinemann Educational Books**  
London and Edinburgh

Heinemann Educational Books Ltd  
LONDON EDINBURGH MELBOURNE TORONTO  
AUCKLAND JOHANNESBURG SINGAPORE HONG KONG  
IBADAN NAIROBI NEW DELHI

ISBN 0 435 71532 1 (cased)

ISBN 0 435 71533 X (limp)

© C. R. Webb and A. R. Luxmoore

First published 1971

Published by Heinemann Educational Books Ltd  
48 Charles Street, London W1X 8AH  
Printed in Great Britain at the Pitman Press, Bath





## ***Editors' Foreword***

Experimentation is essential in engineering. But despite the growth of elaborate undergraduate laboratories, experimental tuition has rarely kept pace with the increasing theoretical content of engineering courses. This series of books grew from a belief that the process of learning in engineering laboratories would be enhanced by the ready availability of comment and advice such as is provided in these texts. Although intended primarily for use in universities and colleges of technology, certain sections may also serve as more general references to experimental practice. SI units have been adopted throughout, supplemented in some instances by the British system of units.

Volume I contains an introduction to the general requirements of experimental method, and describes the principles and applications of some modern instruments. Volume II (Applied Mechanics) and Volume III (Thermodynamics, Fluid Mechanics, and Heat Transfer) outline sets of experiments which range from the simple to the difficult, and from the first to the final year of an undergraduate course. The outlines are not, of course, intended to be followed slavishly but to offer material on which coherent laboratory courses can be based.

We are indebted to many sources of information, which are recorded in the successive volumes. We record also our appreciation of the patience shown by the publisher in what soon became a complex task. But most of all our thanks are due to the authors for the way in which they have co-operated to realize the original idea. It is they who have written the series and any virtues it may possess are due to them.

1971

L.M.

S.D.P.



## *Preface to Volume II*

Part I of this volume describes experiments associated with syllabuses in the subject normally called 'Mechanics of Machines'. With reference to a three-year full-time honours course, the first eight experiments are intended for the first year, the next six for the second year and the last four for the final year, though the boundaries and the order of presentation may be changed as required.

It is now quite normal to include an introductory study of vibrations in courses on machines and, more recently, automatic control and analogue computation have been added. For the first year we have included simple experiments to assist in the understanding and engineering applications of mechanisms, epicyclic gears, friction, balancing and free vibration, and others to illustrate the momentum and energy principles, moments of inertia and dynamic loading. For the second year, more ambitious experiments take vibrations a stage further, deal with gyroscopic precession and shaft whirling and introduce some applications of automatic control. The last four experiments assume that the reader has acquired a good understanding of principles and a reasonable knowledge of laboratory methods. These more-involved experiments on advanced vibrations, control and analogue computation are outlined for the reader to develop according to his own interests.

Part II is concerned with stress analysis, though this has been extended slightly by including several experiments on structural analysis. The first five experiments are intended for the first year, the next four for the second, and then three for the final year. The emphasis is on practical techniques, leading the student through simple examples of experimental stress analysis. The impact of computers has resulted in an increasing concentration upon mathematical techniques in undergraduate courses. However much of engineering still depends on empirical relationships and experience, and this requires a sound appreciation of such techniques of measurement and analysis as are described in this section.

It is hoped that the actual execution of the majority of the experiments described will assist the reader in appreciating the subject and will introduce him to the wide variety of engineering applications involved. The reader is encouraged to bear in mind, at all stages, the measurement and computation errors involved and to try to assess the accuracy of the results which he obtains.

1971

C.R.W.  
A.R.L.



# Contents

Page

Editors' Foreword

v

Preface to Volume II

vii

## Part I Statics and Dynamics

by C. R. Webb

### *Experiment*

1	Simple Mechanisms	3
2	Epicyclic Gears	8
3	Moments of Inertia	12
4	Friction in Machines	17
5	Balancing of Rotating Bodies	24
6	Free Vibration of a Simple System	30
7	Dynamic Loading of a System with One Degree of Freedom	35
8	A Momentum and Energy Experiment	40
9	Forced Vibration of a Simple System	45
10	Free Vibration of a System with Two Degrees of Freedom	50
11	Shaft Whirling	55
12	Simple Gyroscope	60
13	First-Order Process Lag	63
14	Position Control System	67
15	Transverse Vibration of an Elastic Beam	72
16	Vibration of a Multi-mass System	76
17	Speed Control System	82
18	Analogue Computation	91

## Part II Stress Analysis

by A. R. Luxmoore

19	Elastic Constants	103
20	Torsion of a Circular Shaft	106



	<i>Page</i>
21 Simple Bending	109
22 Bending of an L-Shaped Cantilever	113
23 Compound Stress and Strain	116
24 Elastic Stability of Struts	120
25 Resistance Strain Gauges	124
26 Proving Rings	130
27 Structural Analysis by Indirect Models	134
28 The Photoelastic Method of Stress Analysis	139
29 Measuring Deflections by the Moiré Method	147
30 Brittle Lacquer Methods	152
Index	155

## **Part I**

---

# **Statics and Dynamics**



## Simple Mechanisms

### (a) Crank-slider

#### Theory

Kinematic mechanisms with turning and sliding pairs of mechanical elements appear commonly in engineering practice. One of particular importance is the four-bar linkage with three turning and four sliding pairs in the form of the so-called 'crank-slider mechanism' illustrated in Figure 1.1.

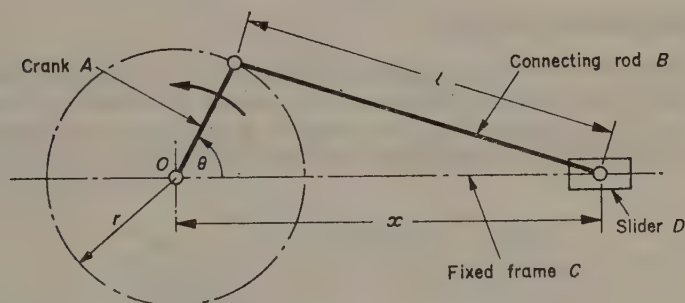


FIGURE 1.1 Crank-slider mechanism.

The crank  $A$  of radius  $r$  rotates about a fixed point  $O$  in the frame  $C$ ,  $O$  being regarded as the origin. Its angular displacement  $\theta$  is measured as shown in the figure. The connecting rod  $B$  of length  $l$  is pivoted to the crank and to the slider  $D$ , the latter being constrained to move along a straight line in the frame through  $O$ . The motion is two-dimensional in the plane of the paper. The displacement of  $D$  (relative to  $O$ ) is given by

$$x = l + r \left[ \cos \theta - \frac{1}{2q} \sin^2 \theta - \frac{1}{8q^3} \sin^4 \theta - \dots \right] \quad (1.1)$$

where

$$q = l/r \quad (1.2)$$

In most practical applications,  $\dot{\theta}$  is assumed to be constant and equal to  $\omega$ , where  $\omega/2\pi$  is the frequency of rotation of the crank. In this case the velocity and acceleration of  $D$  are given by

$$\dot{x} = -\omega r \left[ \sin \theta + \frac{1}{2q} \sin 2\theta + \frac{1}{8q^3} (\sin 2\theta - \frac{1}{2} \sin 4\theta) + \dots \right] \quad (1.3)$$

$$\ddot{x} = -\omega^2 r \left[ \cos \theta + \frac{1}{q} \cos 2\theta + \frac{1}{4q^3} (\cos 2\theta - \cos 4\theta) + \dots \right] \quad (1.4)$$

Unless  $q$  is very small, the expansions given in equations (1.1), (1.3) and (1.4) converge rapidly and, for  $q$  in the common range 3 to 4, it is normal practice to re-write (1.3) and (1.4) as

$$\dot{x} \simeq -\omega r \left[ \sin \theta + \frac{1}{2q} \sin 2\theta \right] \quad (1.5)$$

$$\ddot{x} \simeq -\omega^2 r \left[ \cos \theta + \frac{1}{q} \cos 2\theta \right] \quad (1.6)$$

For  $q$  very large, the second terms in the above expressions become negligibly small, so that the motion of  $D$  approximates to simple harmonic.

## Experimental Details

Given a crank-slider with a typical value of  $q$  of about 3, a useful experiment would be to investigate to what extent the motion of  $D$  differs from simple harmonic. Using equation (1.1), the theoretical comparison for displacement is shown in Figure 1.2. The greatest difference occurs at  $\theta = 90^\circ$  and  $270^\circ$ .

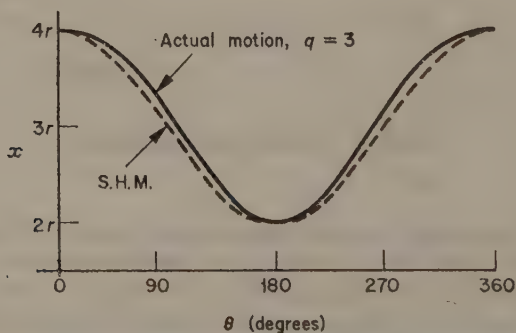


FIGURE 1.2 Motion of slider compared with simple harmonic motion.

It would be adequate to measure  $x$  for increments in  $\theta$  of  $30^\circ$  between  $\theta = 0$  and  $\theta = 360^\circ$ . Provided the test mechanism is manufactured reasonably accurately, any disagreement with theory should arise solely from inaccurate measurement of  $\theta$  and  $x$ .



## Discussion

Experimental verification of equations (1.3) and (1.4) or their approximate forms (1.5) and (1.6) would be difficult. Would you, however, accept these results having confirmed the validity of equation (1.1)?

## (b) Hooke's Joint

### Theory

Rotary motion is often transmitted between a pair of shafts, the axes of which are non-parallel but intersect, by means of a Hooke's joint, as shown diagrammatically in Figure 1.3.

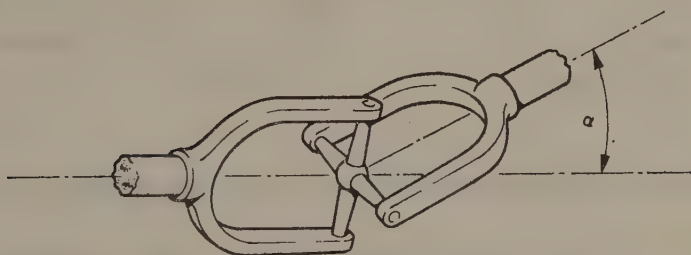


FIGURE 1.3 Hooke's joint.

For a pair of shafts out of line by an angle  $\alpha$ , the relation between their angles of rotation is

$$\tan \phi = \tan \theta \cos \alpha \quad (1.7)$$

where  $\theta$  and  $\phi$  are the angles of rotation of, say, the driver and the driven shaft, and are measured from the position where the arm of the 'cross' associated with the driver lies in the plane of the angle  $\alpha$ . The angular speeds of the shafts are related by

$$\dot{\phi} = \frac{\cos \alpha}{1 - \sin^2 \theta \sin^2 \alpha} \dot{\theta} \quad (1.8)$$

For constant angular speed  $\dot{\theta}$  of the driver, the acceleration of the driven shaft is

$$\ddot{\phi} = \frac{\cos \alpha \sin^2 \alpha \sin 2\theta}{1 - \sin^2 \theta \sin^2 \alpha} \dot{\theta}^2 \quad (1.9)$$

This is zero only when  $\theta = 0, 90^\circ, 180^\circ$ , etc. because when the input speed is constant the output speed fluctuates during each revolution.

For  $\alpha$  equal to  $20^\circ$ , equation (1.7) enables a graph of  $(\phi - \theta)$  against  $\theta$  to be drawn as in Figure 1.4; the curve is for one complete revolution, that

for each half-revolution being identical. The speed ratio  $\dot{\phi}/\dot{\theta}$  is shown in the same figure. Although the maximum difference in position compared with a constant-ratio transmission is less than  $2^\circ$ , the speed fluctuates by

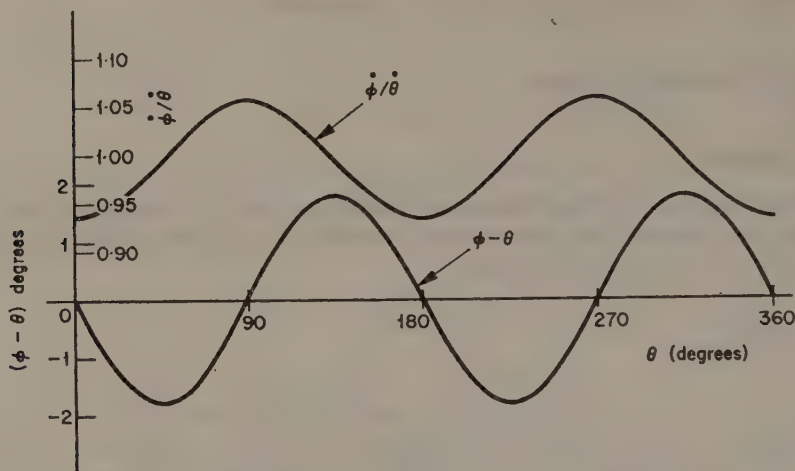


FIGURE 1.4 Displacement difference and velocity ratio for Hooke's joint.

nearly  $\pm 7\%$ . Such a speed fluctuation could result in severe vibration and excessive stress variation with resulting fatigue in many engineering applications. Can you quote any?

## Experimental Details

A simple experiment may be arranged to measure  $(\phi - \theta)$  for various values of  $\theta$  to compare with the first of the curves of Figure 1.4. Increments in  $\theta$  of  $15^\circ$  between  $\theta = 0$  and  $\theta = 180^\circ$  would give a satisfactory result; it is necessary to take a few points in the range  $\theta = 180^\circ$  to  $360^\circ$  to check that the motion is repeated. It is evident that, since  $(\phi - \theta)$  is likely to remain small, both  $\theta$  and  $\phi$  must be measured very accurately, i.e. to within about 1 minute. Any slackness in the bearings of the joint would lead to measurement errors comparable with the values of  $(\phi - \theta)$ .

A drive may be transmitted between two Hooke's joints in turn, and if  $\alpha$  is the same for each and the arms of the crosses associated with each end of the intermediate shaft are parallel, the velocity ratio will be constant. Where this is essential, e.g. for use in a front-wheel-drive vehicle, the two joints may be assembled effectively as a single joint. Variations of this are the Rzeppa and Birfield joints. To check such a drive, two similar Hooke's joints may be arranged in series and the above experiment repeated. You should confirm that a constant-ratio transmission results when the input and output shafts of the assembly are either parallel, i.e. the angle  $\alpha$  for one joint cancels that for the other, or lie at an angle of  $2\alpha$  to one another.

## Discussion

Do your tests confirm the behaviour of the mechanism as predicted by the theory? Do you consider that the errors between the theoretical and experimental curves are due entirely to lack of experimental precision and not because of any shortcomings in the theory? Can you give a theoretical justification for the last result of the final experiment?

## Epicyclic Gears

One important modern application of epicyclic gears is the self-changing gearbox fitted to many road and rail vehicles. This utilizes either a train of helical spur gears or an arrangement of angled-bevel gears. Whereas ordinary gear pairs are easy to understand from the point of view of speed and torque ratios, the methods used for calculating these ratios in epicyclic trains are not always convincing and experimental study can be valuable.

### Theory of Epicyclic Gear Trains

Consider the simple gear shown in Figure 2.1. The sun wheel *A* meshes with one or more planet wheels *B* which in turn mesh with an internally-toothed

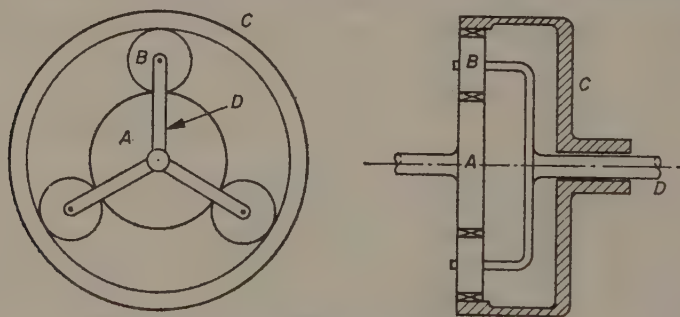


FIGURE 2.1 Simple epicyclic gear train.

wheel *C*. The planets are pivoted on shafts fixed to the carrier or cage *D*. Suppose that  $N_A$ ,  $N_B$ , and  $N_C$  are the numbers of teeth on wheels *A*, *B*, and *C* respectively; let the speeds likewise be  $\omega_A$ ,  $\omega_B$ , and  $\omega_C$ . Because the pitch must be common, it follows that

$$N_C = N_A + 2N_B$$

With the cage fixed, the speed ratio between *A* and *B* is inversely proportional to the ratio of teeth numbers; thus

$$\omega_A/\omega_B = -N_B/N_A$$

the negative sign being necessary because of the opposite direction of motion of the wheels. When the cage moves at speed  $\omega_D$ , it follows that

$$(\omega_A - \omega_D)/(\omega_B - \omega_D) = -N_B/N_A \quad (2.1)$$

In using these formulae, a sign convention must be adopted for positive speed and used throughout. We may also write

$$(\omega_A - \omega_D)/(\omega_C - \omega_D) = -N_C/N_A \quad (2.2)$$

in which it should be noted that  $N_B$  does not appear.

Compounding of two or more epicyclic trains is commonly practised. Consider, as a specific example, the gear found in a modern automobile transmission which is shown diagrammatically in Figure 2.2. The output is

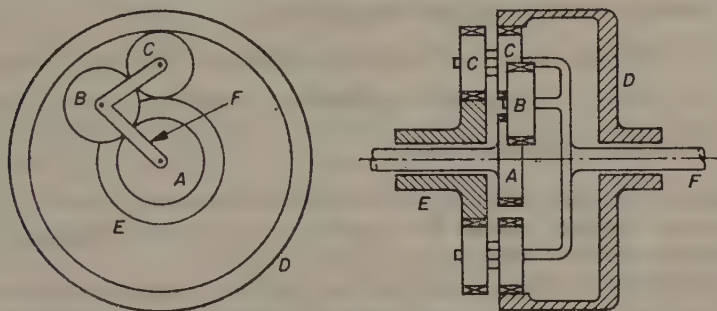


FIGURE 2.2 Compound epicyclic gear train.

always taken from  $D$ . The input may be applied at  $A$  or at  $E$ . The wheels  $C$  are keyed together and have 30 teeth. Wheel  $E$  has 55 teeth and hence  $D$  has 115. Wheel  $A$  has 48 teeth. Wheels  $B$  are carried in the same carrier  $F$  as are wheels  $C$  but are offset as shown so that they can have a practical number of teeth. It should be noted that the actual number of teeth of  $B$  is immaterial.

Similar formulae to those used earlier may be written

$$(\omega_E - \omega_F)/(\omega_D - \omega_F) = -N_D/N_E \quad (2.3)$$

$$\text{and} \quad (\omega_A - \omega_F)/(\omega_D - \omega_F) = +N_D/N_A \quad (2.4)$$

In equation (2.4), a positive sign is used because the drive from  $A$  to  $D$  passes through the extra wheels  $B$ . The gearbox is used as follows.

- (a)  $F$  is fixed and  $E$  is free. The drive is applied at  $A$ . Equation (2.4) gives

$$\omega_A/\omega_D = 115/48 = 2.39$$

which provides first gear.

- (b)  $E$  is fixed and  $F$  is free. The drive is again applied at  $A$ . Equation (2.3) gives

$$-\omega_F/(\omega_D - \omega_F) = -115/55$$



Equation (2.4) gives

$$(\omega_A - \omega_F)/(\omega_D - \omega_F) = 115/48$$

We have two equations connecting three variables. By eliminating  $\omega_F$ , we obtain the following ratio

$$\omega_A/\omega_D = (1/48 + 1/55)/(1/115 + 1/55) = 1.45$$

which provides second gear.

- (c) *A* and *E* are locked together and both are driven. The whole turns as one unit, thus

$$\omega_A/\omega_D = 1$$

which provides third gear (direct drive).

- (d) *F* is fixed and *A* is free. The drive is applied at *E*. From (2.3) we obtain

$$\omega_E/\omega_D = -115/55 = -2.09$$

which provides reverse gear.

It may appear that first and reverse ratios are somewhat small for automobile use; however, where this gearbox is used, a hydrokinetic torque converter provides a further ratio of 2 when required.

In practice, input torque is applied to *A* or *E* by hydraulic clutches and *E* or *F* are fixed by means of band brakes. It is important to know how much torque must be applied to *E* or *F* to prevent rotation when maximum torque is being transmitted through the gearbox. By assuming that the torque ratio between input and output is the same as the speed ratio, we may find the torque required to hold *E* or *F* in terms of the input torque, both in magnitude and direction.

## Experimental Details

It is assumed that a compound epicyclic gear is available for test. This should be equipped, as shown in Figure 2.3, to enable torques to be measured under static conditions. Taking the gear described above as an example, condition (b) requires a cord to be wrapped round a pulley connected to *A* and tensioned with a body of known mass. Similar cords in connection with *E* and *D* are restrained by spring balances. Condition (a) is provided for in a similar manner. If the gear enables a reversing condition to be provided, i.e. like (d) above, the cord associated with *D* must apply a restraining torque in the reverse direction compared with (a) and (b).

Count the number of teeth on the various wheels and determine the theoretical speed ratio under various conditions in the manner shown in the example. To check the ratios experimentally, lock the appropriate parts and measure the angle of rotation of the driver which corresponds to one complete revolution of the driven shaft.

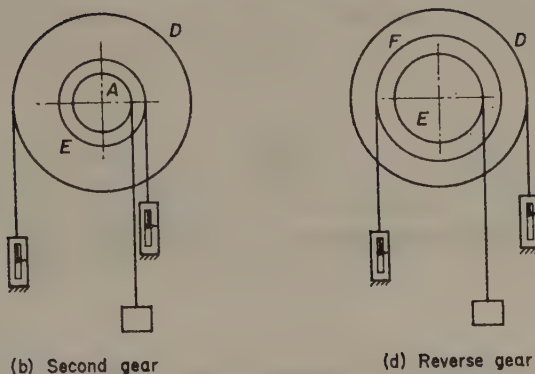


FIGURE 2.3 Measurement of torque reaction.

Using the equipment for static torque determination, find the torque ratio between input and output shafts. Note to what extent this differs from the speed ratio under each condition.

## Discussion

Did your tests confirm that the relationships given in equations (2.1) to (2.4) are correct?

When in motion, the transmission efficiency is given by the torque ratio divided by the speed ratio. From the results of your tests, are you able to judge how efficient the gearbox would be in use?

Suggest why the transmission of a road vehicle usually consists either of a simple gearbox (with alternative ratios) in conjunction with a dry friction clutch or of an epicyclic gearbox combined with a hydrokinetic coupling, i.e. why you would not expect to find alternative combinations of these units.

## Moments of Inertia

Moments of inertia frequently appear in the equations of angular motion of rigid bodies. For a body of regular shape, its moments of inertia can be found from measurements of its mass and physical dimensions, but the shape of an engineering component is often too complicated for this approach to be feasible. The alternative is to measure the values experimentally. Two such experiments, both based on simple vibration theory, are outlined below. Their application is wide but, to fix ideas, we shall apply them to the particular case of a connecting rod of a reciprocating engine.

### Definitions

The outline in Figure 3.1 represents an irregularly shaped body in relation to three mutually perpendicular axes  $OX$ ,  $OY$ ,  $OZ$  intersecting at some chosen

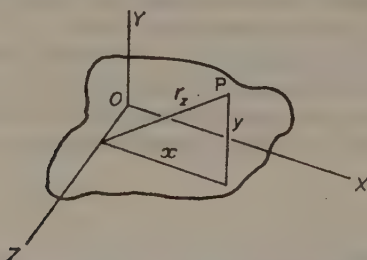


FIGURE 3.1 Mutually perpendicular axes of a body.

origin  $O$ . The body is assumed to be made up of particles of which one of mass  $\delta m$  at  $P$  is typical. The mass moment of inertia of the body about  $OZ$  is defined as

$$I_z = \sum r_z^2 \delta m \quad (3.1)$$

where  $r_z$  is the perpendicular distance of  $P$  from  $OZ$  and the summation includes all the particles in the body. In the limit this becomes

$$I_z = \int r_z^2 dm = \int (x^2 + y^2) dm \quad (3.2)$$

If we require the moment of inertia about a parallel axis  $O'Z'$  (Figure 3.2), it can be shown that  $I_{z'}$  and  $I_z$  are related simply by

$$I_{z'} = I_z + ma^2 \quad (3.3)$$

where  $m$  is the total mass of the body and  $a$  is the perpendicular distance of  $O'Z'$  from  $OZ$ . Equation (3.3) must be used with care; it applies to all shifted but parallel axes  $O'Z'$  *only* if the centre of mass  $G$  of the body lies in  $OZ$ .

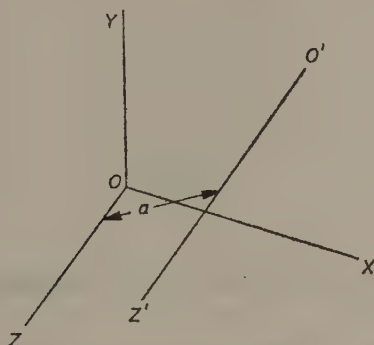


FIGURE 3.2 Parallel axes.

Frequently we are concerned only with axes perpendicular to one given plane ( $OXY$  in our case), and it is convenient to re-write (3.3) as

$$I = I_G + ma^2 \quad (3.4)$$

where  $I$  is the moment about some axis distant  $a$  from the centre of mass and  $I_G$  is the moment about  $G$  itself.

## Theory of the Compound Pendulum

Consider a rigid body, e.g. the connecting rod shown in Figure 3.3, free to swing in a vertical plane about a horizontal pivot at  $A$ . For a small angle of swing, the free oscillation is governed by the local gravitational field according to the equation of motion

$$I\ddot{\theta} + mga\theta = 0 \quad (3.5)$$

where  $I$  is the moment of inertia about  $A$ ,  $\theta$  is the angle of swing,  $m$  is the body mass and  $a$  is the distance  $AG$ . The periodic time  $T_A$  of the motion is given by

$$T_A = 2\pi(I/mga)^{\frac{1}{2}} \quad (3.6)$$

Note that, since  $I$ ,  $m$  and  $a$  are invariable properties of the body, the periodic time depends on the value of  $g$  at the place where the experiment is performed. By equation (3.4), we obtain

$$I_G = (mgaT_A^2/4\pi^2) - ma^2 \quad (3.7)$$

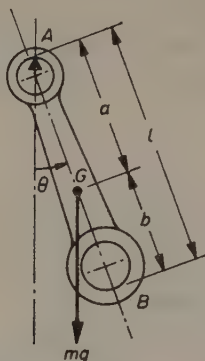


FIGURE 3.3 Free vibration of a connecting rod.

Similarly, for small free oscillations about  $B$ , we obtain

$$I_G = (mgbT_B^2/4\pi^2) - mb^2 \quad (3.8)$$

Since  $l = a + b$ , eliminating  $I_G$  between equations (3.7) and (3.8) we can obtain  $a$  (or  $b$ ) in terms of  $l$ , i.e.

$$a = \frac{gIT_B^2 - 4\pi^2l^2}{gT_A^2 + gT_B^2 - 8\pi^2l} \quad (3.9)$$

which enables the position of  $G$  to be found. (It is assumed, of course, that  $G$  lies in  $AB$ .)

## Theory of the Trifilar Suspension

Figure 3.4 shows a uniform and circular table suspended in a horizontal plane by three equidistant flexible vertical wires of equal length  $l$ , each being attached to the table at radius  $r$  from its centre  $O$ . We are interested in the free angular vibration of the table about a vertical axis through  $O$ .

For small amplitude oscillation, the equation of motion is

$$I_T\ddot{\phi} + (m_Tgr^2/l)\phi = 0 \quad (3.10)$$

where  $\phi$  is the angular displacement about  $O$  and  $I_T$  and  $m_T$  refer to the table. The period of the motion is given by

$$T_T = 2\pi(I_Tl/m_Tgr^2)^{\frac{1}{2}} \quad (3.11)$$

and hence

$$I_T = T_T^2m_Tgr^2/4\pi^2l \quad (3.12)$$



Suppose that we now place the connecting rod on the table, with  $G$  coinciding with  $O$ , so that it moves with the table. The new period  $T$  will be related to the resultant moment of inertia  $I$  by

$$I = T^2 mgr^2 / 4\pi^2 l \quad (3.13)$$

Subtracting (3.12) from (3.13), we obtain  $I_G$  for the connecting rod:

$$I_G = (T^2 m - T_T^2 m_T) gr^2 / 4\pi^2 l \quad (3.14)$$

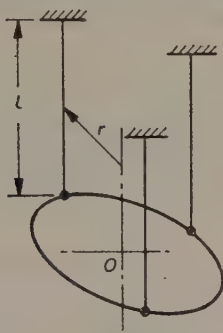


FIGURE 3.4 Trifilar suspension.

## Experimental Details

For the compound pendulum experiment, equation (3.7) shows that we require values for  $m$ ,  $g$ ,  $a$  and  $T_A$ . We can determine  $m$  by using a weighing apparatus and assume the proper value for  $g$ . The reader should devise at least two methods of locating  $G$  directly in order to determine  $a$ . Find  $T_A$  by measuring the time taken for a number of cycles after having set the connecting rod swinging on a knife-edge at  $A$  with small amplitude. This should be done several times, for different numbers of cycles, to determine the range of experimental variation in  $T_A$ . After selecting the best value for  $T_A$ ,  $I_G$  can be calculated from (3.7).

Alternatively  $T_B$  can be found after setting the connecting rod swinging about  $B$ . Then, after measuring  $l$ ,  $a$  can be found from (3.9) and inserted in (3.7). This determination of  $a$  should confirm the earlier direct measurement of  $a$ .

The trifilar suspension test consists of determining the periodic times, in a manner similar to the above, with and without the connecting rod in position on the table. Measure the mean length  $l$  of the three wires and check that this does not alter significantly with the added weight of the connecting rod. Also measure the mean value of  $r$ . Remove the wires from the table and measure  $m_T$  with a weighing apparatus. In determining  $I_G$  from equation (3.14), remember that  $m$  is the combined mass of table and connecting rod.

## Discussion

State the major assumptions in the theory leading to equations (3.6) and (3.11) and discuss how well these were satisfied in your experiments.

Comment on the main sources of error in each experiment and estimate their effect on the  $I_G$  values found, i.e. estimate the percentage accuracy in each value.

What are the important factors in the design of the experimental apparatus? For example, must (a) the knife edge for the pendulum be sharp and truly horizontal, (b) the trifilar wires be truly flexible and of negligible mass, (c)  $l \gg r$  in the trifilar suspension?

## *Friction in Machines*

Friction is both the enemy and the friend of the engineer. In this composite experiment we shall investigate the frictional resistance caused by conventional bearings, a source of power loss in rotating machinery. We shall also study the deliberate use of friction in clutches and belt drives.

### **Theoretical Assumptions**

Consider a body of moment of inertia  $I$  rotating freely at angular speed  $\omega$  and apply a resisting torque  $T_R$ . The equation for the subsequent motion is

$$I d\omega/dt = -T_R \quad (4.1)$$

It is normal to assume that  $T_R$  takes one of two forms. 'Dry' or Coulomb friction assumes that  $T_R$  is constant, and it follows that the speed of the body decreases at a constant rate. Viscous friction occurs when  $T_R$  varies directly with  $\omega$ . Let  $T_R = a\omega$  where  $a$  is a constant. Substitution in (4.1) and integrating gives

$$\omega = \omega_1 \exp \{-(a/I)t\} \quad (4.2)$$

which means that  $\omega$  decreases exponentially with time from the initial speed  $\omega_1$ .

### **Belt Theory**

When power is transmitted from one shaft to another by means of a dry belt in tension, it is assumed that Coulomb friction acts between the contact surfaces of the belt and pulleys. This gives rise to the idea of a coefficient of friction  $\mu$  relating the maximum possible friction force to the normal force. When motion is transmitted in the normal way, the ratio of these forces is less than  $\mu$  and we assume that no slipping occurs between the surfaces. A knowledge of  $\mu$  enables us to estimate the maximum power which can be transmitted. If we prevent the driven shaft from rotating, the belt slips on one or both of the pulleys, and under these circumstances we assume that the ratio of the forces is equal to  $\mu$ .

In Figure 4.1, the tensions at each end of the stationary flat belt are  $F_1$  and  $F_2$ , and the belt is in contact with the pulley over an angle  $\theta$ , the angle of lap. The pulley, of radius  $r$ , is rotating at constant speed  $\omega$ . Simple flat-belt theory relates the tensions by the following

$$F_1/F_2 = \exp \mu\theta \quad (4.3)$$

If the inertia associated with the pulley shaft is  $I$ , equation (4.1) applies. The resisting torque afforded by the belt is given by

$$T_R = (F_1 - F_2)r \quad (4.4)$$

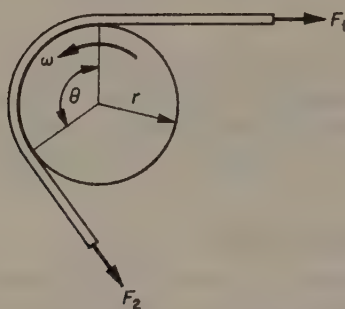


FIGURE 4.1 Friction between a belt and a pulley.

We assume that  $F_1$  and  $F_2$  (and therefore  $T_R$ ) remain constant as  $\omega$  decreases. Eliminating  $F_2$  from (4.3) and (4.4) and substituting in (4.1) gives

$$\text{Integrating,} \quad I d\omega/dt = -F_1[1 - \exp(-\mu\theta)]r \quad (4.5)$$

where  $\omega_1$  and  $\omega_2$  are the speeds at times  $t_1$  and  $t_2$ . Suppose the initial speed is  $\omega_1$ ; hence  $t_1 = 0$ . Let the speed fall to zero at  $t_2$ ; hence  $\omega_2 = 0$ . Rearrangement of (4.5) enables us to write

$$\mu = [-\ln(1 - I\omega_1/rF_1t_2)]/\theta \quad (4.6)$$

This shows that for constant  $\mu$  the expression in the square brackets varies directly with  $\theta$ . Note that  $F_2$  does not appear explicitly.

For a V-shaped belt, of included angle  $2\alpha$ , (4.3) is modified to

$$F_1/F_2 = \exp \mu\theta \operatorname{cosec} \alpha \quad (4.7)$$

and hence (4.6) becomes

$$\mu = [\{-\ln(1 - I\omega_1/rF_1t_2)\} \sin \alpha]/\theta \quad (4.8)$$

## Clutch Theory

In Figure 4.2, torque is transmitted between two shafts in line by using a plate clutch in which contact occurs between radii  $r_1$  and  $r_2$ . Two distinct

theories exist. The first assumes that the pressure is uniform over the area of contact; this results in the relation

$$T_R = \frac{2}{3}\mu P(r_1^3 - r_2^3)/(r_1^2 - r_2^2) \quad (4.9)$$

where  $P$  is the axial force between the plates and  $\mu$  is the friction coefficient acting when slip occurs under torque  $T_R$ .

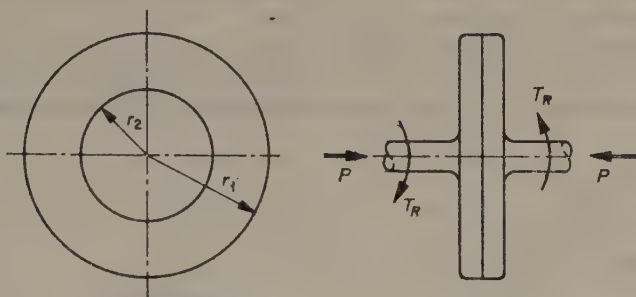


FIGURE 4.2 Friction in a plate clutch.

The second theory assumes 'uniform wear' which is taken to mean that the pressure varies inversely with the radius. This results in the alternative relation

$$T_R = \frac{1}{2}\mu P(r_1 + r_2) \quad (4.10)$$

Equation (4.9) gives the larger value for  $T_R$  but the difference is small except when  $r_1 \ll r_2$ .

## Experimental Details

We shall envisage a composite test rig on the lines of Figure 4.3. A d.c. electric motor  $A$ , having a maximum power output of about 1 kW at 2000

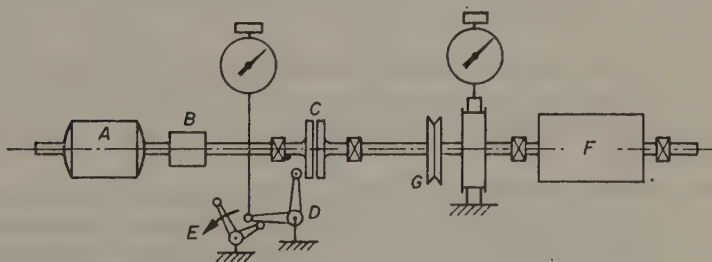


FIGURE 4.3 Apparatus for studying friction in machines.

rev/min, drives a gearbox  $B$  of speed ratio 0.25. The output shaft drives one side of a single-plate clutch  $C$ . Axial force is applied to the clutch by a spring

balance operating through an equal-arm bell-crank lever  $D$ . The clutch may be engaged by hand by turning a second bell-crank lever  $E$ .

The clutch output shaft carries a massive body  $F$  and two pulleys, one flat and one V-shaped. The appropriate belt may be wrapped round either pulley by apparatus at  $G$ , a spring balance being provided to measure the larger tension  $F_1$ ; the angle of lap  $\theta$  may be varied in discrete steps of  $30^\circ$  from zero to  $180^\circ$ . The speed of the output shaft may be measured by a hand tachometer applied to the end of the shaft.

(a) *Bearing Friction and Windage.* After starting the motor, the output shaft is run up to full speed by hand operation of the clutch with both spring balances slackened off. The clutch is then disengaged and the times for the

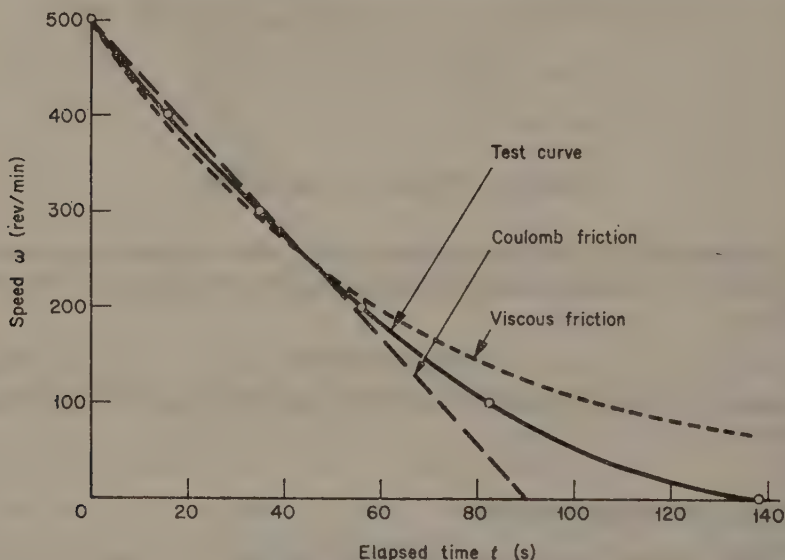


FIGURE 4.4 Bearing friction and windage.

output shaft speed to fall successively to 400, 300, 200, 100 and zero rev/min are found with the aid of the tachometer and a stop watch. This should be repeated to check consistency. A curve is drawn through the readings plotted, as in Figure 4.4.

To compare with equation (4.1) (for  $T_R$  constant) and with (4.2), a curve for each law is shown plotted in Figure 4.4. In drawing these curves the time taken for the speed to fall to half of the initial speed is assumed to be common. It is evident that  $T_R$  in the test depends on both Coulomb and viscous friction.

(b) *Belt Investigation.* Starting with the flat belt, for various combinations of  $\theta$  and  $F_1$  (as set on the spring balance) the output shaft is run up to full speed by using the clutch. The speed  $\omega_1$  is read and the clutch disengaged:



the time  $t_2$  taken by the shaft to stop rotating is measured. It should be observed that  $F_1$  remains sensibly constant during the deceleration and that the deceleration is constant.

Given that  $I$  for the output shaft is  $0.504 \text{ kg m}^2$  and that the mean diameter of the flat belt is  $18.1 \text{ cm}$ , the numerator of the right-hand side of (4.6) can be calculated for each run. Some typical results are tabulated below.

$\theta$ (rad)	$\pi/6$	$\pi/3$	$\pi/3$	$\pi/2$	$2\pi/3$	$5\pi/6$	$5\pi/6$	$\pi$
$F_1$ (N)	100	100	40	60	80	40	80	40
$\omega_1$ (rev/min)	498	486	495	496	492	493	483	492
$t_2$ (s)	9.1	4.9	11.6	6.0	3.4	6.0	3.0	5.3
$-\ln(1 - I\omega_1/rF_1t_2)$	0.18	0.34	0.37	0.51	0.75	0.92	0.89	1.13

These results are plotted in Figure 4.5. It is reasonable to draw a straight line through the test points (to intersect the origin), the slope of which is the coefficient of  $\mu$ .

The test is repeated using the V-belt and pulley. It is given that the belt mean diameter is  $16.8 \text{ cm}$  and  $\alpha = 19^\circ$ . A similar set of results gives the second curve of Figure 4.5, from which  $\mu$  for the V-belt can be measured.

Note that it has been assumed that bearing friction plays a negligible part in decelerating the shaft during the belt tests. Comparison of the times taken with those in test (a) shows this assumption to be reasonable.

(c) *Clutch Investigation.* In this test, a stroboscope is used to illuminate the edges of the clutch plates which are marked with a pattern in contrasting colours. When the flash frequency is synchronized with the shaft speed, it is easy to tell whether or not the clutch is slipping. In this test the flat belt is used as a brake. Choosing  $\theta = \frac{1}{2}\pi$  and using the  $\mu$ -value found in the previous test, the proportionality between braking torque  $T_R$  and  $F_1$  on the spring balance can be established as

$$T_R = kF_1 \quad (4.11)$$

The motor is started and the axial load  $P$  on the clutch is set between  $80 \text{ N}$  and  $280 \text{ N}$  by means of the spring balance at the clutch.  $F_1$  is increased until the clutch is observed to slip. A typical curve of  $F_1$  against  $P$  is shown in Figure 4.6. This is evidently a straight line, the slope of which relates  $F_1$  to  $P$ . Using (4.11) and (4.9) and given that the external and internal diameters of the clutch face are  $15.9 \text{ cm}$  and  $10.8 \text{ cm}$  respectively,  $\mu$  for the uniform pressure theory can be found. Using (4.10) instead of (4.9),  $\mu$  can be again found, this time for the 'uniform wear' theory.

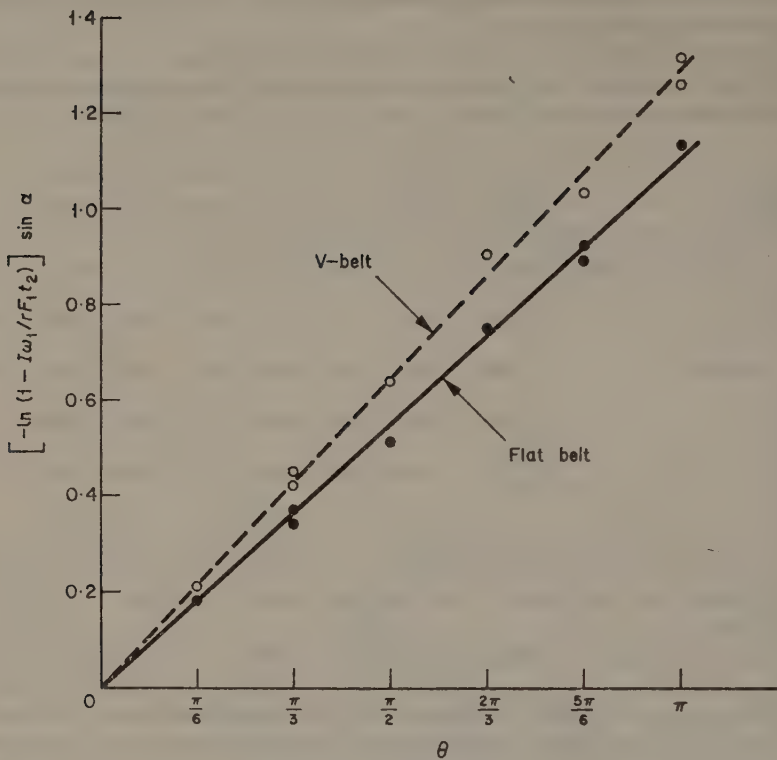


FIGURE 4.5 Belt friction.

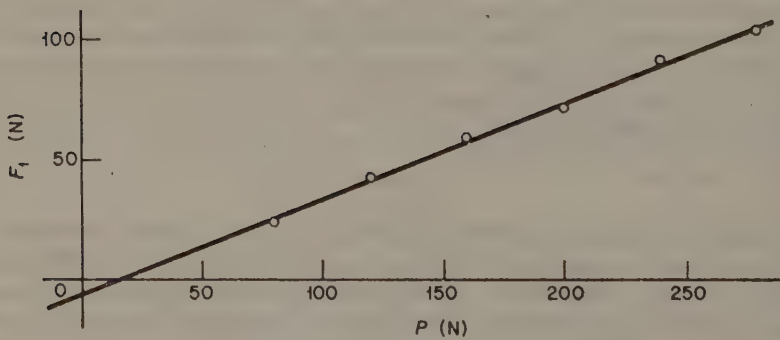


FIGURE 4.6 Clutch friction.

## Discussion

Check that you can obtain equations (4.2), (4.3), (4.7), (4.9) and (4.10) and note the assumptions made.

Does your bearing friction test confirm Figure 4.4? Comment on the accuracy of calculating  $\ln(1 - I\omega_1/rF_1t_2)$  for low and high values of  $\theta$ . Were you justified in ignoring the bearing friction during the belt tests?

Confirm that you arrive at the same  $\mu$ -value (to two significant figures) for the clutch using both theories. Why are they so similar in this case? Can you conclude that either of the theories is the more correct? Can you explain the reason for the intercept on the vertical axis of the curve in Figure 4.6?

## Balancing of Rotating Bodies

Lack of balance in machines causes vibration. For various reasons such vibration should be avoided or, at least, minimized. This experiment is concerned with the balancing of a set of bodies rotating about a common axis.

### Theory

Consider a small body  $A$  of mass  $m_A$  attached to a rigid shaft by means of a light rigid rod so that, when the shaft is constrained by frictionless bearings,  $A$  rotates at radius  $r_A$  as in Figure 5.1. When the shaft is other than vertical,

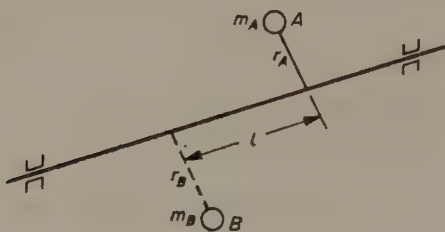


FIGURE 5.1 Static balance.

because of gravity it will turn until the body  $A$  is at its lowest possible position. Clearly it would not turn if another body  $B$  was placed *opposite*  $A$ , provided that

$$m_B r_B = m_A r_A \quad (5.1)$$

It is not necessary for  $A$  and  $B$  to be in the same plane of rotation. Under these circumstances, we say that  $A$  and  $B$  are in *static balance*.

When we rotate the shaft at angular speed  $\omega$ ,  $A$  exerts a force  $m_A r_A \omega^2$  radially outwards on the shaft. We can again balance  $A$  by means of a body  $B$  according to equation (5.1), since  $\omega$  is common. However, it is now essential for  $A$  and  $B$  to be in the *same* plane. This is elementary *dynamic balance*. Note that static and dynamic balance depend on gravitational and centrifugal effects, respectively.

For  $A$  and  $B$  situated in planes  $l$  apart, the equal dynamic forces give rise

to a couple  $m_A r_A l \omega^2$  in a plane containing the shaft and rotating therewith. Complete dynamic balance is not obtained unless an equal and opposite couple is provided.

We must now replace  $B$  by two bodies  $C$  and  $D$  opposite to  $A$ , as shown in Figure 5.2. For the centrifugal forces to balance, since  $\omega^2$  is common,

$$m_A r_A = m_C r_C + m_D r_D \quad (5.2)$$

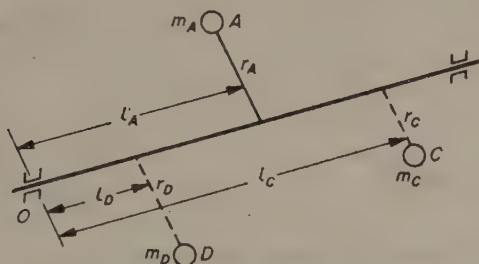


FIGURE 5.2 Dynamic balance.

Now take moments in the plane of the bodies about any point  $O$  in the shaft; for dynamic balance the resultant moment must vanish. Since  $\omega^2$  is common,

$$m_A r_A l_A - m_C r_C l_C - m_D r_D l_D = 0 \quad (5.3)$$

Obviously we can place  $O$  where we like in the shaft but, should it then be necessary to measure one of the  $l$ 's in a direction opposite to the others, its sign must be changed in equation (5.3). It is often convenient to eliminate one

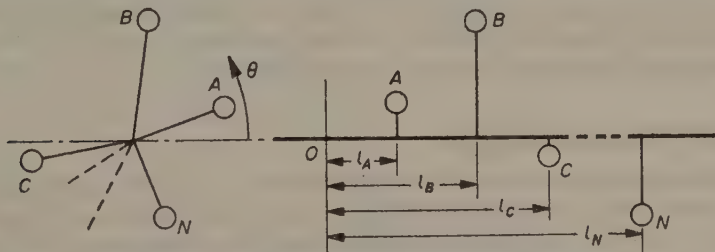


FIGURE 5.3 General situation for dynamic balance.

of the terms in equations like (5.3) by placing  $O$  in the plane of the appropriate body. Both equations (5.2) and (5.3) must be satisfied for dynamic balance; it follows that static balance is achieved at the same time.

To study the dynamic balance of a large number of rotating bodies, we require a more general theory leading to the construction of force and moment polygons. The bodies need not be set opposite one another, as in Figures 5.1 and 5.2, but may be arranged as shown in Figure 5.3. Consider bodies  $A, B, C, \dots, N$ , set at angles  $\theta_A, \theta_B$ , etc. from some datum direction,

rotating in planes distant  $l_A, l_B$ , etc. along the shaft from some reference plane at  $O$ .

It is now convenient to represent the centrifugal forces by vectors and to draw a force polygon with component vectors proportional to  $mr$  in magnitude. Instead of equation (5.2), dynamic balance requires that we obtain a closed polygon, as in Figure 5.4. It does not matter whether we draw each vector in

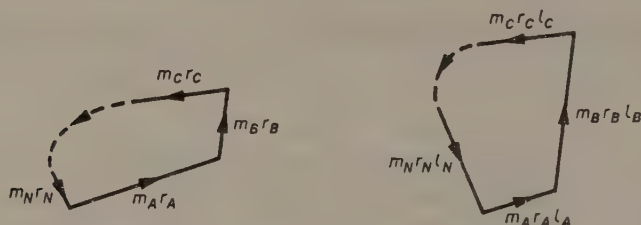


FIGURE 5.4 Force and moment polygons.

direction radially outwards or radially inwards so long as we follow the same rule throughout.

The moments can likewise be represented by vectors. Now the vector representation of a moment is a line drawn normally to the plane of the moment. Such vectors give rise to a moment polygon, as in Figure 5.4. Strictly, each moment vector should be perpendicular to the corresponding force vector, but there is no need to make this distinction. To correspond to equation (5.3) it is only necessary for the moment polygon to close. Where the  $l$ 's are measured on both sides of the reference plane, the direction of the moment vectors must be reversed accordingly. It is usually convenient to take the reference plane at one of the bodies for which  $m, r$  and/or  $\theta$  is unknown; this eliminates the corresponding vector from the moment polygon.

## Experimental Details

A suitable apparatus consists of a horizontal shaft carried in bearings attached to a frame which is suspended by light springs, as shown in Figure 5.5. Keyed to the shaft are four (or more) discs, the whole being in dynamic balance. The shaft is driven by an electric motor *via* a flexible drive at an angular speed  $\omega$  below its whirling speed but such that  $\omega/2\pi$  is above the resonant frequency of the frame on its suspension (see later experiments).

The discs are slotted to permit the fixing of bodies of various mass at various  $r$  and  $\theta$  by means of bolts and knurled nuts. Any lack of dynamic balance introduced is shown by movement of the frame on its suspension.

First, to investigate the static balance, remove the flexible drive and fix a body  $A$  to one of the discs. Note that the shaft rotates under gravity until  $A$  is in its lowest position. Now fix a body  $B$  opposite to  $A$ , both to the same and to another disc, such that equation (5.1) is satisfied. Note that the shaft will remain in equilibrium in any position.



With  $B$  on the same disc as  $A$ , re-connect the flexible drive and switch on the motor. Note dynamic balance which is shown by the lack of movement of the frame on its suspension.

Using three different discs, fix two bodies  $C$  and  $D$  both opposite to  $A$ ,

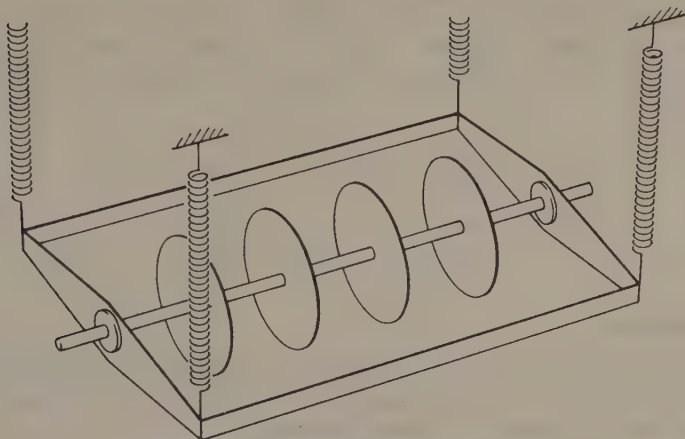


FIGURE 5.5 Dynamic balance machine.

at radii which obey both equations (5.2) and (5.3). Choose values for  $m$  and  $r$  which permit  $C$  and  $D$  to be (a) one either side of  $A$ , (b) both on the same side of  $A$ . In both cases switch on the motor and check the dynamic balance.

Now suppose that you are given the information in the following table.

Plane	$m$ (kg)	$r$ (cm)	$\theta$	$l$ (cm)	$mr$	$mrl$
$A$				0		
$B$	1.0	4.0	$180^\circ$	7.4		
$C$			$265^\circ$	13.4		
$D$			$40^\circ$	20.8		

Note that it is assumed that  $A, B, C, D$  are placed in order along the shaft and that the plane of  $A$  is regarded as the reference plane. You are required to find values for  $m_A, m_C, m_D, r_A, r_C, r_D$  and  $\theta_A$ . Each vector polygon will reveal two unknowns, leaving some arbitrary choice for the remaining quantities.

Since  $mrl$  for  $B$  is known, first draw the closed moment polygon, using the given angles; because  $mrl$  for  $A$  is zero, you do not need  $\theta_A$ . This will reveal  $mrl$  for  $C$  and  $D$ . Now calculate  $mr$  for  $B, C$  and  $D$  and draw the closed force polygon. This will reveal  $mr$  and  $\theta$  for  $A$ . You now have some choice in the selection of the unknown  $m$  and  $r$  values.

Fix bodies to the discs according to your completed table and check the dynamic balance.

As a further example, complete the following table with the aid of vector diagrams and confirm your results by a test.

Plane	$m$ (kg)	$r$ (cm)	$\theta$	$l$ (cm)	$mr$	$mrl$
<i>A</i>			$10^\circ$	0		
<i>B</i>	1.5	3.0		7.4		
<i>C</i>	1.0	4.0		13.4		
<i>D</i>	1.0	3.0		20.8		

## Discussion

What principles of mechanics are invoked in the theory of dynamic balancing? Why is it possible to draw the vectors of the moment polygon in the same directions as those of the force polygon?

Note any shortcomings in the experimental equipment. Did you take into account the different lateral displacements of the centres of mass of different sized bodies relative to their respective discs? Does it matter that the bodies used in the tests are of finite size?

## Note on the Balancing of Reciprocating Bodies

In an earlier experiment we considered the crank-slider mechanism. From equation (1.6), for a reciprocating body of mass  $m_R$ , the accelerating force at the body is very nearly  $-m_R\omega^2r\{\cos\theta + (\cos 2\theta)/q\}$ . This consists of two forces, the first,  $-m_R\omega^2r \cos\theta$  being called the *primary force*, and the

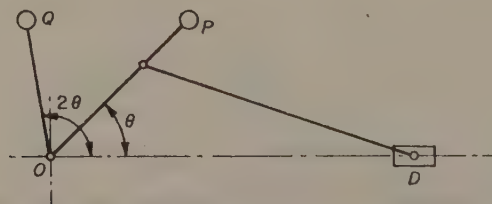


FIGURE 5.6 Primary and secondary cranks.

second,  $(-m_R\omega^2r \cos 2\theta)/q$  being called the *secondary force*. The reactions of these forces on the crankshaft are equal and opposite.

We may now visualize a body *P* rotating with the crank and another *Q* also rotating about *O* but at *twice* the speed of the crank, as depicted in Figure 5.6. These could be arranged to provide exactly the same variation of

reaction on the crankshaft in the direction  $OD$ , as is caused by the motion of the reciprocating body considered above. This is why problems on reciprocating balance are similar to those on rotating balance except that two sets of polygons must be drawn. By equation (1.4), forces exist in addition to the primary and secondary forces, but these are almost always too small to matter.

In a reciprocating engine,  $m_R$  is taken as the mass of the piston plus some portion of the mass of the connecting rod. The remaining connecting rod mass is taken as acting at the crank pin, where it can be regarded as a simple rotating body.

## Free Vibration of a Simple System

The natural frequency or frequencies of vibrating systems are of great importance and must often be determined experimentally. A system vibrates in its natural or free mode(s) when any disturbing agents from without the system are zero or constant in magnitude. A familiar example is the vertical motion of a body suspended by a tension spring from a fixed support; it is necessary to disturb the system in order to set the body in motion, but we are interested in the free motion after the disturbance has been removed.

The example chosen for the present experiment is a one-degree-of-freedom linear torsional system.

### Theory

Consider the system shown in Figure 6.1, which comprises a body suspended at its centre of mass by a light rod or wire from a fixed support. This system

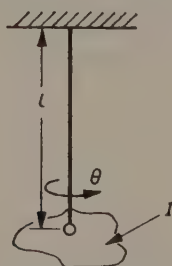


FIGURE 6.1 Simple torsional system.

can vibrate freely in a number of ways. We could cause the body (a) to swing from side to side like a pendulum, or (b) to move bodily in a circular horizontal path without rotating, or (c) to rotate about its centre of mass causing the wire to twist. We say that the system has several *degrees of freedom*. We are interested only in (c) above and we must restrain the system from vibrating in any other manner.

Suppose that the wire is circular and of uniform diameter  $d$  and length  $l$ . From the simple theory of torsion (see Experiment 20),

$$T/J = G\theta/l \quad (6.1)$$

where  $\theta$  is the angle of rotation of the body and is therefore the angle of twist over the whole length of the wire,  $T$  is the torque imposed on the wire by the body (and by the support),  $G$  is the modulus of rigidity of the material of the wire, and  $J$  is the second moment of area of the wire about the axis of twist and is equal to  $\pi d^4/32$ . We are interested in the *stiffness*  $k$  of the wire, i.e. the torque per unit angle of twist; hence

$$k = T/\theta = GJ/l = G\pi d^4/32l \quad (6.2)$$

For convenience, take the body as being a circular disc of mass moment of inertia  $I$  about its point of support (centre of mass). The reader should note the essential difference between  $J$  and  $I$ . Suppose that a cylinder fitted under the body rotates within a fixed cylinder, the space between the cylinders being filled with a viscous medium, Figure 6.2. This constitutes a dashpot, the

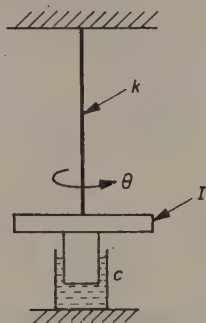


FIGURE 6.2 Damped torsional system.

viscous friction coefficient of which we suppose is  $c$ , i.e.  $c$  is the resisting torque on the body per unit angular speed. Then, equating torques for some arbitrary  $\theta$ , we obtain the system equation of motion

$$I\ddot{\theta} + c\dot{\theta} + k\theta = 0 \quad (6.3)$$

This is a second-order homogeneous linear differential equation in  $\theta$ . It has several solutions depending on the relative magnitudes of  $I$ ,  $c$  and  $k$ . For  $c^2 < 4Ik$ , when the body is released from an angle  $\bar{\theta}$  measured from the equilibrium position, we obtain the damped oscillation

$$\theta = \bar{\theta}(1 + a^2/b^2)^{1/2} e^{at} \cos(bt + \beta) \quad (6.4)$$

where  $a$  is the damping factor,  $b/2\pi$  the natural damped frequency and  $\beta$  the damping angle, given by

$$\left. \begin{aligned} a &= -c/2I \\ b &= (k/I - c^2/4I^2)^{\frac{1}{2}} \\ \beta &= \arctan (a/b) \end{aligned} \right\} \quad (6.5)$$

Two other cases are of interest. For no damping,  $c = 0$  and instead of (6.4), we obtain the undamped oscillation

$$\theta = \bar{\theta} \cos b_n t \quad (6.6)$$

where the natural undamped frequency,  $b_n/2\pi$  is given by,

$$b_n = (k/I)^{\frac{1}{2}} \quad (6.7)$$

For  $c^2 = 4Ik$ , we obtain the aperiodic solution

$$\theta = \bar{\theta} e^{at} (1 - at) \quad (6.8)$$

The three results are compared in Figure 6.3. For  $c = 0$ , the motion is said to be *undamped*; for  $c^2 < 4Ik$ , it is *underdamped*; for  $c^2 = 4Ik$ , it is

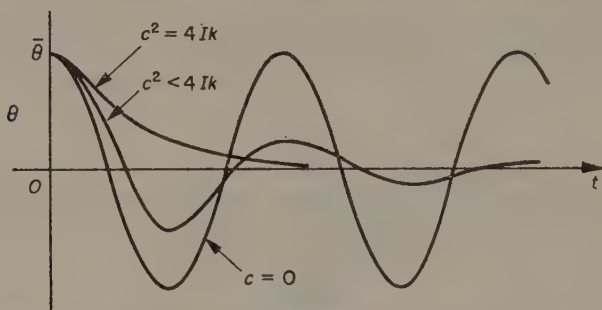


FIGURE 6.3 Free motion of the system.

*critically-damped*. There is a fourth case known as *overdamped*, when  $c^2 > 4Ik$ , but this is of no interest in the present experiment.

## Experimental Details

This follows the lines of Figure 6.2. In a typical case, the suspension wire is of steel, 0.90 mm in diameter and 0.91 m long. The modulus of rigidity is  $81.5 \times 10^9$  N/m<sup>2</sup>. The disc, with cylinder attached, is of brass and is well-balanced about its point of attachment to the wire. Its moment of inertia is 0.002 64 kg m<sup>2</sup> and the cylinder diameter is about 10 cm. The upper surface of the disc is graduated in degrees around the periphery. A means is provided for releasing the disc from an angular position displaced from the equilibrium position; for convenience,  $\bar{\theta}$  is made 180°, and it is essential that this does not twist the wire beyond its elastic limit.



The fixed cylinder is arranged so that it can be moved vertically relative to the moving cylinder. The radial clearance must remain uniform and equal to about 0.5 cm. This cylinder is filled with a mixture of fuel oil and lubricating oil gauged so that, over the range of vertical movement of the cylinder, the effective viscous damping coefficient covers most of the range

$$0 < c^2 < 4Ik$$

i.e. so that the free motion of the system can be investigated over most of the underdamped region.

Practise releasing the disc from its displaced motion until you are able to set it in smooth angular motion. Check that the equilibrium position of the disc corresponds to  $0^\circ$  on the scale.

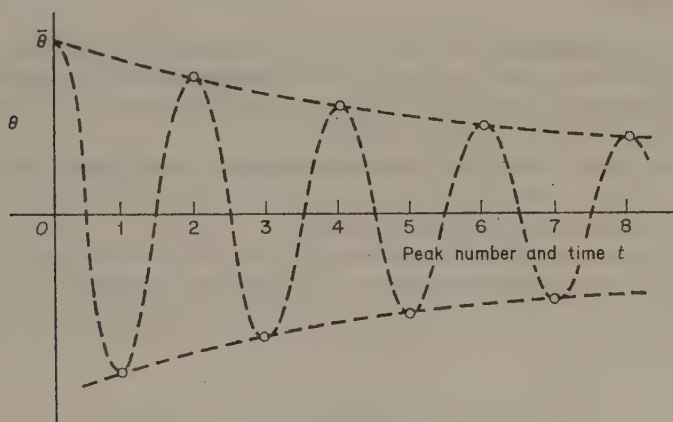


FIGURE 6.4 Free underdamped response.

Lower the fixed cylinder until the moving cylinder is clear of the oil. Start the vibration and record the amplitude each time the disc comes to rest, until about ten complete cycles have been completed. This can be done easily and accurately after a little practice, especially if one person reads whilst another records. Repeat the experiment to check consistency and measure, with a stop watch, the total time for the ten cycles. Find  $b_n$  and compare with the value calculated from equations (6.7) and (6.2); for the latter, you will need to take given values for  $I$  and  $G$  and to ensure that you have a very accurate value of  $d$ . It is to be expected that the free motion will be slightly damped even though no oil damping is used.

Next adjust the lower cylinder until  $c$  is large enough to ensure that the amplitude decreases from  $180^\circ$  to about  $20^\circ$  after ten complete cycles. Repeat the test as above and estimate  $b$  by time-averaging over the whole ten cycles. Do not time from the instant of release but from the first occasion when the disc stops. Now try to measure  $b$  separately during the early and late part of the transient; there should be no difference if the system is truly linear.

Plot the amplitude against peak number (which is proportional to elapsed time) following the style of Figure 6.4. Draw smooth curves to represent the envelope of the vibration, and sketch in the disc displacement between peaks; from equation (6.4), the envelope should be the curves  $\pm \theta e^{at}$ . Also plot the logarithm (to base  $e$ ) of the amplitude against peak number. The envelope should now consist of straight lines of slope  $\pm a$ .

Using equation (6.5), find  $c$  from the slope of the logarithmic envelope. Also check that the following relation is obeyed:

$$b_n^2 = b^2 + a^2 \quad (6.9)$$

Repeat the above but with about twice the amount of effective damping.

## Discussion

Did your calculated and test values of  $b_n$  agree closely? If not, what do you consider to be the primary source of error? What caused the slight damping which occurred when the dashpot was rendered inoperative? Did this cause any significant error in the determination of  $b_n$ ?

What part does gravity play in this experiment? Does it affect any of the results? Why is it necessary to avoid timing between the moment the disc is released and when it first comes to rest?

Can you assess whether the oil damping was truly viscous or otherwise? Can you obtain equation (6.9) from the theory given earlier? Did  $b$  differ greatly from  $b_n$ ?

## Dynamic Loading of a System with One Degree of Freedom

When a system is in equilibrium with a load imposed upon it, we speak of static loading. When potential and/or kinetic energy is transferred to the system *during* the imposition of the load, we have dynamic loading. It is important to appreciate that the stresses arising in the system during dynamic loading may be many times greater than those occurring under static loading *for the same load*.

### Theory

Consider the system with one degree of freedom shown in Figure 7.1, which consists of a body of mass  $m$  and a massless spring of linear stiffness  $k$ . Motion

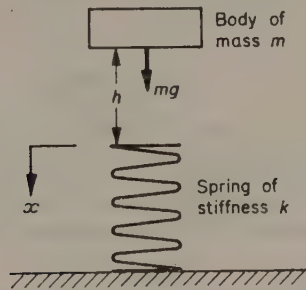


FIGURE 7.1 Simple spring-body system.

is restrained to the vertical direction along the axis of the spring. The lower end of the spring is attached to a fixed support and the upper end is free to move. Suppose that the deflection of the spring (displacement of the upper end) under the action of the load is  $x$ , measured as positive in the *downward* direction.

First suppose that the body is *gently* lowered until its weight  $mg$  is supported by the spring in equilibrium. The *static* deflection is clearly given by

$$x_s = mg/k \quad (7.1)$$

The stress in the spring is proportional to  $x$ , say equal to  $\phi x$ ; hence the static spring stress is of magnitude  $\phi mg/k$ .

Now suppose the body is released to fall freely under gravity through a vertical distance  $h$  until it reaches the upper end of the spring, and suppose that it then attaches itself to the spring. The system will *first* come to rest when the spring has moved through its dynamic deflection  $x_d$ . Assuming no loss of energy, we may equate the strain energy of the spring to the reduction of potential energy of the body.

$$\frac{1}{2}kx_d^2 = mg(h + x_d) \quad (7.2)$$

Solving for  $x_d$  gives

$$x_d = \frac{mg}{k} \left[ 1 \pm \left( 1 + \frac{2hk}{mg} \right)^{\frac{1}{2}} \right] \quad (7.3)$$

Consider the special case when  $h = 0$ . Equation (7.3) then shows that

$$x_d = 2mg/k \quad \text{or} \quad 0 \quad (7.4)$$

The first value gives the dynamic deflection when the system *first* comes to rest; we note that this is twice the value of  $x_s$  given by equation (7.1). The spring stress is likewise twice the static stress, i.e.  $2\phi mg/k$ . In this position the spring force is  $2mg$ , sufficient to return the body towards its initial position. In fact, the second value of  $x_d$  given by equation (7.4) shows that the system *next* comes to rest when the body has returned precisely to its initial position.

It is now evident that an undamped free oscillation of the system has been initiated, the (downward) displacement of the body being

$$x = \frac{1}{2}x_d(1 - \cos b_n t) \quad (7.5)$$

where, according to equation (6.7),  $b_n$  is given by

$$b_n = (k/m)^{\frac{1}{2}} \quad (7.6)$$

The amplitude is  $x_d/2$ , in this case  $x_s$ .

It is instructive to apply the impulse-momentum equation (see Experiment 8) to this phenomenon. The net downward force on the body  $F$  may be written

$$\begin{aligned} F &= mg - kx \\ &= mg - \frac{k}{2} \frac{2mg}{k} (1 - \cos b_n t) \\ &= mg \cos b_n t \end{aligned} \quad (7.7)$$

The time integral of  $F$  equals the change of momentum of the body, i.e.

$$\Delta(m\dot{x}) = \int mg \cos b_n t \, dt \quad (7.8)$$

The momentum of the body is zero initially. The body reaches its static equilibrium position after one quarter-cycle, i.e. when  $t = \pi/2b_n$ . At this instant, the momentum is given by equation (7.8) as  $mg(m/k)^{\frac{1}{2}}$ . This shows

that the (downward) velocity is  $g(m/k)^{1/2}$ , which may be confirmed by differentiating equation (7.5). Similarly, after one half-cycle the momentum of the body is found to be again zero, which accords with the facts.

In the general case, when  $h > 0$ , the body first comes to rest when  $x_d > 2mg/k$ , see equation (7.3), the spring stress then being greater than when  $h = 0$ . It is evident that for large  $h$  the stress can be many times greater than that occurring under static loading. The subsequent motion of the body is again undamped oscillatory motion about the static equilibrium position. Its amplitude is now greater than  $x_s$ , so that during part of each cycle the spring is in tension, reversal of stress taking place when the spring deflection is negative (i.e. upwards).

An alternative analysis can be applied when  $h > 0$ . When the body has fallen through  $h$ , its reduction in potential energy given by  $mgh$  equals the kinetic energy acquired given by  $\frac{1}{2}m\dot{x}_0^2$ , assuming that no energy has been lost. Instead of equation (7.2), we may write

$$\frac{1}{2}kx_d^2 = \frac{1}{2}m\dot{x}_0^2 + mgx_d \quad (7.9)$$

Solving for  $x_d$  gives

$$x_d = \frac{mg}{k} \left[ 1 \pm \left( 1 + \frac{\dot{x}_0^2 k}{mg^2} \right)^{1/2} \right] \quad (7.10)$$

Since, in this case,  $\dot{x}_0 = (2gh)^{1/2}$ , equation (7.10) is identical to equation (7.3),

In practice, due to inherent damping effects which have been neglected, the amplitude of the motion will gradually decay to zero as energy is transferred as heat, leaving the system in its static equilibrium configuration. We have, of course, neglected any loss of energy due to impact where this applies.

## Experimental Details

It is convenient to use a light elastic cantilever rather than a coil spring; this is supported in a rigid frame, as shown in Figure 7.2, and the load is

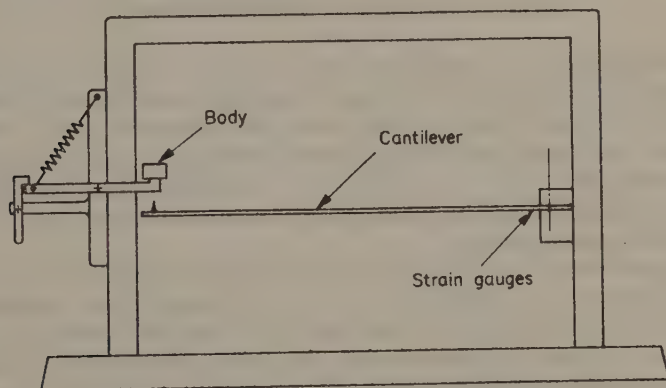


FIGURE 7.2 System for dynamic loading.



applied at the free end. In conjunction with a body of mass 50 g, a suitable cantilever is one made of high-tensile steel having the following dimensions: length 30 cm, width 2 cm, thickness 1 mm. For these parameters,  $k$  is about 38 N/m and  $x_s$  is about 1.3 cm; the natural period of the system is about 0.22 s. To avoid overstressing the material of the cantilever,  $x_d$  should be restricted to about 8 cm, which requires  $h$  to be limited to about 15 cm.

Strain gauges (see Experiment 25) are fixed to the upper and lower faces of the cantilever near the fixed end; these feed recording apparatus which is calibrated to indicate the stress in the cantilever and also the deflection under the load (which are proportional to each other). A signal displayed on a cathode-ray oscilloscope (C.R.O.) provides a deflection-time record.

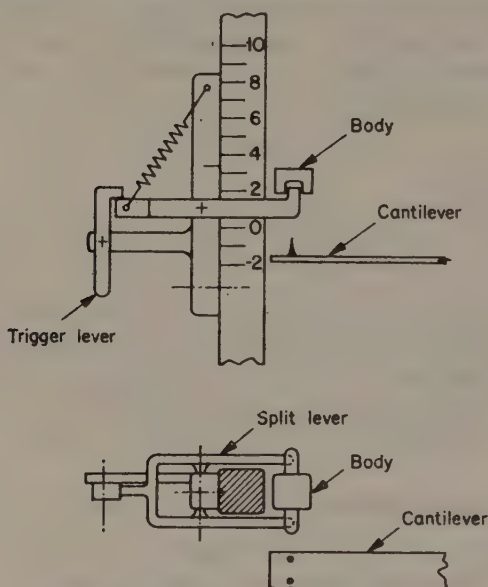


FIGURE 7.3 Detail of release mechanism.

The mechanism for releasing the body is shown in detail in Figure 7.3; in the plan view, the cantilever is shown displaced from the body for clarity. The body is shaped with two ears which are supported by the ends of a split lever. The latter is retained against the tension of a spring by the trigger lever. When the split lever is released, the ends supporting the body move with an acceleration well in excess of  $g$ , thus permitting the body to begin its fall freely under gravity.

The underside of the body is fitted with a cork insert which, on contact with the cantilever, is penetrated by a pair of sharp spikes attached to the cantilever. The friction between the spikes and the cork assists the body and cantilever to move together during the subsequent motion. The whole release assembly may be moved vertically relative to the frame and fixed according to a scale which indicates the value of  $h$ .



Move the cantilever by hand and check the calibration of the deflection indicator and the C.R.O. Fix the body to the cantilever and measure the static deflection  $x_s$ . Cock the release mechanism and offer this up to the body until the ends of the split lever just touch the ears; check that the scale reads  $x_s$  (negatively). The scale may then be relied upon to indicate  $h$ . Check that the spikes on the cantilever penetrate the cork insert in the body sufficiently to ensure that the body rests firmly on the cantilever following release of the load from any height between zero and 10 cm.

Start the tests by releasing the load with  $h$  set at zero. Note  $x_d$  and the stress when the system first comes to rest, and observe the subsequent motion. Repeat several times to check consistency. Carry out similar tests at about eight different values of  $h$  between zero and 10 cm.

## Discussion

Compare the behaviour of the system with that predicted by the theory. To what extent do the measured and calculated values of  $x_d$  differ as  $h$  is altered? Give reasons for the differences, taking into account

- (a) the energy lost in impact,
- (b) friction and damping effects,
- (c) the mass of the cantilever, and
- (d) the shortcomings of the test equipment, including dynamic attenuation of the stress signal.

## *A Momentum and Energy Experiment*

As a consequence of Newton's Second Law we have the Principle of the Conservation of Momentum, which states that the momentum of a system of bodies is constant provided that no external forces act on the system. Momentum is a vector quantity so that we may apply the principle only in one direction at a time.

Unlike momentum, we can rarely assume that the energy of a mechanical system is conserved. Energy, a scalar quantity, occurs in many forms; in mechanics, the common forms are kinetic, potential and strain. In any analysis of a system based on energy, possible energy conversion into heat and other forms must be taken into account. Such conversion was seen to take place in Experiment 7.

### Theory

For a system of finite bodies acted upon by a single force  $F$ , we may write:

$$F = \Sigma (m\dot{v}) \quad (8.1)$$

where  $m$  is the mass of one of the bodies and  $v$  is the velocity of the same body *measured in the same direction as  $F$* . Equation (8.1) can be rewritten as follows:

$$\int F dt = \Sigma \int m dv \quad (8.2)$$

when it is known as the impulse-momentum equation. The time integral of the force is the impulse, and this is seen to equal the change of momentum of the system. When  $F$  is zero, this leads at once to the principle of the conservation of momentum.

Equation (8.1) can be re-written alternatively as

$$\int F ds = \Sigma \int m v dv \quad (8.3)$$

where  $s$  is the distance through which the force acts in the direction of the force. In this form, we have the work-energy equation. The left-hand side is the work done *on* the system by the external force, and the right-hand side

is the increase in kinetic energy of the system. When  $F$  is zero, the kinetic energy is conserved.

These equations have analogous forms when applied to rotational motion about a fixed axis. We simply replace  $F$ ,  $m$ ,  $s$  and  $v$  as in the table below:

<i>Linear motion</i>	<i>Rotational motion</i>
force $F$	torque $T$
mass $m$	moment of inertia $I$
displacement $s$	angular displacement $\theta$
velocity $v$	angular velocity $\omega$
momentum $mv$	angular momentum $I\omega$

It is important to measure the relevant quantities about the axis of rotation of the system. We can construe the angular momentum to mean the aggregate of the moments of linear momentum of the system of bodies, when the term moment of momentum is appropriate.

## Experimental Details

Figure 8.1 shows the important items of a suitable test apparatus. The turntable is about 30 cm in diameter and the periphery is flanged to hold a

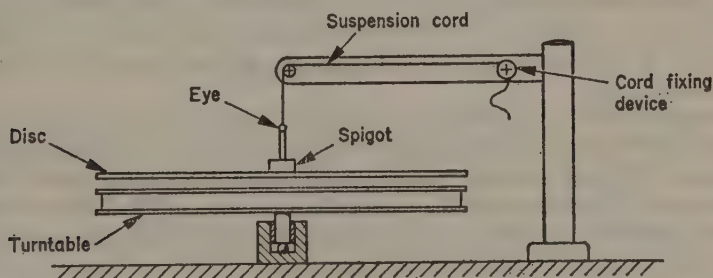


FIGURE 8.1 General arrangement of test equipment.

strip of recording paper 2 cm wide. It is pivoted as freely as possible by using a single steel ball to support the plain end of the shaft, the latter being of polished steel of diameter 1 cm; lateral support is provided by a nylon bush. A suitable weight for the turntable is 50 N.

A flat disc, of the same diameter as the turntable and weighing about 15 N, is supported by a light strong cord attached to the eye of a thin shaft fixed to the disc centre. By supporting the disc at a point well above its mass centre, it is easy to ensure that when the disc is held stationary its surface

is parallel to the surface of the turntable. The rigid supporting frame is fixed to the base of the apparatus so that the disc and turntable shafts are coaxial. The cord is fastened off by means of a spring-loaded split washer such as is used to tension the upper thread on a sewing machine.

A spigot on the disc is used to locate additional plain discs in order to increase the inertia when required; a suitable number of additional discs is three, each weighing about 15 N.

The turntable is put into motion by transferring to it the energy of a compressed coil spring. A simple trigger mechanism is used to start the motion. The proportions of the mechanism are such that the initial speed imparted to the turntable is between 2 and 3 rad/s. A stop is fitted to halt the motion after rather less than one revolution.

Measurement of velocity is carried out by using a freely-vibrating cantilever to make a sinusoidal trace on recording paper wrapped around the

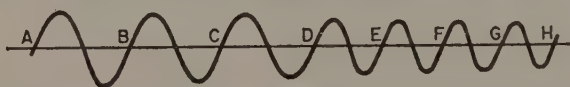


FIGURE 8.2 Measurements from the recording.

periphery of the turntable. A suitable natural frequency for the cantilever is 8 to 10 Hz (c/s). It is essential that the pen causes a minimum of retardation of the turntable. For this reason a very light stylus is used in conjunction with electrically-sensitive paper; an a.c. mains supply is suitable with a 10 k $\Omega$  5 W resistance in series. Pen and bearing friction reduce the initial turntable speed by no more than 10 per cent over the whole of the working displacement (a bigger reduction than this would render the apparatus unsuitable). The stylus is released by the same triggering mechanism which initiates the turntable motion.

In use, the horizontal portion of the disc suspension cord is severed when the turntable has rotated through between one quarter and one half of a revolution. Slipping occurs over about 5° of rotation, after which the disc and turntable move together. The velocities of the turntable before the disc is released and after slipping has ceased are assessed from measurements of the sinusoidal trace on the recording paper.

Measure the natural frequency of the cantilever by means of an accurately-calibrated stroboscope and mark the cantilever accordingly. Measure the moment of inertia of the turntable and of each disc by suspending each as a trifilar suspension (as described in Experiment 3) and mark the items with the appropriate values.

Carry out the test proper by starting the unloaded turntable and releasing the main disc after the turntable has moved through one quarter to one half of a revolution. The initial clearance between the disc and the turntable is not critical and need be no more than 1 cm. You will have recorded a sinusoidal trace as shown in Figure 8.2. With the stylus in its equilibrium position, mark the centre line on this recording, and measure  $AB$ ,  $BC$ ,  $CD$ ,

etc. Plot these measurements against time, as in Figure 8.3, taking the time interval between points to be equal to the known period of the cantilever. Your plot will represent angular *velocity* to an appropriate scale, and there will be a noticeable step over the interval during which impact occurred. Draw the best straight lines through several points in each group either side of the step.

The above lines will not be horizontal because friction will have decelerated the system. Neither are they likely to be parallel because the magnitude of the deceleration probably will have changed. It is necessary to make accurate

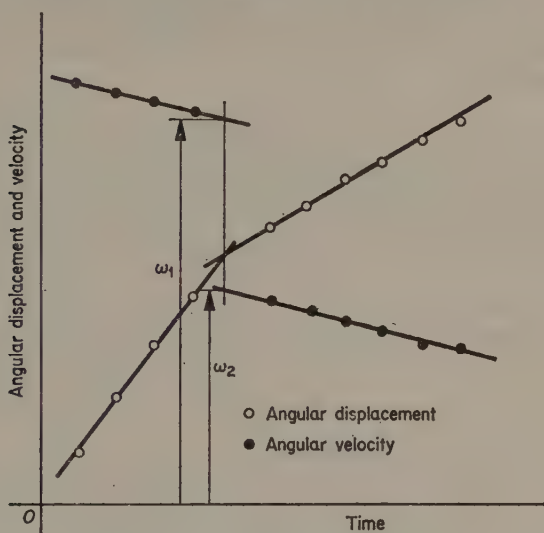


FIGURE 8.3 Angular displacement and velocity.

assessments of the velocity just before impact and just after slipping ceased and, for this purpose, an estimate is required of the time at which impact may be supposed to have occurred. Hence now measure  $AB$ ,  $AC$ ,  $AD$ , etc. from your trace and plot these values against time to represent the angular *displacement* of the turntable, as in Figure 8.3. Again you will have points in two distinct groups. Draw the best straight lines through several points in each group adjacent to the interval over which impact occurred. Suppose that the point of intersection of this pair of lines represents the time of impact. Measure the velocities  $\omega_1$  and  $\omega_2$  from the velocity lines corresponding to the time of impact as found above. You may suppose that these values represent the velocity of the turntable before and after impact.

You are now in a position to check that, over the short period covering the impact between the two bodies, the principle of momentum has been obeyed. You may also calculate the loss of kinetic energy due to impact as a percentage of the kinetic energy of the turntable just prior to impact.

Repeat with the main disc loaded with one, two and three additional discs.



## Discussion

Did your results confirm that the momentum principle was obeyed to the same degree of accuracy in all four tests? If not, discuss the main sources of error under the following headings, and suggest possible remedies:

- (a) design of the apparatus,
- (b) execution of the test, and
- (c) interpretation of the results.

Are you satisfied that the amount of energy lost varied in the expected manner according to the amount of the added inertia? To what extent does the initial clearance between the disc and the turntable affect the application of the energy principle?



## *Forced Vibration of a Simple System*

We consider in this experiment the behaviour of a system with one degree of freedom as a result of imposing a continuously-varying disturbance from outside the system. To simplify the analysis, it is usual to take a disturbance which varies sinusoidally. Since the frequency of the disturbance can be varied over a wide range, this procedure can provide much useful information about the system.

The system chosen for experiment has the same mathematical form as that used in Experiment 6, but the components are arranged in a different manner in order to facilitate the tests.

### **Theory**

Consider the rotary system shown in Figure 9.1, in which the elastic member is a torsion spring of angular stiffness  $k$ , one end of which is displaced forcibly through an angle  $\theta_1$  by some external agency; we can refer to this as

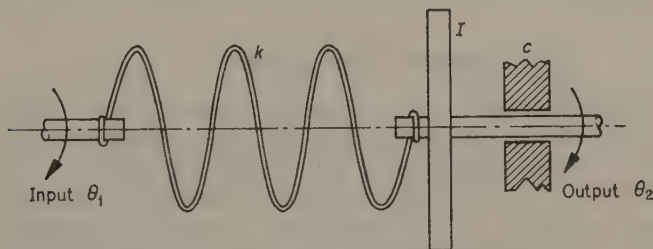


FIGURE 9.1 System with one degree of freedom.

the *input* to the system. The other end of the spring is attached to and rotates with a massive disc which moves through an angle  $\theta_2$ , the system *output*. Movement of the output shaft is resisted by a viscous damper of coefficient  $c$  and the total inertia associated with the output shaft is  $I$ . Instead of the homogeneous equation (6.3) we now have

$$I\ddot{\theta}_2 + c\dot{\theta}_2 + k\theta_2 = k\theta_1 \quad (9.1)$$

It is evident that the complementary function solution in  $\theta_2$  of equation (9.1) is identical to the solution of (6.3) in  $\theta$ . In other words, when the input shaft is held stationary, the *free* motion of the output shaft is of the form given by equations (6.4) to (6.9), depending on the relative values of  $k$ ,  $I$  and  $c$ .

For the purpose of this experiment we are also interested in the particular integral solution of (9.1) when  $\theta_1 = \bar{\theta}_1 \sin \omega t$ , i.e. when the input shaft is given simple harmonic motion of amplitude  $\bar{\theta}_1$  and frequency  $\omega/2\pi$ .

Because the system is of second order, it must be possible to describe it by no more than two parameters. To simplify the analysis it is therefore convenient to replace  $k$ ,  $I$  and  $c$  by

$$\text{and} \quad \left. \begin{aligned} \tau &= 1/b_n = (I/k)^{\frac{1}{2}} \\ \zeta &= c/2(Ik)^{\frac{1}{2}} \end{aligned} \right\} \quad (9.2)$$

where  $\tau$ , which has the dimensions of time, is called the *time constant* and  $\zeta$ , which is dimensionless, is called the *damping ratio*. The latter name arises since  $\zeta$  is the ratio of the actual value of  $c$  to the value it would need to assume in order to impose critical damping. Note that  $\tau$  is inversely proportional to the undamped natural frequency. A further useful substitution is to put

$$\lambda = \omega\tau = \omega/b_n$$

where  $\lambda$  is clearly dimensionless and is called the *frequency ratio*, i.e. the ratio of the forcing frequency to the undamped natural frequency.

The particular integral solution to equation (9.1) for the given input function may now be expressed as

$$\theta_2 = \bar{\theta}_1 \sin(\omega t + \psi) / \{(1 - \lambda^2)^2 + 4\zeta^2\lambda^2\}^{\frac{1}{2}} \quad (9.3)$$

where

$$\psi = -\arctan \{2\zeta\lambda/(1 - \lambda^2)\} \quad (9.4)$$

The complete solution in  $\theta_2$  includes, of course, both complementary function and particular integral components. In all practical cases the former is transitory and soon disappears. In forced vibration work we are concerned solely with the latter, called the *steady-state* solution. Equation (9.3) shows this to be an oscillation of the same frequency as the input, having an amplitude depending on  $\bar{\theta}_1$ ,  $\zeta$  and  $\lambda$ , i.e. on  $\bar{\theta}_1$ ,  $k$ ,  $I$ ,  $c$  and  $\omega$ . It lags behind the input because the phase angle  $\psi$ , which depends on  $k$ ,  $I$ ,  $c$  and  $\omega$ , is negative.

Note that, because the system is linear, the output amplitude is directly proportional to the input amplitude  $\bar{\theta}_1$ ; we can therefore make  $\bar{\theta}_1$  any angle convenient to the experiment. It is best to express the steady-state forced behaviour by the so-called *magnification ratio*  $M$ , meaning the ratio of the output magnitude to the input magnitude, together with the phase difference  $\psi$ . Hence (9.3) can be replaced by

$$M = 1/\{(1 - \lambda^2)^2 + 4\zeta^2\lambda^2\}^{\frac{1}{2}} \quad (9.5)$$

In Figure 9.2 curves of  $M$  and  $\psi$  against  $\lambda$  for various  $\zeta$  are drawn. The curves indicate that  $M$  for certain  $\zeta$  passes through a maximum at a particular  $\lambda$ . This maximum can be found by differentiating the r.h.s. of (9.5) with respect to  $\lambda$  and equating to zero. Thus

$$M_{\max} = 1/\{2\zeta(1 - \zeta^2)^{\frac{1}{2}}\} \quad \text{at} \quad \lambda = (1 - 2\zeta^2)^{\frac{1}{2}} \quad (9.6)$$

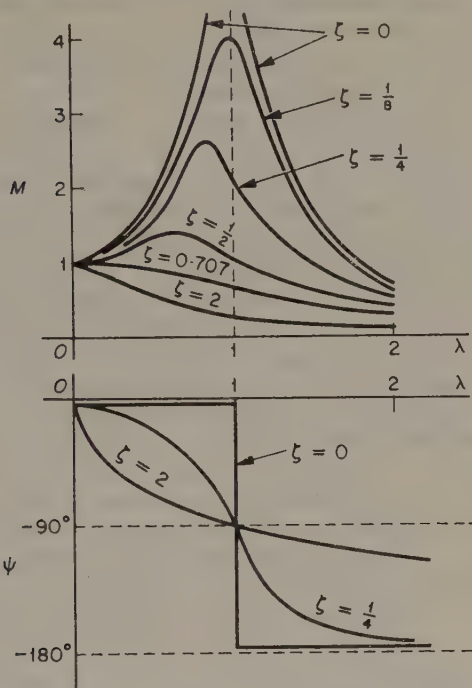


FIGURE 9.2 Amplitude ratio and phase spectrum.

When this maximum occurs at  $\lambda > 0$ , we describe the phenomenon as *resonance*. Further analysis shows that resonance can be avoided by making  $\zeta \geq 0.707$  and equation (9.6) applies only when  $\zeta < 0.707$ . Resonance can be very destructive in certain engineering applications and it is important that the conditions under which it might occur can be foreseen. Note that  $M \rightarrow 0$  as  $\lambda \rightarrow \infty$  for all  $\zeta$ .

### Experimental Details

It is desirable that the input shaft is displaced with undistorted simple harmonic motion. To avoid cyclic variation of  $\omega$  we may employ a Velodyne, though, if a relatively large motor is used (0.5 kW), ordinary armature control of a d.c. machine would be adequate. The motor drives a crank-slider mechanism at about one-tenth motor speed; if space prevents the use of a

large connecting rod to crank ratio, a Scotch-yoke mechanism can be employed instead.

The output is converted to oscillatory motion of the input shaft by means of a rack engaging a gearwheel keyed to the shaft; a suitable value for  $\theta_1$  is  $15^\circ$ . The mechanism should be free from backlash throughout. A suitable range of the input frequency  $\omega/2\pi$  is from zero to 2.5 Hz; a speed indicator on the motor shaft enables  $\omega$  to be measured. Choosing a spring of stiffness about 0.08 N m/rad and a total inertia at the output shaft of about 0.0012 kg m<sup>2</sup> gives us a value for the undamped natural frequency of about 1.3 Hz, which is mid-way within the range of  $\omega/2\pi$ .

In this application it is convenient to use a damper in the form of an eddy-current brake. The inertia disc may be supported on the shaft of a small induction motor which is supplied with direct current; this provides a braking torque very nearly proportional to angular speed, as is required for viscous damping. In a typical installation the current can be varied to alter the effective  $c$ , the maximum of 1 A providing rather more than critical damping.

To record  $\theta_1$  and  $\theta_2$  it is only necessary to fit light pulleys to the input and output shafts which drive light cords attached to the pens of a strip-chart recorder. The steady-state result would then appear as a pair of sinusoids for which  $M$  and  $\psi$  could be determined. This determination is laborious, however, and it is not possible to find  $\psi$  with acceptable accuracy. Hence the alternative arrangement described below is advisable.

An oscillating platform replaces the strip chart of the recorder; this is driven in a direction perpendicular to that of the output pen by a second drive taken from the input motor. The input pen is no longer required. By using a differential, a deliberate phase lag is introduced between the motion of the platform and of  $\theta_1$ ; this angle can be varied by means of a handwheel and is indicated by a pointer on a dial. In use, this 'bias' lag is made equal to

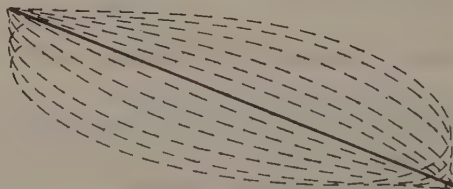


FIGURE 9.3 Lissajous figure on recording paper.

$\psi$  in the system and the value of  $\psi$  appears on the indicator. The record on the paper attached to the platform now appears as a Lissajous figure which, in general, will have an elliptical shape. When the handwheel is turned until the ellipse is converted to a line, the system lag  $\psi$  is indicated on the dial;  $\psi$  can be determined to an accuracy of  $\pm 1^\circ$ , which is some five times better than when using strip-chart recording. A typical record is illustrated in Figure 9.3; this was made with a light electric stylus on electrically-sensitive paper.

Of course  $M$  is directly proportional to the absolute travel of the stylus



since  $\bar{\theta}_1$  is kept constant; it is thus an easy matter to determine  $M$  from the record.

In order to work in terms of  $\lambda$ , it is necessary first to determine  $b_n$ . With zero damping current, turn the disc through about  $180^\circ$  and release it; time the nearly-free motion over about ten cycles. Repeat to check consistency.

Now set a high value of damping current and switch on the input motor. Vary  $\omega$  over its entire range and observe the motion of  $\theta_2$ ; check the calibration of the speed indicator by measuring the period of the oscillations.

Continue the experiment with less damping; now care must be exercised in the region of resonance to avoid damaging the apparatus. Assess the minimum value of damping current which should be set when the system is taken through resonance.

The object of the experiment is to produce a family of experimental curves to compare with Figure 9.2. Aim at investigating the system behaviour for about five constant settings of damping current over the range provided. For each setting, carry out two or three tests with  $\lambda < 1$  and a similar number with  $\lambda > 1$ , making use of the full speed-range of the input motor. It will be found that the steady-state condition will always be reached very quickly. All that is then necessary is to vary the bias angle to the platform drive until the best line recording is obtained. Then read the speed indicator; finally read  $\psi$  and determine  $M$  from the record.

Plot  $M$  and  $\psi$  against  $\lambda$  and sketch in the best curves for each value of damping current.

## Discussion

Make sure that you can obtain equation (9.1) and can solve for the steady-state output motion given by (9.3) and (9.4). Differentiate equation (9.5) and obtain (9.6) for  $\zeta < 0.707$ .

Try to relate damping current to effective  $\zeta$  and also to effective  $c$  if  $I$  and  $k$  are known. Does your experimental family of curves differ significantly from Figure 9.2? If so, can you trace the reason or reasons? If, for various  $\lambda$ ,  $\zeta$  for the same damping current changes markedly, this will suggest non-linear damping.

Were any of your line recordings other than straight? If so, can you suggest why?

## Free Vibration of a System with Two Degrees of Freedom

We now study a conservative system having two principal natural modes and an infinite number of combined modes. The experiment introduces the phenomenon of beating which occurs commonly in engineering assemblies subjected simultaneously to two vibrations of almost identical frequency.

### Theory

Consider the system shown in Figure 10.1, which consists of two simple pendulums coupled together with a spring. For simplicity the pendulums are

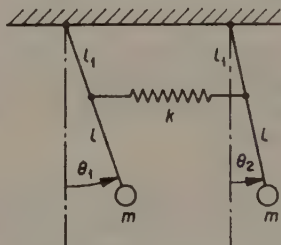


FIGURE 10.1 System comprising coupled pendulums.

similar, each having a length  $l$  and a bob of mass  $m$ . Of course, they both swing in the same vertical plane from supports which are at the same height. The spring, of stiffness  $k$ , is attached at  $l_1$  from each point of support and is unstressed when the angles of swing  $\theta_1$  and  $\theta_2$  are both zero. There is no damper.

Only the linear behaviour is considered, i.e. the amplitudes are taken to be small enough to assume that  $\sin \theta_1 \simeq \theta_1$  and that  $\sin \theta_2 \simeq \theta_2$ . The equations of motion for the two pendulums may then be written

$$ml^2\ddot{\theta}_1 + mgl\theta_1 + kl_1^2(\theta_1 - \theta_2) = 0 \quad (10.1)$$

$$ml^2\ddot{\theta}_2 + mgl\theta_2 + kl_1^2(\theta_2 - \theta_1) = 0 \quad (10.2)$$



This is a pair of simultaneous second-order homogeneous equations. For convenience we introduce the following:

$$\theta_1 = p + q; \quad \theta_2 = p - q \quad (10.3)$$

Equations (10.1) and (10.2) may now be written in terms of  $p$  and  $q$  and, after considerable manipulation, we obtain the following independent solutions for  $\theta_1$  and  $\theta_2$ :

$$\theta_1 = \bar{p} \cos(b_1 t + \psi_1) + \bar{q} \cos(b_2 t + \psi_2) \quad (10.4)$$

$$\theta_2 = \bar{p} \cos(b_1 t + \psi_1) - \bar{q} \cos(b_2 t + \psi_2) \quad (10.5)$$

where  $\bar{p}$  and  $\bar{q}$  are the amplitudes of  $p$  and  $q$  respectively,  $b_1$  and  $\psi_1$  are associated with the motion  $p$  and likewise  $b_2$  and  $\psi_2$  with the motion  $q$ ;  $b_1$  and  $b_2$  are in fact given by

$$b_1 = (g/l)^{\frac{1}{2}} \quad (10.6)$$

$$b_2 = \{(mgl + 2kl_1^2)/ml^2\}^{\frac{1}{2}} \quad (10.7)$$

In any solution of (10.4) and (10.5),  $\bar{p}$ ,  $\bar{q}$ ,  $\psi_1$ , and  $\psi_2$  depend on the initial conditions. We shall consider several special cases.

- (a) At  $t = 0$ , suppose that  $\theta_1 = \theta_2 = A$ ,  $\dot{\theta}_1 = \dot{\theta}_2 = 0$ . Substitution in (10.4) and (10.5) and their derivatives results in  $\psi_1 = \psi_2 = 0$ ,  $\bar{p} = A$  and  $\bar{q} = 0$ . Hence

$$\theta_1 = \theta_2 = A \cos b_1 t \quad (10.8)$$

Equation (10.8) describes the first principal mode of the system, in which the two pendulums have exactly the same motion. The frequency is determined by (10.6) which does not contain  $k$ . In fact the spring remains undeflected during the motion, each pendulum moving independently under gravity as if the spring was not present.

- (b) At  $t = 0$ , suppose that  $\theta_1 = A$ ,  $\theta_2 = -A$ ,  $\dot{\theta}_1 = \dot{\theta}_2 = 0$ . Similar substitution results in  $\psi_1 = \psi_2 = 0$ ,  $\bar{p} = 0$  and  $\bar{q} = A$ . Hence

$$\left. \begin{aligned} \theta_1 &= A \cos b_2 t \\ \theta_2 &= -A \cos b_2 t \end{aligned} \right\} \quad (10.9)$$

Now the two pendulums move in anti-phase but otherwise similarly at a higher frequency as given by (10.7). This is the second principal mode, the spring deflecting so that its mid-point remains stationary. For large  $k$  or  $l_1$ ,  $b_2$  is considerably greater than  $b_1$  and we say that the coupling is strong. For small  $k$  or  $l_1$ ,  $b_2$  is slightly greater than  $b_1$  and we refer to the coupling as being weak.

We have an infinite number of further choices of initial conditions, all of which result in more complex modes than the above, modes which combine oscillations of both frequencies  $b_1/2\pi$  and  $b_2/2\pi$ . We choose a third special case.

(c) At  $t = 0$ , suppose  $\theta_2 = A$ ,  $\theta_1 = \dot{\theta}_1 = \dot{\theta}_2 = 0$ . Similar substitution results in  $\psi_1 = \psi_2 = 0$ ,  $\bar{p} = \frac{1}{2}A$  and  $\bar{q} = -\frac{1}{2}A$ . Hence

$$\theta_1 = -\frac{1}{2}A(\cos b_2 t - \cos b_1 t) \quad (10.10)$$

$$\theta_2 = \frac{1}{2}A(\cos b_2 t + \cos b_1 t) \quad (10.11)$$

which may be written as

$$\theta_1 = \{A \sin \frac{1}{2}(b_2 - b_1)t\} \sin \frac{1}{2}(b_2 + b_1)t \quad (10.12)$$

$$\theta_2 = \{A \cos \frac{1}{2}(b_2 - b_1)t\} \cos \frac{1}{2}(b_2 + b_1)t \quad (10.13)$$

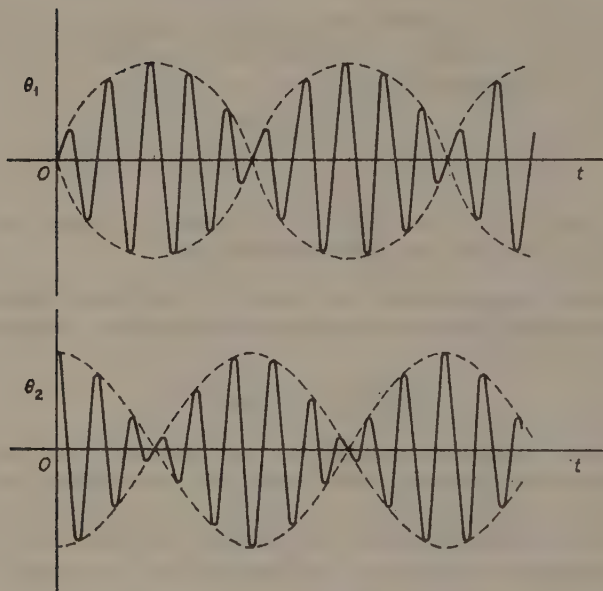


FIGURE 10.2 The phenomenon of beating.

We can translate equation (10.12) as meaning an oscillation of frequency mid-way between the principal mode frequencies, having an amplitude which varies sinusoidally. For a weak coupling, the variation of amplitude is slow. The motion is illustrated in Figure 10.2 (upper part) and is an example of beating. The period at which the beat recurs is  $2\pi/(b_2 - b_1)$  and hence the beat frequency is  $(b_2 - b_1)/2\pi$ .

Beating becomes evident whenever a structure is simultaneously subjected to two vibrations of similar frequency. For the special case above, where the two vibrations are of the same amplitude, see equation (10.10), the resulting amplitude becomes zero once every beat period.

We note that, for our present system, the two pendulums vibrate in the same manner, see (10.12) and (10.13), except that they beat alternately;

see Figure 10.2. Being a conservative system, the total energy remains constant. As the vibration of one pendulum dies away, that of the other builds up due to the transfer of energy from one part of the system to the other *via* the spring.

## Experimental Details

It is desirable first to match a pair of pendulums, about 80 cm long, and to ensure that each is suspended in bearings as free from friction as possible. A spring should be chosen and fitted such that  $2kl_1^2$  is between 0.25 and 0.35 of  $mg/l$  to provide a weak coupling. To ensure that the spring retains the same stiffness in compression as in tension, it should be made with a small number of turns of large diameter and anchored to the pendula in bearings free from friction and from backlash. Of course the spring should be unstressed when the system is in equilibrium.

Remove the spring and set the separate pendulums in motion in phase with each other with a similar amplitude not exceeding  $10^\circ$ . Check that they remain in phase over a long period; otherwise lengthen one of the pendulums accordingly. Also check that both decay in amplitude at about the same rate; it is desirable that this rate of decay is as small as possible though it cannot be reduced to zero in practice because of friction and windage.

Re-fit the coupling spring and check that it is unstressed when both pendulums hang freely. Practise setting the system in motion in its principal modes; this is not a simple matter because of the special nature of the modes. Measure the two periods over a large number of cycles and calculate  $b_1$  and  $b_2$ .

Now set the system to beat. This is comparatively simple since it is necessary only to release one pendulum from a displaced position at the same time as the other is released from its equilibrium position. Measure the beat frequency and check its relationship to  $b_1$  and  $b_2$ . Measure the frequency of swing of each pendulum and check whether this is given by the mean of  $b_1$  and  $b_2$ . Study carefully the overall motion of the system and check that the pendulums beat alternately. Also check whether the amplitude of each becomes zero during each beat period; if not, you have not started the motion precisely according to the conditions stated in (c) above. Check that the pendulums swing  $90^\circ$  out of phase with each other, i.e. that one is at maximum displacement when the other passes through its equilibrium position, as suggested by equations (10.12) and (10.13) and by Figure 10.2.

Now set the system in motion without attempting to impose any special initial conditions. In general you should still find that each pendulum beats but that the amplitude of the beat no longer reduces to zero.

## Discussion

Check that you are able to write down equations (10.1) and (10.2), and that you can obtain (10.6), (10.7) and (10.8) to (10.13).

Describe the ease or otherwise of initiating the various kinds of motion

called for in the procedure; what conclusions do you draw from your experience?

To what extent did frictional effects make the experiment difficult to carry out or the various frequency components difficult to measure? Were you able to assign causes to the various ways in which the experimental behaviour departed from the theory?

Describe examples of beating which you have experienced, e.g. (a) the vibration of a diesel railcar when stationary with the engine idling, (b) the motion of the floor of the turbine hall of a power station, (c) piano tuning.

Analyse the process of energy transfer during beating between the two pendulums of the system you have tested; you should start with an expression for the energy in terms of  $A$ ,  $g$  and the system parameters.

## Shaft Whirling

Whenever a shaft to which rotors are attached is caused to rotate, it is found that whirling occurs at a certain speed or speeds however well the system is balanced. This means that the shaft has deflected and rotates in its bent form. Often whirling does not occur within the normal operating speed range of a system, but the phenomenon is common whenever a fairly flexible shaft and/or several heavy rotors are involved, e.g. turbine machinery. Because of the excessive stresses involved, a knowledge of the whirling speeds of a system is essential in order that such speeds are avoided when the system is operated.

This experiment investigates the phenomenon for a system with one degree of freedom, and shows how it is related to the transverse vibration of the same system.

### Theory

First consider the free transverse vibration of a simply-supported uniform, light, straight beam, of length  $l$ , to which a single concentrated body, of mass  $m$ , is attached at distance  $p$  from one end, as in Figure 11.1.

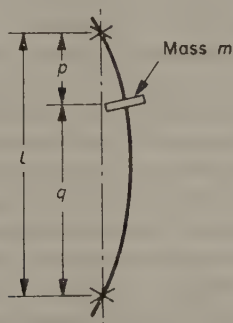


FIGURE 11.1 Transverse vibration of a beam.

Elementary bending theory (see Experiment 21) informs us that the force  $F$  required at the body to deflect the body by  $\delta$  is given by

$$F = 3EI\delta/(pq)^2 \quad (11.1)$$



where  $E$  and  $I$  are respectively Young's modulus for the beam material and the relevant second moment of area of the beam section. Hence, in transverse vibration, the beam may be assumed to act as a simple spring of stiffness  $k$  given by

$$k = F/\delta = 3EI/(pq)^2 \quad (11.2)$$

By comparison with equations (6.6) and (6.7), the frequency of free transverse vibrations is given by

$$\frac{b_n}{2\pi} = \frac{(k/m)^{\frac{1}{2}}}{2\pi}$$

where

$$b_n = \frac{(3EI/m)^{\frac{1}{2}}}{pq} \quad (11.3)$$

Note that we have ignored damping from any cause and beam deflection due to shear; also that, by neglecting the mass of the beam, we obtain only one mode of vibration. Clearly, as the body is moved along the beam, the

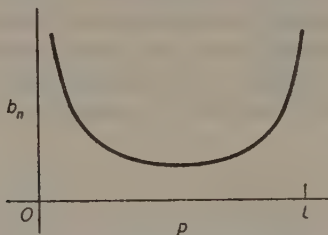


FIGURE 11.2 Variation of natural frequency with the position of the body.

natural frequency changes, being a minimum when the body is sited mid-way between the ends; this variation of frequency is illustrated in Figure 11.2. We have ignored the tilting of the body when sited away from the mid-point.

Now consider a uniform, light, circular shaft of length  $l$ , having the same  $E$  and  $I$  as above, supported freely in self-aligning bearings at its ends, as in Figure 11.3. A disc of mass  $m$  is firmly attached to the shaft at distance  $p$  from one bearing, and the whole is rotating at angular speed  $\omega$ . Figure 11.3 also shows a view in the direction from one bearing to the other, in which  $O$  is the centre of rotation (the centre-line of the bearings),  $A$  is the centre of the deflected shaft (the geometrical centre of the disc) and  $C$  is the centre of mass of the disc. The distance  $OA$  is  $r$  and the distance  $AC$  is the eccentricity  $e$ . In practice  $e$  is often very small but it can never be assumed to be zero; in general  $AC$  is not in line with  $OA$ . The configuration  $OAC$  remains fixed during rotation and the shaft is said to whirl; although there is no change in the deflection of the beam, nevertheless it is convenient to assume that some aerodynamic damping force exists and, furthermore, to assume that this acts radially inwards, i.e. in the same direction as the force due to the beam stiffness in bending.



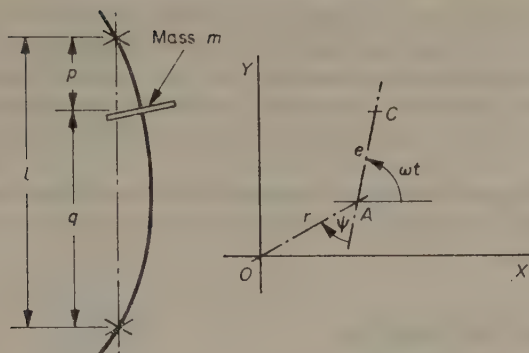


FIGURE 11.3 Whirling of a shaft.

Taking the co-ordinates of  $A$  as  $x, y$ , we may write the equations of motion for the displacements of the body in the  $X$  and  $Y$  directions as follows:

$$\left. \begin{aligned} m\mathbf{D}^2(x + e \cos \omega t) + c\mathbf{D}x + kx &= 0 \\ m\mathbf{D}^2(y + e \sin \omega t) + c\mathbf{D}y + ky &= 0 \end{aligned} \right\} \quad (11.4)$$

where  $c$  is the 'damping coefficient' and  $\mathbf{D}$  is the differential operator  $d/dt$ . The solutions of the above in the steady state are

$$\left. \begin{aligned} x &= r \cos(\omega t + \psi) \\ y &= r \sin(\omega t + \psi) \end{aligned} \right\} \quad (11.5)$$

$$\left. \begin{aligned} \text{where} \quad r &= e\lambda^2 / \{(1 - \lambda^2)^2 + 4\zeta^2\lambda^2\}^{\frac{1}{2}} \\ \text{and} \quad \psi &= -\arctan [2\zeta\lambda / (1 - \lambda^2)] \end{aligned} \right\} \quad (11.6)$$

where  $\lambda = \omega/b_n$  and  $\zeta = c/2(mk)^{\frac{1}{2}}$ , these symbols having been introduced in Experiment 9.

Ignoring the damping, the shaft deflection at the body,  $r$ , becomes  $e\lambda^2/(1 - \lambda^2)$ . This shows that when  $\omega = b_n$ , i.e. when  $\lambda = 1$ ,  $r$  is infinite. This is the condition which must be avoided in practice to prevent violent deflection and sudden fracture of the shaft. The *critical speed* is  $b_n/2\pi$  and is identical to the frequency of free transverse vibrations of the shaft. The phase angle  $\psi$  is zero when  $\lambda < 1$  and  $\pi$  when  $\lambda > 1$ ; this means that  $O, A$  and  $C$  are in line when damping is absent. Below the critical speed,  $A$  is between  $O$  and  $C$ , and above the critical speed  $C$  is between  $O$  and  $A$ . For  $\lambda > 1$ ,  $C$  approaches  $O$  more nearly as the speed is increased, which explains the smoothness with which a shaft runs above its critical speed.

The critical speed varies with the position of the body along the shaft in the same manner as the transverse mode frequency, as shown in Figure 11.2.

When damping is not ignored, it is seen that  $\psi \rightarrow 0$  for  $\lambda \rightarrow 0$  and that  $\psi$  increases in magnitude gradually to  $\frac{1}{2}\pi$  as  $\lambda$  is increased to unity. For  $\lambda > 1$ , the magnitude of  $\psi$  increases further and reaches  $\pi$  at  $\lambda = \infty$ .

In the above analysis, we have ignored shear deflection, the mass of the shaft and the gyroscopic effect (see Experiment 12) due to the tilt of the disc when situated away from the mid-point of the shaft. The latter increases or decreases the critical speed depending on whether the gyroscopic precession is in the same or opposite direction compared with the direction of rotation of the shaft.

It must be appreciated that when more than one disc is attached to the shaft and/or when the shaft mass cannot be ignored, there will be more than one critical speed.

## Experimental Details

A suitable apparatus is shown in Figure 11.4. This utilizes a steel shaft, of diameter 1 cm, supported horizontally in two spherical self-aligning bearings 80 cm apart. A pair of guard rings is fitted to prevent excessive deflection of the shaft. A disc, of diameter 10 cm and mass 1.2 kg, is fitted with a collar to enable it to be fixed at any point along the shaft. These values result in a natural transverse mode frequency, by equation (11.3), of about 14 Hz when the disc is situated at the mid-point of the shaft.

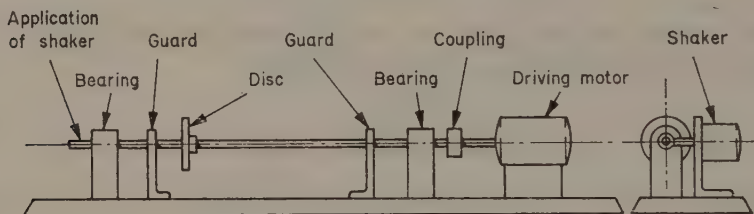


FIGURE 11.4 Test apparatus.

For whirling tests, one end of the shaft is driven, through a flexible coupling, by a variable-speed electric motor having a maximum speed of 2000 rev/min. A radial line marked on the disc enables a stroboscope to be used to measure the shaft speed.

For transverse vibration tests, an electromagnetic shaker is used to oscillate the shaft horizontally at a point close to one of the bearings. The shaker is driven by a power oscillator, the combination being capable of providing a maximum force amplitude of 10 N, the displacement amplitude being restricted to 2 mm, over a frequency range from 5 to 10 000 Hz; the upper end of this range is not required in the test.

With the shaker disconnected, fix the disc mid-way along the shaft and start the electric motor. Slowly increase the motor speed until the critical speed is reached, i.e. until the deflection reaches a maximum (damping provided by the bearings should obviate excessive deflection). Increase the speed beyond critical and note the smooth running of the shaft. Return to the critical speed and measure this by means of the stroboscope.

Fix the disc at a minimum of ten different measured positions along the shaft and find the critical speed in each case.

Connect the shaker, return the disc to mid-way along the shaft and apply a small-amplitude force at the lowest possible frequency. Slowly increase the frequency until resonance is obtained, i.e. until the natural transverse mode is excited. Note the frequency on the calibrated dial of the oscillator. Repeat for the same positions of the disc as used in the whirling tests.

Calculate  $b_n/2\pi$ , using equation (11.3), for the range of values of  $p$  used in the tests.

Plot the theoretical frequency against distance of the disc along the shaft. Also plot the critical frequency values found in the whirling tests and the natural frequency values found in the transverse vibration tests to the same axes.

## Discussion

Compare the three curves you have plotted and discuss the discrepancies between them, taking into account the following:

- (a) mass of the shaft,
- (b) shear deflection of the shaft,
- (c) damping of the motion,
- (d) twisting of the disc in transverse vibration, and
- (e) gyroscopic effect in whirling.

## Simple Gyroscope

The precessional behaviour of a gyroscope, as described in an analytical treatment, is somewhat surprising when met for the first time. It is therefore particularly valuable to examine this behaviour in the laboratory.

### Theory

Referring to Figure 12.1, consider a thin circular disc attached to a shaft lying in the axis  $Z_1Z_2$ . The instantaneous plane of rotation of the disc is

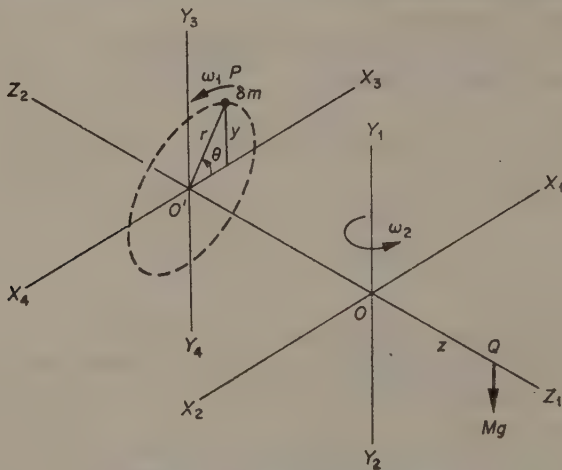


FIGURE 12.1 Gyroscopic precession.

$X_3O'Y_3$  and the disc rotates at uniform speed  $\omega_1$  in the direction indicated. At the same time the shaft  $Z_1Z_2$  rotates about some vertical axis  $Y_1Y_2$  at uniform speed  $\omega_2$  in the direction shown; by this means the disc is said to *precess*.

Consider a particle  $P$  in the disc, of mass  $\delta m$ , rotating about  $O'$  at radius  $r$ . At some instant,  $O'P$  makes an angle  $\theta$  with  $O'X_3$ . The velocity  $\dot{x}$  of  $P$  relative to  $O'$  in the direction  $X_3X_4$  is given by

$$\dot{x} = \omega_1 r \sin \theta$$

But  $Z_1Z_2$  is rotating about  $Y_1Y_2$  at speed  $\omega_2$ ; hence

$$\text{Coriolis acceleration of } P = 2\omega_2 (\omega_1 r \sin \theta) = 2\omega_1\omega_2 y$$

This is in the direction  $Z_2Z_1$ . It follows that

$$\text{Inertia force on } P = 2\omega_1\omega_2 \delta m y$$

which is also in the direction  $Z_2Z_1$ . This force has a clockwise torque about  $X_2X_1$  given by

$$\text{Inertia torque} = 2\omega_1\omega_2 \delta m y^2$$

For the entire disc, we may write

$$\begin{aligned} \text{Total inertia torque} &= 2\omega_1\omega_2 \Sigma \delta m y^2 \\ &= 2\omega_1\omega_2 I_x \end{aligned}$$

where  $I_x$  is the moment of inertia of the disc about its diameter  $X_3X_4$ . But  $I_x = \frac{1}{2}I$ , where  $I$  is the polar moment of inertia about  $Z_1Z_2$ . Hence

$$\text{Total inertia torque} = \omega_1\omega_2 I \quad (12.1)$$

Suppose that the shaft  $Z_1Z_2$  is supported freely at  $O$ ; then the above torque can be provided by hanging a body of mass  $M$  at  $Q$ , distant  $z$  from  $O$ , such that

$$Mgz = C = \omega_1\omega_2 I \quad (12.2)$$

The above analysis shows that when a couple  $C$  is applied to the system, it does not turn about the axis of the couple but about an axis which is perpendicular to both the couple axis and the axis of spin of the disc. Of course, there is a rule connecting the directions of  $\omega_1$ ,  $\omega_2$  and  $C$ ; a reversal of couple direction requires the reversal *either* of  $\omega_1$  *or* of  $\omega_2$  and the couple can remain unchanged if  $\omega_1$  and  $\omega_2$  *both* change. Note that  $Y_1Y_2$  can be any vertical axis including  $Y_3Y_4$ .

For a full examination of gyroscopic precession, the reader is referred to Arnold and Maunder [1].

## Experimental Details

Suitable apparatus is shown in Figure 12.2. A straight bar supports an electric motor driving a circular disc at one end and a balance body at the other end. The speed of the motor can be varied in the range 1000 to 6000 rev/min. The bar is supported at its centre of mass on a rigid stand by means of a cup-and-cone pivot bearing. Current is fed to the motor through a mercury cup surrounding the bearing into which dips a stainless steel pin attached to the bar; the current is returned *via* the pivot bearing.

Grooves are cut in the bar at 2.5, 5.0, 7.5, etc. cm from the pivot to locate a hanger for supporting one or more small bodies. The gravitational force on the body, together with the pivot reaction, provides the applied couple  $C$ . A stroboscope is used to illuminate the disc in order to measure  $\omega_1$ . The



bar precesses slowly about its pivot, and to measure  $\omega_2$  it is only necessary to provide means for assessing accurately the time for a few complete revolutions.

Set the motor speed control at maximum and allow several minutes for the speed  $\omega_1$  to settle. Hang a small body in a groove near the pivot and

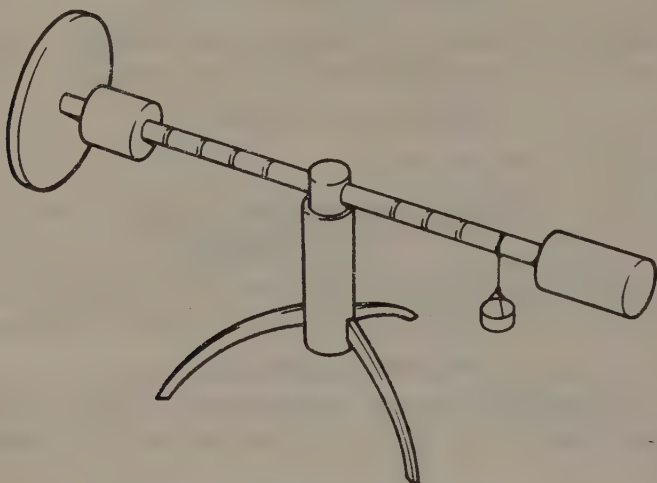


FIGURE 12.2 Simple gyroscope apparatus.

observe the slow precession of the bar. Now hang the body on the other side of the pivot and note that the precession reverses its direction. Should the bar gradually assume an angle of inclination to the horizontal, it must be returned to the horizontal by applying light finger pressure *horizontally* on the appropriate side of the pivot. Care should be taken not to set the bar into oscillation about the pivot.

For the test proper, run the disc at about four different values of  $\omega_1$ . In each case, apply various couples in both directions to the bar by using the small bodies of known mass. In a typical apparatus having a disc of inertia about  $2 \times 10^{-3} \text{ kg m}^2$ , a suitable maximum value for the applied couple  $C$  is  $0.7 \text{ N m}$ . Measure  $\omega_2$  and check  $\omega_1$ .

Plot  $\omega_2$  against  $C$  for each  $\omega_1$ . If  $I$  is known, draw the theoretical curves on the same diagram by using equation (12.2).

## Discussion

Compare the test points with the theoretical curves and try to explain any discrepancies.

What is the effect of the small frictional drag at the pivot? Will this have affected the accuracy of the experiment?

## Reference

1 .ARNOLD, R. N., and MAUNDER, L., *Gyrodynamics and Its Engineering Applications*, Academic Press, 1961.



## First-Order Process Lag

This very common dynamic process lag is met in many branches of engineering [1]. A knowledge of its behaviour is essential in the application of linear control system theory.

### Theory

A process having an input  $\theta_1$  and an output  $\theta_2$ , both functions of time and preferably having the same dimensions, may obey the following linear equation:

$$\tau \dot{\theta}_2 + \theta_2 = \theta_1 \quad (13.1)$$

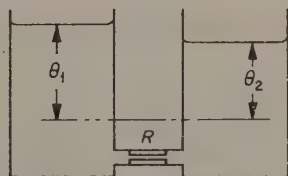


FIGURE 13.1 Liquid level process.

where  $\tau$  has the dimensions of time and is called the *time constant*. Equation (13.1) may be expressed more conveniently in terms of the differential operator  $\mathbf{D}$ ; thus

$$\theta_2 = \left( \frac{1}{1 + \tau \mathbf{D}} \right) \theta_1 = T(\mathbf{D})\theta_1 \quad (13.2)$$

where the so-called *transfer operator*  $T(\mathbf{D})$  relates the output to the input. The transfer operator in this case is  $1/(1 + \tau \mathbf{D})$  and is known as the *exponential lag* or the *first-order lag*.

The process chosen for experiment is shown in Figure 13.1. Incompressible liquid is contained in a pair of tanks connected by a restriction. The gravitational head  $\theta_1$  in the left-hand tank is regarded as the input, and likewise  $\theta_2$  is the output. It is assumed that the flow through the restriction is laminar.

Hence, if  $I$  is the volume flow-rate and  $R$  is the resistance to flow, we may write

$$\theta_1 - \theta_2 = RI \quad (13.3)$$

Thus  $R$  is a property of the restriction, meaning the volume flow-rate/pressure drop, and depends on (a) the physical dimensions of the restriction and (b) the properties of the liquid. The flow through the restriction must equal the flow into the right-hand tank; hence

$$I = CD\theta_2 \quad (13.4)$$

where the capacitance of the process  $C$  is in this case simply the cross-sectional area of the right-hand tank.

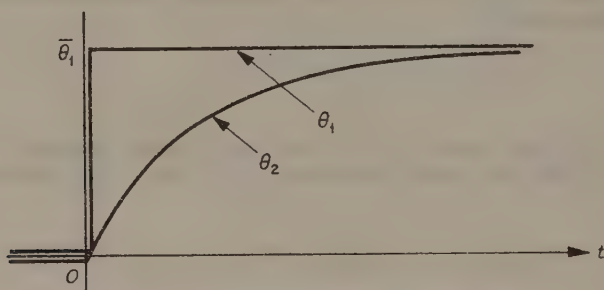


FIGURE 13.2 Step response of first-order lag.

Eliminating  $I$  between (13.3) and (13.4) and putting  $\tau$  for  $CR$ , we obtain (13.2). Hence the process is an example of a first-order lag.

It should be noticed that the cross-sectional area of the left-hand tank does not enter the analysis. However, it is essential for  $C$  to be constant throughout the right-hand tank.

The apparatus available for test lends itself to the measurement of the transient behaviour of the process, in particular the transient response in  $\theta_2$  to a step change in  $\theta_1$ . It is convenient to measure  $\theta_1$  and  $\theta_2$  from some datum level above the restriction to permit of negative values occurring. Suppose that initially both are zero. Now suddenly make  $\theta_1 = \bar{\theta}_1$  and keep it constant at this value. The relevant solution of (13.1) or (13.2) may be written [1]

$$\theta_2 = \bar{\theta}_1(1 - e^{-t/\tau}) \quad (13.5)$$

and is illustrated in Figure 13.2 together with the step in  $\theta_1$ .

Eventually  $\theta_2$  becomes equal to  $\theta_1$  but in general it lags behind  $\theta_1$ ; it approaches  $\theta_1$  exponentially. This explains the name 'exponential lag'. Two properties of this response curve are worth noting. The initial slope is  $\bar{\theta}_1/\tau$  and  $\theta_2$  reaches  $0.865 \bar{\theta}_1$  in time  $2\tau$ .

In practice it is unlikely that the flow through a restriction will be laminar except at very low rate. It follows that we cannot expect the linear analysis above to be obeyed precisely in the test apparatus where a commercial valve is employed. The value of the experiment lies in noting the differences in behaviour of a real process compared with the behaviour predicted by the simple theory.

## Experimental Details

Two sections of Perspex cylindrical tube of 8 cm diameter are mounted with their axes vertical as shown in Figure 13.3. Cylinder *A* is closed at both

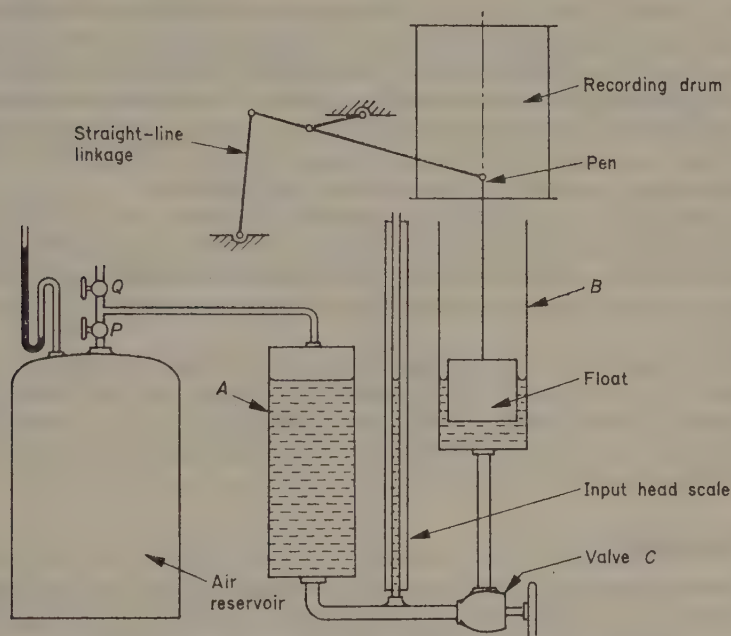


FIGURE 13.3 Apparatus for process-lag response tests.

ends but cylinder *B* is open at the top. The cylinders are connected by a pipe of diameter 1.5 cm containing a commercial screw-down valve *C*. A manometer with a scale is fitted to the pipe on the left-hand side of *C*. The assembly is filled with water to the level indicated.

A hollow brass float in *B* is connected to a straight-line linkage to move a pen vertically over a recording chart fitted to a drum which is driven at a uniform speed about a vertical axis by a small electric motor.

The effective liquid head to the left of *C* is adjusted by admitting air under pressure into *A*. The air is supplied from a reservoir which is pressurized by a hand pump to about  $15 \times 10^3 \text{ N/m}^2$ . Air is admitted through the

needle regulating valve  $P$  and exhausted to atmosphere through a similar valve  $Q$ .

With all the valves open, check that the water level is at an appropriate point on the manometer scale. Check the recording drum drive and measure the paper speed, which should be between 20 and 25 cm/min. Close valve  $P$  and pressurize the air reservoir.

Set the screw-down valve  $C$  at half-turn open. Close valve  $Q$ . Start the drum and, when the pen has traversed about 2 cm, gently open valve  $P$  and regulate it continuously so as to maintain the level in the manometer at 10 cm above the starting level. This will cause the float to rise in cylinder  $B$ . As the float motion terminates it will again be necessary to close valve  $P$  completely. Stop the drum.

With  $P$  closed, start the drum and gently open valve  $Q$  and regulate it so as to maintain the manometer level at its original reading. At the termination of this second response test, valve  $Q$  will be open. Again stop the drum.

You have tested the process comprising  $B$  and  $C$  with forward and reverse steps of input head. You have recorded curves of output head change against time. Carry out similar tests for step changes of 2, 4, 6, 8, and 10 cm, with  $C$  one-quarter, one-half, three-quarters and one turn open.

For each part of a selection of recordings, determine  $\tau$  by measuring (a) the initial slope and (b) the time to reach 0.865 of the step. Under certain circumstances these will not be the same because of non-linear behaviour. Construct a true exponential curve through the origin based on the  $\tau$ -value found in (b).

Now take the record for the 10 cm step when the valve was one turn open. Measure  $(\theta_1 - \theta_2)$  and  $D\theta_2$  for a selection of points on each curve. Plot logarithms of these values. Note that, in practice,  $(\theta_1 - \theta_2)$  varies with  $(D\theta_2)^n$  where  $n$  is a number other than unity. From your graph note how  $n$  varies with  $(\theta_1 - \theta_2)$ .

## Discussion

How does the real process lag differ in behaviour from a linear exponential lag? What changes occur in the apparent 'time constant' of the lag as the magnitude of the step is altered? How does the lag vary with valve opening? How does the direction of motion through the valve affect the lag?

What restriction must be placed upon input changes in order that the transfer operator given by equation (13.2) may represent the process?

## Reference

1. WEBB, C. R., *Automatic Control*, McGraw-Hill, 1964.

# 14

## Position Control System

Following the last test which investigated the behaviour of a simple transfer lag, this experiment deals with a complete closed-loop control system, arranged to control the angular position of a shaft. We start with a basic proportional system and then add conventional compensation to improve the performance.

### Theory

Let  $\theta_o$  be the angular position of a shaft to which a disc of inertia  $I$  is attached, as in Figure 14.1. The motion of the shaft is resisted by viscous friction of

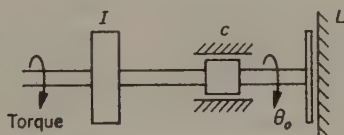


FIGURE 14.1 Physical system to be controlled.

coefficient  $c$  and by an external load torque  $L$ . In the basic system, torque is applied to the shaft by an amplifier and servo motor; this torque is propor-

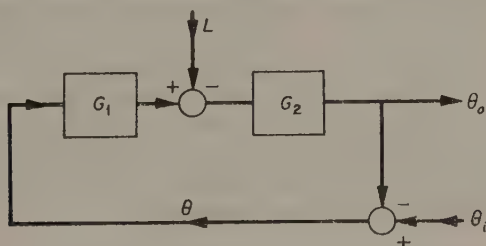


FIGURE 14.2 Basic block diagram.

tional to the error  $\theta$  between the desired position  $\theta_i$  and the actual position  $\theta_o$ . The block diagram is shown in Figure 14.2, where the transfer operator



represents the controller (amplifier) and servo motor and  $G_2$  the process parameters  $I$  and  $c$ . The following equations apply [1]:

$$k\theta - L = (ID^2 + cD)\theta_o \quad (14.1)$$

$$\theta = \theta_i - \theta_o \quad (14.2)$$

where  $k$  is the proportional control coefficient, i.e. (input torque)/(position error).

Eliminating  $\theta_o$  from (14.1) and (14.2), we obtain

$$(ID^2 + cD + k)\theta = (ID^2 + cD)\theta_i + L \quad (14.3)$$

which gives the error as a function of  $\theta_i$  and  $L$ . The coefficient of  $\theta$  shows the system to be mathematically similar to the free and forced simple vibrating systems considered earlier. The quantities defined by equation (9.2) apply here also; we restrict our attention to the underdamped case, i.e.  $\zeta < 1$ . Whenever a disturbance is made in  $\theta_i$  or in  $L$ , the system response is damped oscillatory as given by equation (6.5).

We are also concerned with the error which persists after the transient has faded, i.e. the steady-state error  $\theta_{ss}$ . By equation (14.3), for constant  $L$  and  $\theta_i$ , the steady-state error is given by

$$\theta_{ss} = L/k \quad (14.4)$$

Hence, in the absence of external load,  $\theta_{ss}$  is zero. Note how the controller (amplifier) gain, which contributes to  $k$ , affects the value of  $\theta_{ss}$ .

When the desired *speed* is suddenly changed from zero to  $D\theta_i$  and held uniform, i.e. a ramp input function is applied, the steady-state error, now called the *velocity lag*, is given by

$$\theta_{ss} = (c/k)D\theta_i + L/k \quad (14.5)$$

Clearly, steady-state errors can be reduced by increasing  $k$ , and the consequent increase in the response frequency  $b/2\pi$  is beneficial. However,  $\zeta$  becomes smaller which is unstabilizing, and hence the simple system cannot be stable without exhibiting velocity lag. An equally important drawback of the simple system is the inherent load imposed on the servo motor by the viscous drag but, of course, the latter is required for stability.

We first seek a means of artificially replacing the viscous drag which will permit the use of a less powerful controller and servo motor but without loss of stability. We measure the speed  $D\theta_o$  of the output shaft and apply an additional torque  $-k_1 D\theta_o$  to the process; this is called *output-velocity feedback* and results in (14.5) being modified to

$$\theta_{ss} = [(c + k_1)/k]D\theta_i + L/k \quad (14.6)$$

The parameter  $c$  is no longer required for stability since  $k_1$  takes over this function. We may therefore specify bearings exerting negligible resistance and consequently a less powerful servo motor.



We now add a further path to the system to reduce the velocity lag. Another additional torque,  $+k_1 D\theta_i$ , called *input-velocity feedforward* (because of its positive sign), is applied to the process. Omitting  $c$  altogether, the steady-state error now reduces to

$$\theta_{ss} = L/k \quad (14.7)$$

Thus in the absence of external load, there is no velocity lag.

## Experimental Details

Small components as used in instrument servo mechanisms are employed in the apparatus described below and shown in Figure 14.3, which is one of several suitable arrangements.

A two-phase 115 V 400 Hz a.c. servo motor *A* drives the output shaft through reduction gearing, a scale on the shaft indicating  $\theta_o$ . Viscous friction

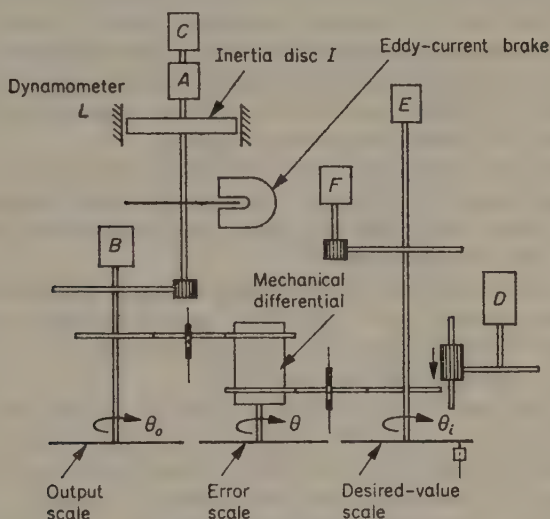


FIGURE 14.3 Layout of components of position control system.

is provided artificially by an eddy-current brake, the current through the coil, and therefore  $c$ , being adjustable. A disc is keyed to the motor shaft to provide the inertia  $I$ . For experimental purposes,  $I$  is made large deliberately to ensure a low operating frequency in the range 0.3 to 0.5 Hz. The actual position  $\theta_o$  is measured by the synchro transmitter *B* and  $D\theta_o$  by the tachogenerator *C*. A band brake acts as a dynamometer and provides the external load  $L$ .

The desired-value shaft can be turned by hand or driven at various values of uniform speed in either direction by a d.c. motor *C*. The actual position  $\theta_i$ , which is indicated on a scale, is measured by the synchro transmitter *E*, and  $D\theta_i$  is measured by the tachogenerator *F*. For convenience, a mechanical differential enables the error  $\theta$  to be indicated on a third scale.

The synchros supply an a.c. amplifier which in turn supplies the control phase of the servo-motor,  $k$  being adjustable by a knob on the amplifier. Signals from the tachogenerators also feed the amplifier, there being a separate knob to vary  $k_1$ .

The steps given below are suggested in order to demonstrate the successive improvements in the system indicated by the theoretical outline.

(a) First set up the equipment as follows:

- (i) set  $k_1$  at zero,
  - (ii) set  $k$  at maximum,
  - (iii) set  $L$  at zero,
  - (iv) declutch the drive from  $D$ , and
  - (v) switch off the eddy-current brake.
- (b) Switch on the amplifier. The equipment should operate according to equation (14.3) with  $c$  and  $L$  both equal to zero, i.e. with  $\theta_i$  constant the  $\theta_o$  and  $\theta$  shafts should oscillate continuously (hunt) because of the lack of damping. Measure the undamped natural frequency  $b_n/2\pi$ .
- (c) Switch on the eddy-current brake and set  $c$  at maximum. Apply a step in  $\theta_i$  and note the highly-damped response in  $\theta_o$  and  $\theta$ ; check that  $\theta$  returns to zero. Note also that the maximum speed of the servo motor is limited. Try several steps with smaller  $c$ .
- (d) Switch off the brake. Switch on the output-velocity feedback and set  $k_1$  to maximum. Try a step in  $\theta_i$  and note that there is a similar response to the above except that the servo motor maximum speed is much greater. Repeat with smaller  $k_1$ .
- (e) Switch off the output-velocity feedback. Apply a moderate load  $L$  at the dynamometer. Try a step in  $\theta_i$  and verify that  $L$  stabilizes the response. Note the steady-state error. For a large  $L$ , verify that the maximum speed of the motor is limited.
- (f) Re-set  $L$  to zero. Connect the drive from the motor  $D$  to the  $\theta_i$  shaft. Switch on  $D$  and adjust  $D\theta_i$  to about 1 rev/min. Note that  $\theta_o$  follows in a non-uniform manner and that  $\theta$  hunts about zero. Reverse the direction of  $D$  and check that the response is similar.
- (g) Switch on the eddy-current brake and adjust for a moderate value of  $c$ . Check that the hunting is damped out but that there is a steady velocity lag. Also observe that the servo motor can only just overcome the viscous drag at the desired speed demanded.
- (h) Switch off the eddy-current brake. Apply the output velocity feedback with moderate  $k_1$ . Observe that the rapid and stable response to the ramp demand even when  $D\theta_i$  is increased to 2 rev/min and that the velocity lag remains.
- (i) Apply input-velocity feedforward. Check that the velocity lag disappears. Reverse the direction of  $D$  and further check that the response is rapid and stable and without steady-state error.
- (j) Apply a small load  $L$  at the dynamometer. Check that this causes a velocity lag which increases with  $L$  until the servo motor is no longer able to keep up with the demanded speed.

## Discussion

Make sure that you can formulate equations (14.1) and (14.2) and that you can obtain the derived equations.

Compare the results of the various tests you have carried out with the linear theory given and try to explain any anomalies.

## Reference

1. WEBB, C. R., *Automatic Control*, McGraw-Hill, 1964.

## *Transverse Vibration of an Elastic Beam*

This experiment is concerned with the vibration of a system with an infinite number of degrees of freedom. This occurs whenever the mass is distributed instead of being concentrated at one or more points in the system. We shall confine our attention to the transverse vibration of a cantilever due solely to the mass of the cantilever itself.

### Theory

Consider a uniform slender straight beam, of length  $l$  and mass  $m$ , supported in some manner which we shall discuss later. Suppose that the beam is vibrating transversely and freely. At a distance  $x$  along the beam from some arbitrary point, let the deflection at some instant be  $y$ . Consider a section  $\delta x$  long having mass  $(m/l)\delta x$ ; this requires an accelerating force  $F$  given by

$$F = \frac{m}{l} \delta x \frac{\partial^2 y}{\partial t^2} \quad (15.1)$$

This force arises because of the change of shear force  $(\partial Q/\partial x)\delta x$ , where the shear force for simple bending deflection is given by

$$Q = -EI \frac{\partial^3 y}{\partial x^3} \quad (15.2)$$

Therefore

$$F = \frac{\partial Q}{\partial x} \delta x = -EI \frac{\partial^4 y}{\partial x^4} \delta x \quad (15.3)$$

Eliminating  $F$  from equations (15.1) and (15.3), we obtain

$$\frac{\partial^4 y}{\partial x^4} = -\frac{m}{lEI} \frac{\partial^2 y}{\partial t^2} \quad (15.4)$$

We may assume that the motion at  $x$  is simple harmonic, i.e.

$$y = \bar{y} \cos b_n t \quad (15.5)$$

where  $\bar{y}$  is the amplitude at  $x$  and  $b_n/2\pi$  is the natural frequency, damping being assumed negligible. Substituting this expression for  $y$  in equation (15.4) and simplifying we get

$$\frac{\partial^4 \bar{y}}{\partial x^4} = \frac{mb_n^2}{EI} \bar{y}$$

which, for convenience, is re-written

$$\frac{\partial^4 \bar{y}}{\partial x^4} - \alpha^4 \bar{y} = 0 \quad (15.6)$$

where

$$b_n = (\alpha l)^2 (EI/ml^3)^{1/2} \quad (15.7)$$

The solution of equation (15.6) is

$$\bar{y} = A \cos \alpha x + B \sin \alpha x + C \cosh \alpha x + D \sinh \alpha x \quad (15.8)$$

In the above equation,  $A$ ,  $B$ ,  $C$  and  $D$  are arbitrary constants depending on the end conditions of the beam. Variations are numerous: the beam can be freely supported at both ends, fixed at one end and freely supported at the other, etc. For the particular case of a uniform cantilever considered here, suppose that the origin is at the fixed end. Then, since the deflection and the slope are both zero at the fixed end we have

$$\bar{y} = 0, \quad \frac{\partial \bar{y}}{\partial x} = 0 \quad \text{at } x = 0$$

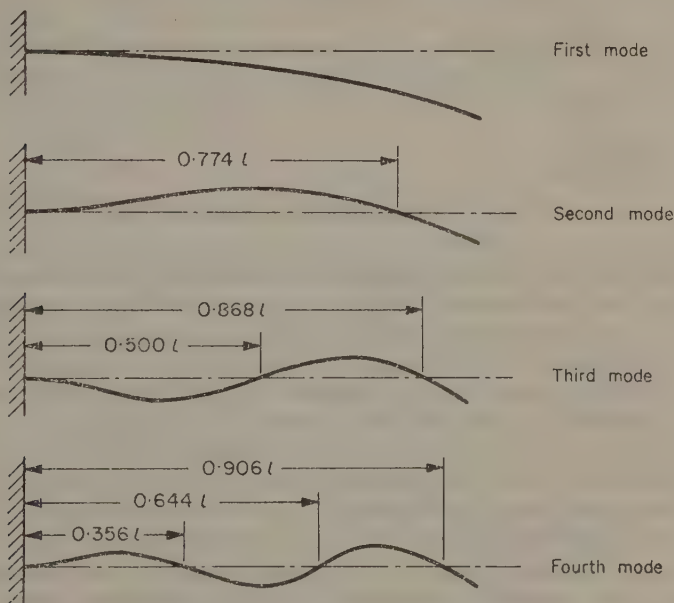


FIGURE 15.1 First four natural modes.



Also, since the bending moment and the shear force are zero at the free end, we have:

$$\frac{\partial^2 \bar{y}}{\partial x^2} = 0, \quad \frac{\partial^3 \bar{y}}{\partial x^3} = 0 \quad \text{at } x = l$$

Substituting these four conditions into equation (15.8) and its derivatives leads to the condition

$$\cos \alpha l \cosh \alpha l = -1 \quad (15.9)$$

Values of  $\alpha l$  satisfying equation (15.9) are 0.87, 4.69, 7.85, 11.0, . . . , enabling  $b_n$  for the first four modes to be found from equation (15.7). The cantilever shapes when vibrating in these modes are shown in Figure 15.1, the theoretical positions of the nodes being indicated.

### Experimental Details

The material and dimensions of the cantilever to be tested should be chosen so that the first four natural frequencies are within the range of a single exciter; also the cantilever should be sufficiently flexible to enable the displacement amplitude at the modes to be large enough to enable the mode shapes to be clearly discernable with the naked eye. A suitable test cantilever is one made of mild steel strip, of free length  $l = 1$  m, width  $b = 12.7$  mm and thickness  $d = 3.17$  mm. Such a cantilever has a density of  $7700 \text{ kg/m}^3$ , so

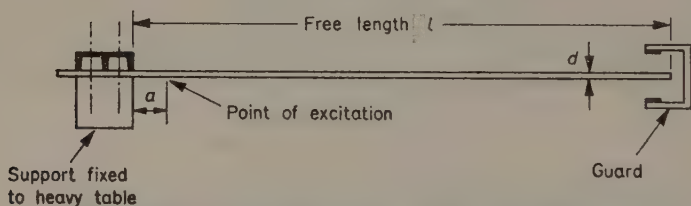


FIGURE 15.2 Arrangement of test cantilever.

that  $m = 310$  g.  $I$  about the appropriate neutral axis (parallel to the width  $b$ ) is found to be  $33.4 \text{ mm}^4$ . Taking  $E = 207 \times 10^9 \text{ N/m}^2$ , the theoretical value of  $b_n$  for the first mode may be found from equation (15.7) to be  $16.6 \text{ rad/s}$ . This corresponds to a frequency of  $2.64 \text{ Hz}$ . Similarly frequency values for the next three modes may be calculated as  $16.5$ ,  $46.3$  and  $90.7 \text{ Hz}$ .

It is convenient to support the cantilever horizontally, and the clamp must anchor the fixed end as rigidly as possible. This may be arranged so that the cantilever is free to move either in a vertical plane or in a horizontal plane; the former is preferable to facilitate visual observation, and the dimensions suggested are such that the cantilever does not deflect unduly under its own weight. Figure 15.2 illustrates the general arrangement.

A low-power source of excitation of variable frequency may take the form of an electromagnetic shaker or a simple mechanical shaker driven by an

eccentric. It is important that the excitation is applied at a point which interferes least with the free transverse motion of the cantilever, and this dictates that the distance  $a$  in Figure 15.2 is kept small compared with  $l$ . For the cantilever suggested, a suitable value for  $d$  is 5 cm and, when a positive-displacement mechanical shaker is employed, an excitation amplitude of about 0.10 mm is suitable. The eccentric may be driven by a high-speed electric motor of about 50 W with means for varying the speed sensitively from zero to 10 000 rev/min. Safety considerations demand that a guard is fitted to restrict the amplitude at the free end of the cantilever to about 2 cm.

A more elaborate means of excitation may be adopted to reduce the discrepancies between the test and theoretical mode frequencies. This uses a light inertia-type shaker fixed to the beam and driven by a flexible shaft.

To determine frequency, it is best to measure the speed of the exciting motor with, for example, a magnetic impulse counter.

The amplitudes at resonance should be sufficient to enable the nodes to be detected easily, but the assistance of a stethoscope may be found useful.

The first test suggested is to set the cantilever in free motion by hand (with the shaker removed). Is this the first mode? Check the frequency by a sufficiently accurate method.

Re-connect the shaker and slowly increase the motor speed from zero until resonance occurs at the first mode. Inherent damping should prevent the amplitude becoming excessive. Check the frequency by measuring the motor speed and compare with the value found above. Further increase the motor speed until the second mode is excited. Again measure the frequency. Estimate the position of the single node by marking the cantilever where the amplitude appears to be a minimum and by subsequent measurement when the cantilever is stationary.

Now excite the third and fourth modes and repeat the above measurements. Even for the fourth mode, the amplitude should be sufficient to detect the cantilever shape easily by eye.

## Discussion

Compare the test and theoretical values of natural frequency and the actual node positions with the theoretical positions given in Figure 15.1. Suggest reasons for the differences found.

## Vibration of a Multi-mass System

We now consider systems in which the body masses are concentrated, where the bodies are connected by elastic members assumed to be massless and where frictional damping is neglected. As in the previous experiment, we have a large number of degrees of freedom but now the number is finite. Analytical methods are available for such systems which, in many cases, reliably predict real behaviour; however, the analysis becomes increasingly tedious the greater the number of degrees of freedom. An experimental method is useful, therefore, especially when the general pattern of behaviour is known from theoretical considerations.

### Theory

Consider the torsional system shown in Figure 16.1, which consists of a light elastic shaft to which are attached five rotors. For simplicity, rotors 1 to 4 each have a moment of inertia of  $I$ ; rotor 5 has a moment of inertia of

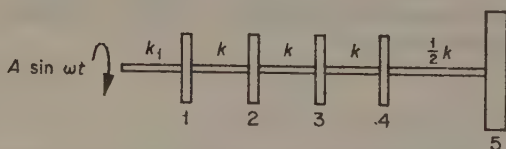


FIGURE 16.1 Multi-mass torsional system.

20  $I$ . Also, the stiffnesses of the shaft sections connecting rotors 1 to 4 are each  $k$ , while that of the section between rotors 4 and 5 is  $0.5k$ . There is a light extension shaft of stiffness  $k_1$  by means of which the system can be forced when required. Suppose that the angular displacements of the rotors are  $\theta_1, \theta_2$ , etc.

In the absence of damping and with no restraint imposed upon the extension shaft, the free motion of the system is given by a set of five equations of which the following is typical:

$$I\ddot{\theta}_2 + k(\theta_2 - \theta_3) + k(\theta_2 - \theta_1) = 0 \quad (16.1)$$

The system has four principal modes. For any of the natural frequencies

$b/2\pi$ , we may substitute  $-b^2\theta_1$  for  $\ddot{\theta}_1$ ,  $-b^2\theta_2$  for  $\ddot{\theta}_2$ , etc. to obtain a further five equations of the form

$$-k\theta_1 + (2k - Ib^2)\theta_2 - k\theta_3 = 0 \quad (16.2)$$

Equations (16.2) may be solved for  $b$  in a number of ways, all of which are tedious, to yield the following non-trivial values:

$$\left. \begin{aligned} b_1 &= (0.099 \, k/I)^{\frac{1}{2}}, & b_3 &= (2.18 \, k/I)^{\frac{1}{2}} \\ b_2 &= (0.813 \, k/I)^{\frac{1}{2}}, & b_4 &= (3.46 \, k/I)^{\frac{1}{2}} \end{aligned} \right\} \quad (16.3)$$

These give the first, second, third and fourth mode frequencies respectively.

The relationship between the angular amplitudes of the rotors depends on which mode is excited. Equations (16.2) are satisfied by the values given in Table 16.1, where the displacement at rotor 1 is taken as unity and positive.

TABLE 16.1

Displacement at rotor no.	Mode			
	<i>first</i>	<i>second</i>	<i>third</i>	<i>fourth</i>
1	1.000	1.000	1.000	1.000
2	0.904	0.187	-1.056	-2.439
3	0.707	-0.778	-0.810	2.562
4	0.457	-1.102	1.201	-1.308
5	-0.155	0.035	-0.014	0.010

A negative sign indicates where a rotor moves in anti-phase with rotor 1. Where a sign change occurs between adjacent rotors, this indicates a node in the connecting shaft; there are as many nodes as the order of the mode. We may draw the elastic curves as shown in Figure 16.2, using the values given in Table 16.1. The ordinate is angular displacement in any convenient unit. Straight lines are drawn between the plotted values since each section of shaft is assumed to twist uniformly along its length. The nodes occur where the lines cross the horizontal axis, the actual positions being found by simple proportion.

For the experiment, the same elastic material with the same cross-section should be used for each portion of shaft. The section between rotors 4 and 5 will be twice as long as each of the other sections in order that its stiffness shall be half as much. Hence, in Figure 16.2, the slope of each line is a direct measure of the maximum shear stress occurring in the section. In practice we must guard against the danger of the effect of resonance, at any of the mode frequencies, permitting excessive shear stress and thus failure of the shaft.

Now suppose that a sinusoidal displacement  $A \sin \omega t$  is imposed at the end of the extension shaft. Theoretically, in the steady state, each rotor

will oscillate at the forcing frequency  $\omega/2\pi$  with some amplitude dependent upon  $A$ ,  $\omega$ ,  $I$ ,  $k$ ,  $k_1$  (and, in general, the rotors will have different amplitudes from each other). Each rotor will move in phase or in anti-phase with the forcing function. When  $\omega = b_1, b_2$ , etc., rotor 1 will have amplitude  $A$  and

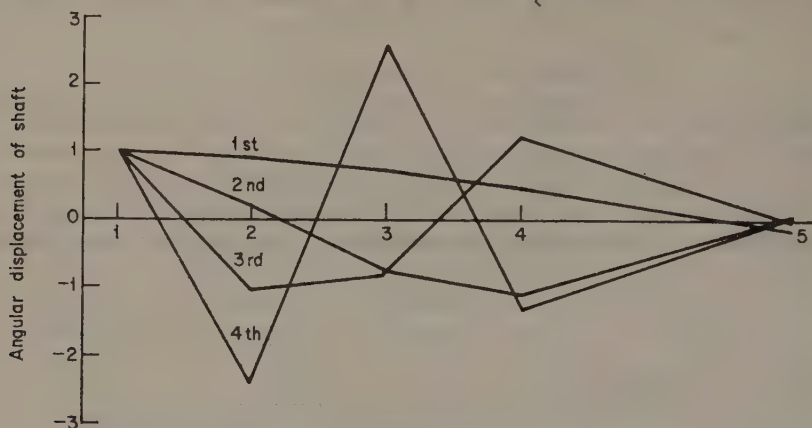


FIGURE 16.2 Elastic curves for multi-mass system.

there will be no stress in the extension shaft; the other rotors will move according to the relative values in Table 16.1. Effectively the system will be vibrating freely.

Of course, in practice there will be some frictional damping which will require a small power input to maintain any of the free modes. This will be provided by the source of the forcing function. The effect of the inherent

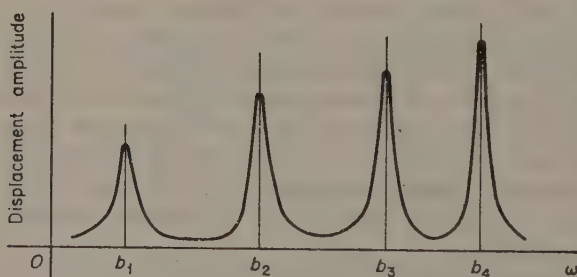


FIGURE 16.3 Forced oscillation at a rotor.

damping on the natural frequency values is likely to be small. The amplitude at each of the rotors may be expected to vary with  $\omega$  in the manner shown in Figure 16.3, rising to a peak at  $b_1, b_2$ , etc.

Were we to impose a sinusoidally-varying *torque* instead of a displacement, the amplitude at resonance would increase theoretically to infinity. There is usually insufficient damping in practice to avoid substantial oscillations of the shaft at the critical frequencies, followed by shaft failure in extreme cases.



## Experimental Details

For experimental purposes it is desirable to keep the natural frequencies as small as possible; this dictates a slender shaft which must be supported in a roller bearing close to each rotor. The general arrangement is shown diagrammatically in Figure 16.4. A steel shaft of diameter 3 mm and length 30 cm has a stiffness  $k$  of about 2.2 N m/rad. This is suitable for the sections between rotors 1 and 2, 2 and 3, 3 and 4, whilst that between 4 and 5 is made 60 cm long. The largest rotor is of steel, of diameter 23 cm and thickness 2 cm; this has a mass of about 6.5 kg and a moment of inertia  $20 I$  of about 0.042 kg m<sup>2</sup>. Corresponding smaller rotors each have a moment of inertia  $I$  of about 0.0021 kg m<sup>2</sup>. By equation (16.3), the natural frequencies should be about 1.6, 4.5, 7.5 and 9.4 Hz.

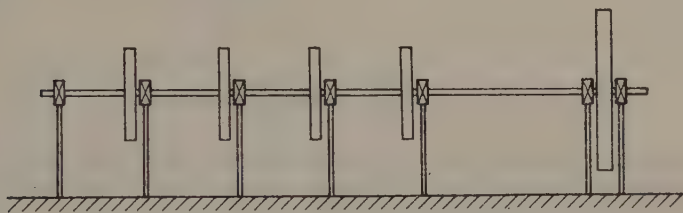


FIGURE 16.4 Arrangement of experimental system.

The other advantage of a slender shaft is that large amplitudes may be excited without overstressing the shaft. Even so, for the suggested shaft, the total twist between any pair of smaller rotors should be limited to 13° or 14°. Light pointers may be attached to each rotor to sweep over fixed scales marked over a range of  $\pm 8^\circ$ . The pointers can be illuminated by a stroboscope set to flash at *near* the frequency of oscillation, so that the pointers appear to oscillate at the beat frequency, which can be made small enough to enable the rotor amplitudes to be read from the scales. It will also be evident whether rotors are oscillating in phase or anti-phase.

An arrangement is required to turn the end of the extension shaft with simple harmonic motion with a maximum amplitude of about  $\pm 6^\circ$ . One possibility is shown in Figure 16.5, a lever of about 10 cm in length being attached to the shaft and moved *via* a long connecting rod by a crank driven by an electric motor. A simple means is required for adjusting the crank throw from 2 mm to 1 cm. Though a 0.5 kW variable-speed d.c. motor will suffice, a Velodyne (speed-controlled) motor is preferred to minimize cyclic speed fluctuations. Accurate speed measurement is essential and may be provided by a digital counter driven by a magnetic or a photo-elastic pick-up on the motor shaft.

If desired, the surface stress fluctuation at one or more of the shaft sections may be detected by a rosette of strain gauges cemented to the shaft with a suitable amplitude-modulated measuring system.

It is instructive first to find the theoretical natural frequencies from equation (16.3) and to determine the corresponding motor speeds.

With the crank throw set at minimum, the motor speed may be slowly increased until the first mode is excited. With the aid of the stroboscope, the amplitudes of the rotors may be checked. Repeat for the other modes in

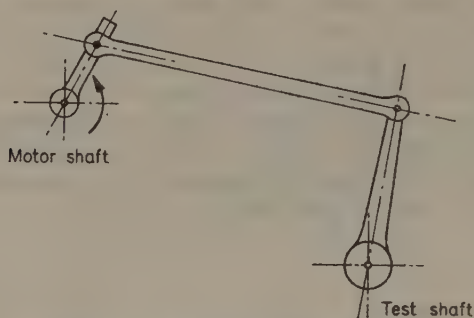


FIGURE 16.5 Means to excite the system.

succession. Use this information to determine the maximum crank throw which may be used at each mode to give the largest possible amplitudes without overstressing the shaft anywhere, and use these values in the subsequent tests.

Concentrate your attention on frequency ranges in the vicinity of the four actual critical frequencies. At each setting of the speed control, measure

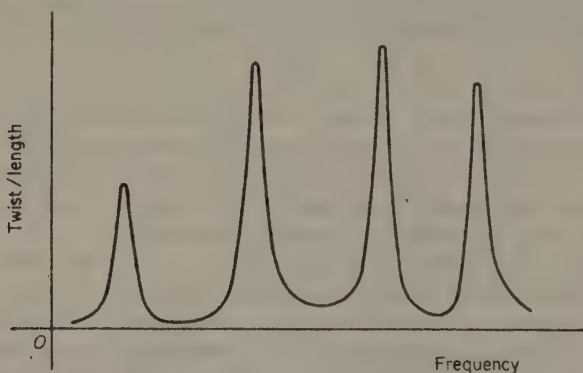


FIGURE 16.6 Twist per length in a section of shaft.

the speed and all the rotor amplitudes. For each shaft section, determine the twist per unit length and plot against frequency in the manner of Figure 16.6. Compare the peaks in your curves with the theoretical natural frequencies. Where strain-gauge equipment is provided, measure the stress and plot against frequency. Compare with the relevant twist-frequency plots and check by simple torsion theory.

## Discussion

Make sure that you can obtain the expressions for the natural frequencies given in equation (16.3). State which method you prefer and why. Check the values given in Table 16.1.

Discuss fully the experimental curves. How do the actual critical frequencies differ from the theoretical values? Give reasons for any substantial discrepancies.

## Speed Control System

Our last control experiment is concerned with the control of the speed of a shaft driven by a prime mover. It is instructive to compare and contrast its behaviour with that of the position control system considered earlier.

### Theory

Figure 14.1 used for the position control system also represents the present process. The important difference is that  $\theta_o$  now means the control *speed* of the driven shaft instead of the controlled position.  $I$  is the moment of inertia of the rotating parts referred to the driven shaft and  $c$  is the coefficient of the viscous damping. The prime mover in the suggested experiment is a reciprocating internal-combustion engine and  $I$  and  $c$  may reasonably represent its dynamics:  $L$  is the external load torque to which the prime mover is subject.

Likewise the block diagram of Figure 14.2 can be used to represent the closed-loop control system.  $\theta_i$  is now the desired *speed*. We may write the following equations [1]:

$$\left[ \frac{k}{1 + \tau_c D} \right] \theta - L = (ID + c)\theta_o \quad (17.1)$$

$$\theta = \theta_i - \theta_o \quad (17.2)$$

Note the difference in the right-hand sides of (17.1) and (14.1) since  $\theta_o$  is now a speed. The operator  $G_1$  is the coefficient of the speed error  $\theta$  on the left-hand side of (17.1). The proportional control, of coefficient  $k$ , is subject to the engine induction lag which is approximated to a simple exponential lag of time constant  $\tau_c$ , the latter depending on the throttle restriction and the manifold capacitance.

Eliminating  $\theta_o$  from (17.1) and (17.2), we obtain

$$\begin{aligned} \{\tau_c ID^2 + (c\tau_c + I)D + (c + k)\}\theta \\ = \{\tau_c ID^2 + (c\tau_c + I)D + c\}\theta_i + (1 + \tau_c D)L \end{aligned} \quad (17.3)$$

which gives the error as a function of  $\theta_i$  and  $L$ . By comparison with equation (14.3) for the position control system, (17.3) shows that once again we have

a second-order system. In practice the parameters  $I$ ,  $c$ ,  $k$  and  $\tau_c$  are such that the system mode is underdamped oscillatory. The steady-state error, for constant  $L$  and  $\theta_i$ , is

$$\theta_{ss} = \{c/(c+k)\}\theta_i + \{1/(c+k)\}L \quad (17.4)$$

Compared with (14.4), we note that a sustained change in  $\theta_i$  gives rise to a steady-state error as well as that given by a load change.

To avoid steady-state error, it is customary to employ integral control action; this means that the controller integrates the error signal with respect to time and the new controller output is added to the proportional action. Instead of (17.1), we now write

$$\left[ \frac{k(1 + 1/\tau_i \mathbf{D})}{1 + \tau_c \mathbf{D}} \right] \theta - L = (I\mathbf{D} + c)\theta_o \quad (17.5)$$

where  $1/\mathbf{D}$  means integration with respect to time and  $\tau_i$  is the integral action time constant. It is usually possible to adjust  $k$  and  $\tau_i$  separately by means of knobs on the controller.

We now eliminate  $\theta_o$  between (17.5) and (17.2), to obtain

$$\begin{aligned} \{\tau_i I \mathbf{D}^3 + (c\tau_c + I)\mathbf{D}^2 + (c+k)\mathbf{D} + k/\tau_i\}\theta \\ = \{\tau_i I \mathbf{D}^3 + (c\tau_c + I)\mathbf{D}^2 + c\mathbf{D}\}\theta_i + (1 + \tau_c \mathbf{D})DL \end{aligned} \quad (17.6)$$

The system is now of third order, there being an aperiodic mode in addition to the principal oscillatory mode. The steady-state error, for constant  $L$  and  $\theta_i$ , is now

$$\theta_{ss} = 0 \quad (17.7)$$

The advantage of integral control action is self-evident. The disadvantage is that the system can easily become unstable if  $k$  is too great or  $\tau_i$  too small. It might be argued that good stability can be restored if a third control action, namely derivative or error, is added. Although of great benefit in many systems, it is useless in the present case for the following reason. There is an inherent cyclic speed fluctuation in a reciprocating engine, the frequency of which in a 4-stroke 4-cylinder design can be easily as high as 150 Hz compared with the principal system mode frequency of about 0.5 Hz. Differentiation of the high-frequency ripple in the error signal amplifies its magnitude by  $2\pi \times \text{frequency}$ . This results in excessive 'noise' associated with the controller output signal and control is lost.

## Experimental Details

*Test Equipment.* It is desirable to avoid non-linearities as far as possible. For this reason, the common inertia 'governor',\* which inherently provides an output proportional to the square of speed, should not be employed.

\* In control terminology, the term 'governor' means a complete closed-loop speed-control system. The 'governor' referred to in texts on machines refers only to the speed-measuring element of the system.



Instead a tacho-generator should be driven by the engine shaft. This has an output in the form of a d.c. electric potential which is proportional to speed  $\theta_0$ ; a suitable type gives 0.04 V/(rev/min). This is fed to a pot-coil relay to give a current signal of 0.05 mA/V input.

It is convenient to employ a commercial proportional-plus-integral electronic process controller with possibly a small modification to extend the  $\tau_i$  range down to 1 second. This includes the system difference element, and hence the pot-coil relay output is fed in directly, zero to 5000 rev/min in  $\theta_0$  changing the controller input over its entire range of zero to 10 mA, moving a pointer over the input scale marked 0–100. A knob on the controller varies the desired speed  $\theta_i$  fed in, there being a second scale marked 0–100. The speed error  $\theta$  is shown by the difference between the two scale readings.

The controller output is also in the range zero to 10 mA and is shown on a third scale marked 0–100. The proportional action is usually calibrated as *proportional band*, which means the percentage of the maximum input change required to cause full-scale output change. Thus, if a difference in the desired and measured value pointers of 50 results in an output scale change of 100, the band is said to be 50 %. The band may be calibrated from 25 to 300 %; the parameter  $k$  of the system is, of course, inversely proportional to the band.

On proportional action alone, it is essential that the controller output should be at about mid-range when the desired and measured pointers are coincident; this permits changes in output for both positive and negative speed errors. The controller should be checked and the zero-error output value noted. This is of no consequence when integral action is used.

A four-cylinder spark-ignition engine, of 1200 cm<sup>3</sup> displacement, has been found suitable for this experiment. The external load would normally be provided by a hydraulic dynamometer but, for the purpose of the experiment, a means is required for rapidly turning the load-setting handwheel.

The throttle valve of the single carburettor is required to be turned in direct proportion to the controller output. It is convenient to use a small pneumatic motor fed *via* an electro-pneumatic converter, both of which need clean air supplied at about 130 kN/m<sup>2</sup> gauge pressure. The lag introduced by this regulating unit is small enough (compared with the main time constants of the system,  $I/c$  and  $\tau_c$ ) to have negligible effect on the system behaviour. Its overall characteristic is linear, as shown by Figure 17.1.

The equipment is completed by installing a two-pen strip-chart current recorder, one pen recording the same as the pointer on the controller input  $\theta_0$  scale and the other that of the controller output scale. The record will then indicate the variation in the controlled speed together with that of the throttle opening, both against time.

It is also convenient to have a manual control knob on the controller, together with a manual/automatic changeover switch. This permits the control loop to be broken and the engine throttle to be adjusted directly by hand.

*Engine and Dynamometer Characteristics.* The only serious non-linearities in the experimental system are due to the engine and dynamometer. Typical

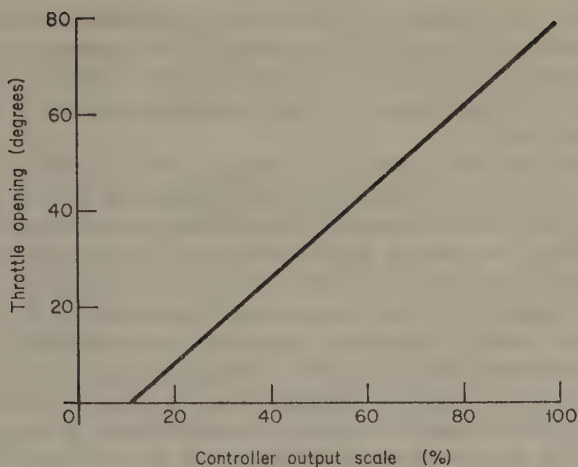


FIGURE 17.1 Regulating unit characteristic.

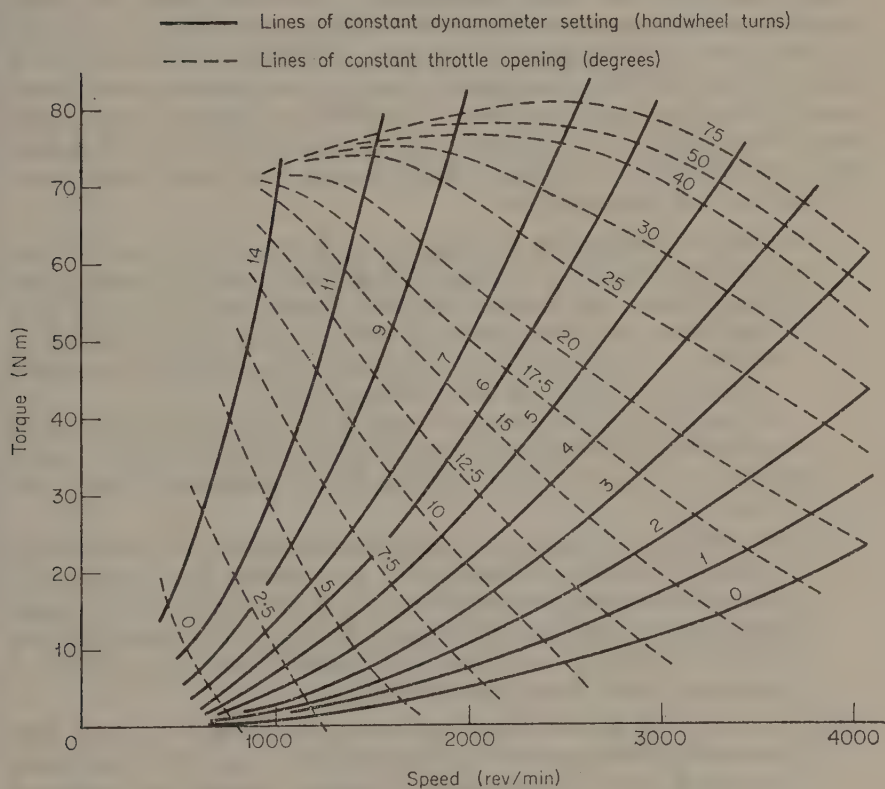


FIGURE 17.2 Engine and dynamometer characteristics.

curves are shown in Figure 17.2. The full curves indicate the load imposed by the dynamometer for various fixed settings of the handwheel (measured in handwheel turns). The dotted curves show the torque output of the engine at various fixed throttle positions. At steady speed, the engine output equals the dynamometer load.

It is evident that the engine output torque is not proportional to throttle opening at any speed. In fact, the system parameter  $k$ , though nominally fixed by the proportional band of the controller, varies both with speed and throttle opening. In order to ensure stable operation under all conditions, the band must be set so as to provide satisfactory response at the speed and load where the spacing of the throttle curves is greatest. The largest variation occurs at low speed,  $k$  being much greater at low load than at high load.

The only convenient way to impose a change in load  $L$  is by re-setting the dynamometer handwheel. The load set is constant only in the absence of a change of speed. Hence, during a transient following a step load change, we must realize that the actual load  $L$  as well as the speed will fluctuate.

*Procedure.* First allow the engine to warm up with moderate load on manual control. Set the controller to work on proportional action only with a proportional band between 100 % and 150 %. Set the dynamometer handwheel at about 5 turns. Set the desired value at about 2000 rev/min and switch to automatic control. If the system tends to hunt, switch back at once to manual control, *raise* the proportional band to stabilize and repeat. Now impose small changes in  $\theta_i$  and check whether the response is oscillatory but reasonably damped. Otherwise adjust the band further. The system is now ready for the following suggested tests.

- (a) With the dynamometer handwheel set at 5 turns and the proportional band at the value chosen above, set  $\theta_i$  to 1500 rev/min (30 on the scale) and allow the system to settle. Start the recorder. Make a step change in  $\theta_i$  to 3500 rev/min (70 on the scale). Allow 10 seconds for the system to settle completely. Now re-set  $\theta_i$  to 1500 rev/min and repeat. You should now have a record on the lines of Figure 17.3.

Repeat for different loads and steps in  $\theta_i$ . For high load and large steps, note that the system may saturate during the early part of each transient, i.e. the throttle may be held at a maximum or minimum opening.

- (b) Re-set the load at 5 turns. Add integral control action of time constant of about 1 second and re-adjust the proportional band if necessary. To avoid saturation, use smaller steps in  $\theta_i$  than in (a). For example, start at 1800 rev/min and make a step change to 3200 rev/min. Figure 17.4 shows the kind of response obtainable. Note the removal of steady-state error. Repeat for different loads.
- (c) With the same controller settings as the above, set  $\theta_i$  at about 2800 rev/min and the dynamometer handwheel to 1 turn. After the system has settled, apply a step change in load by turning the handwheel rapidly to 6 turns. Allow 10 seconds for the system to settle and then

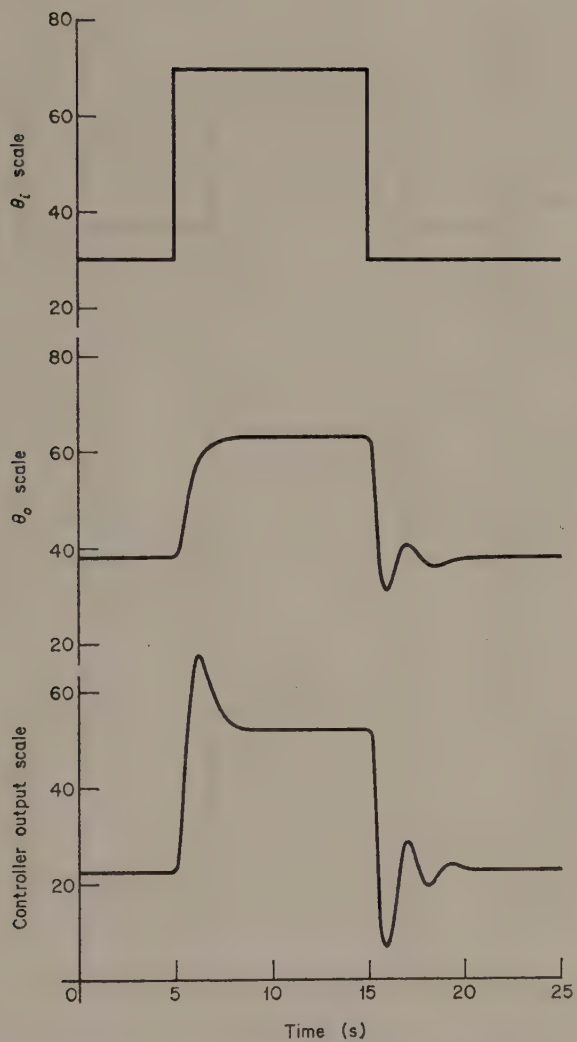


FIGURE 17.3 Response to desired-value change with proportional control.

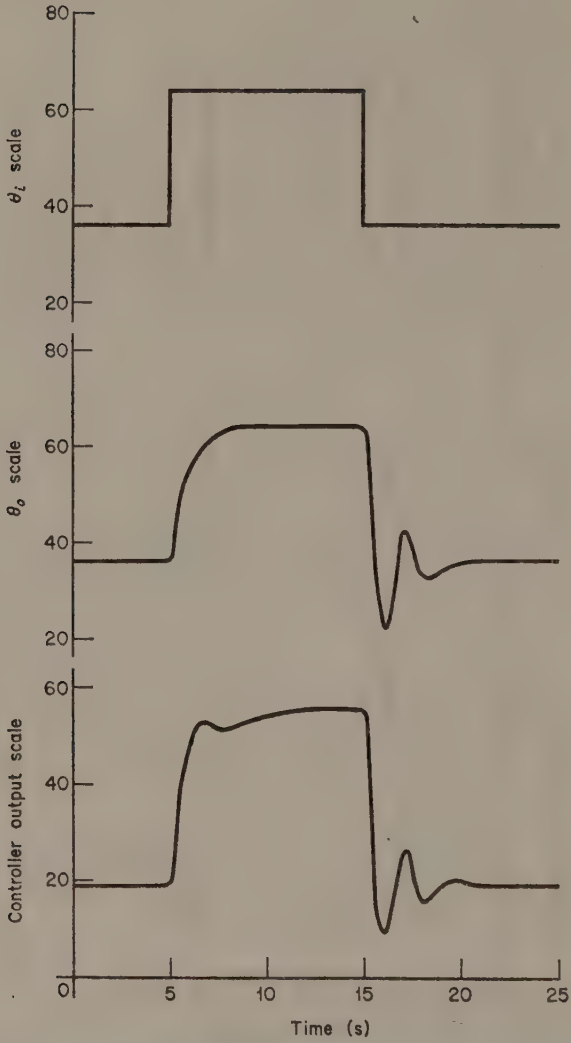


FIGURE 17.4 Response to desired-value change with proportional-plus-integral control.



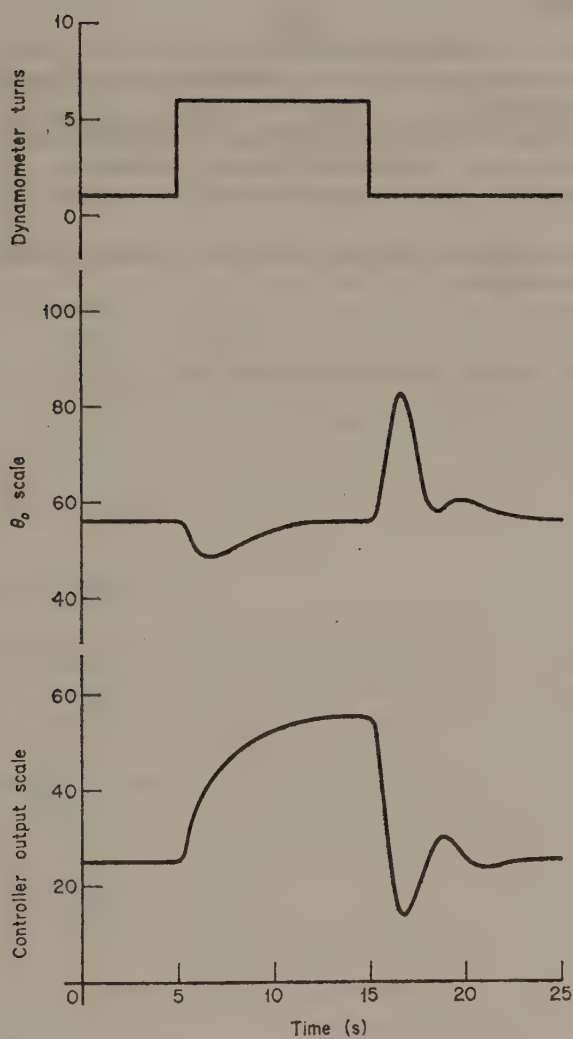


FIGURE 17.5 Response to load change with proportional-plus-integral control.

apply a reverse step in load back to 1 turn. A typical response is shown in Figure 17.5. Repeat for different speeds and steps in load.

## Discussion

Check that you can obtain equations (17.3), (17.4), (17.6) and (17.7). Draw a detailed block diagram of the experimental system, identifying all the components employed.

Explain the large discrepancies between desired and actual speed in the steady state in test (a). In test (b), following the step up, why is there a well in the controller output response followed by a gradual rise to the final value?

Why is the response for the step down more oscillatory than that for the step up in all three tests?

## Reference

1. WEBB, C. R., *Automatic Control*, McGraw-Hill, 1964.

---

## ***Analogue Computation***

An analogue computer is an instrument used for making a mathematical model of a system. Unlike a digital computer, which is fast and accurate and works in small discrete steps, an analogue computer represents variables continuously. It solves the differential equations representing the system directly, and hence is easier to program than a digital machine. It shows to advantage when simulating complex systems which are laborious to analyse by ordinary methods. Its accuracy depends on that of its components and on the skill of the programmer.

We shall confine our attention to the kind of instrument which is based on the d.c. operational amplifier.

### **Computer Elements**

When the output of a high-gain d.c. amplifier is fed back to the input, it acts as an amplifier of gain  $-1$  if the input and feedback resistances are equal. If the former is smaller than the latter, the magnitude of the gain is greater than unity in inverse proportion. Variants of the above are used for addition, subtraction, integration with respect to time, etc. Table 18.1 shows three important forms with their usual symbols. The first can add a number of voltages, multiplying inputs as required by round factors such as 10 or 100; the sign reversal is inherent. The second is a simplified special-purpose form of the first. The third element integrates with respect to time and permits initial conditions (I.C.) to be inserted.

Another important element is the attenuator, which is also shown in Table 18.1. This is simply a precision potentiometer by which the output voltage can be made some fraction  $\lambda$  of the input.

### **A Specific Problem**

The use of a computer is best described with the aid of a particular example. We choose a linear mechanical vibrating system which is just sufficiently difficult to analyse to justify the use of a computer. The same system is used in the actual experiment on the computer. Typical commercial instruments can, of course, deal with much more complex systems which can be non-linear or be represented by partial differential equations.

TABLE 18.1



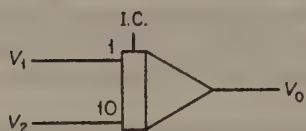
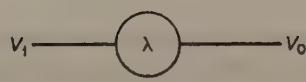
Symbol	Function
	Summing amplifier $V_0 = -(V_1 + 10V_2)$
	Inverter $V_0 = -V_1$
	Integrator $V_0 = -(\int V_1 dt + 10 \int V_2 dt + I.C.)$
	Attenuator $V_0 = \lambda V_1 \quad (\lambda < 1)$

Figure 18.1 shows a lumped system consisting of two bodies, two springs and a viscous dashpot. The following data apply:

$$m_1 = 25 \text{ kg}$$

$$m_2 = 2 \text{ kg}$$

$$k_1 = 10 \text{ N/cm}$$

$$k_2 = 50 \text{ N/cm}$$

$$c = 1 \text{ N/(cm/s)}$$

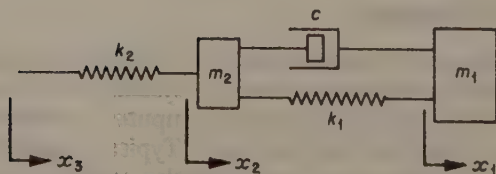


FIGURE 18.1 Lumped mechanical system.

The large differences in the chosen parameters are deliberate in order to illustrate the versatility of the computer. We are interested in the displacements  $x_1$  and  $x_2$  resulting from an input displacement  $x_3$ . The equations of motion may be written as under

$$m_1\ddot{x}_1 + c(\dot{x}_1 - \dot{x}_2) + k_1(x_1 - x_2) = 0 \quad (18.1)$$

$$m_2\ddot{x}_2 + c(\dot{x}_2 - \dot{x}_1) + k_1(x_2 - x_1) + k_2(x_2 - x_3) = 0 \quad (18.2)$$

The first step is to re-write the equations with the higher derivatives on the left and the remainder on the right, i.e.

$$\ddot{x}_1 = -(c/m_1)\dot{x}_1 + (c/m_1)\dot{x}_2 - (k_1/m_1)x_1 + (k_1/m_1)x_2 \quad (18.3)$$

$$\ddot{x}_2 = -(c/m_2)\dot{x}_2 + (c/m_2)\dot{x}_1 - (k_1/m_2)x_2 + (k_1/m_2)x_1 - (k_2/m_2)x_2 + (k_2/m_2)x_3 \quad (18.4)$$

## Amplitude Scaling

We must not exceed the maximum voltages permitted in the computer; otherwise certain circuits will overload (indicated by warning lights) and the problem will not be solved. Assuming that we may work in the range zero to 10 V, positive and negative, we now have to estimate the maximum likely values of the variables and their derivatives.

It is proposed to investigate the transient response in  $x_1$  and  $x_2$  to a step in  $x_3$  of 1 cm. It is then likely, for example, that  $x_1$  will not exceed 2 cm and hence we may represent 2 cm by 10 V. We therefore apply a scale factor of 5 V/cm and represent  $x_1$  by the computer variable  $[5x_1]$ , which of course is measured in volts. Other computer variables are found likewise, as in Table 18.2.

TABLE 18.2

<i>Problem variable</i>	<i>Maximum value</i>	<i>Scale factor</i>	<i>Computer variable</i>
$x_1$	2 cm	10/2	$[5 x_1]$
$x_2$	2 cm	10/2	$[5 x_2]$
$x_3$	1 cm	10/1	$[10 x_3]$
$\dot{x}_1$	5 cm/s	10/5	$[2 \dot{x}_1]$
$\dot{x}_2$	25 cm/s	10/25	$[0.4 \dot{x}_2]$

Since  $\ddot{x}_1$  and  $\ddot{x}_2$  are not to be found, they may be formed as integrator inputs. They may be scaled as we please but it is convenient to use the same



scales as for  $\dot{x}_1$  and  $\dot{x}_2$  respectively, giving the computer variables  $[2\ddot{x}_1]$  and  $[0.4\ddot{x}_2]$ .

We now re-write the equations of motion in terms of the computer variables, i.e.

$$[2\ddot{x}_1] = -\frac{c}{m_1} [2\dot{x}_1] + 5\frac{c}{m_1} [0.4\dot{x}_2] - \frac{2}{5}\frac{k_1}{m_1} [5x_1] + \frac{2}{5}\frac{k_1}{m_1} [5x_2] \quad (18.5)$$

$$\begin{aligned} [0.4\ddot{x}_2] = & -\frac{c}{m_2} [0.4\dot{x}_2] + \frac{1}{5}\frac{c}{m_2} [2\dot{x}_1] - \frac{2}{25}\frac{k_1}{m_2} [5x_2] \\ & + \frac{2}{25}\frac{k_1}{m_2} [5x_1] - \frac{2}{25}\frac{k_2}{m_2} [5x_2] + \frac{1}{25}\frac{k_2}{m_2} [10x_3] \end{aligned} \quad (18.6)$$

## Time Scaling

Using the data, we may find the coefficients of the computer variables given in the above equations. These vary in size from  $(c/m_1)$  which is 4 units to  $\frac{2}{25}(k_2/m_2)$  which is 200 units. We shall assume that the operational amplifiers in the available computer provide gains of either 1 or 10. Clearly it will reduce the number of computer elements needed if we can reduce the magnitude of the larger coefficients. This will automatically reduce the speed at which the computer solves the problems. The process is known as *time scaling*; we apply a factor  $a$  to all the coefficients in (18.5) and (18.6). It should be noted that, for a process which is slow in real time, a fractional value can be chosen for  $a$  in order to make 'computer time' faster than real time. For the present

TABLE 18.3

Attenuator number	Number in equations (18.7) and (18.8)	Expression represented	$\lambda$ value
1	(i)	$c/(am_1)$	0.40
2	(ii)	$c/(2am_1)$	0.20
3,4	(iii), (iv)	$k_1/(25am_1)$	0.16
5	(v)	$c/(10am_2)$	0.50
6	(vi)	$c/(5am_2)$	1.00
7,8	(vii), (viii)	$k_1/(125am_2)$	0.40
9	(ix)	$k_2/(1250am_2)$	0.20
10	(x)	$k_2/(250am_2)$	1.00

problem, a suitable value for  $a$  is 10. The equations are once again re-written as

$$\frac{1}{a} [2\ddot{x}_1] = -1 \text{ (i)} [2\dot{x}_1] + 10 \text{ (ii)} [0.4\dot{x}_2] - 10 \text{ (iii)} [5x_1] + 10 \text{ (iv)} [5x_2] \quad (18.7)$$

$$\begin{aligned} \frac{1}{a} [0.4\ddot{x}_2] = & -10 \text{ (v)} [0.4\dot{x}_2] + 1 \text{ (vi)} [2\dot{x}_1] - 10 \text{ (vii)} [5x_2] \\ & + 10 \text{ (viii)} [5x_1] - 10 \times 10 \text{ (ix)} [5x_2] + 10 \text{ (x)} [10x_3] \end{aligned} \quad (18.8)$$

In the above, the unbracketed coefficients represent amplifier gains, either 1 or 10. The terms in curved brackets are attenuator settings  $\lambda$ ; these must not exceed unity and dictate the choices of amplifier gain. The values of  $\lambda$  are listed in Table 18.3.

We may now draw the computer block diagram, Figure 18.2. Integrators 1 and 3 have inputs corresponding to the right-hand sides of equations (18.7) and (18.8) respectively. Hence the input to integrator 1, for example, represents  $2\ddot{x}_1/a$ , i.e.

$$\begin{aligned} \text{input} &= \frac{2}{a} \frac{d}{dt} (\dot{x}_1) \\ &= 2 \frac{d}{d\tau} (\dot{x}_1) \end{aligned}$$

where  $\tau$  is computer time, equal to  $at$ . Therefore

$$\text{output} = -[2\dot{x}_1]$$

which is the negative of the required computer variable. By a similar argument, the output of integrator 3 is  $[0.4\dot{x}_2]$ , all the terms on the right-hand side of (18.8) being fed in negatively for convenience.

The output from integrator 2 is required to be  $[5x_1]$ , and hence the input must be  $-5\dot{x}_1/a$ , i.e.  $-\frac{1}{2}\dot{x}_1$ . We must therefore insert attenuator 11 of value 0.25. Similarly attenuator 12 in the input to integrator 4 must have a value of 0.125, together with an integrator gain of 10.

Inverters 5, 6 and 7 are needed to reverse signs in certain paths. At this point it should be stressed that the arrangement of Figure 18.2 is not the only one possible. However, it is important to aim at minimizing the number of computer elements required.

## Static Check

The object of this part of the procedure is to check the programming. We make use of the facility of applying initial conditions (I.C.) to the integrators. These need not be realistic but are chosen to ensure that voltages which are neither zero nor greater than 10 V in magnitude are produced in every path in the diagram. We assume the values given in Table 18.4.



TABLE 18.4

<i>Variable</i>	<i>Value of I.C.</i>	<i>Corresponding value of computer variable</i>
$x_1$	1 cm	5 V
$x_2$	-1 cm	-5 V
$\dot{x}_1$	5 cm/s	10 V
$\dot{x}_2$	-10 cm/s	-4 V

For the purpose of the check, only the I.C. signals operate the integrators, the other inputs being switched out. We require -4 V at the output from integrator 3, for example, and must therefore apply 4 V; this is done by applying 10 V (marked 'S.C.') through attenuator 13 having value 0.40. Similar S.C. signals are applied to integrators 1, 2, 4. Another 10 V signal is used to represent the input  $[10x_3]$  (marked 'Input').

We now trace through the computer block diagram, checking that a voltage other than zero but not exceeding 10 V appears at every point. If these requirements are not met, the assumed initial conditions must be changed accordingly. The aggregate inputs to integrators 1 and 3 are then found to be -28 V and -270 V respectively. These are checked by inserting the assumed initial conditions in the original equations (18.3) and (18.4). For example,

$$\begin{aligned}\ddot{x}_1 &= -4(5) + 4(-10) - 40(1) + 40(-1) \\ &= -140 \text{ cm/s}^2\end{aligned}$$

Hence  $\frac{1}{\alpha} [2\ddot{x}_1] = -28 \text{ V}, \quad \text{as required.}$

The above procedure checks the whole of the programming and suggests I.C. values suitable for an actual static check on the computer itself.

## Setting Up the Computer

This varies in detail from one instrument to another and reference should be made to the manufacturer's literature. However, the general procedure is as follows. First make the necessary connections on the patch board to represent the computer diagram, Figure 18.2. Next adjust all the potentiometers to their required values.

Now carry out a static check on the same lines as described above; in most instruments special switching arrangements are available for this. The instrument should not overload anywhere and all the required voltages should be obtained, provided the setting up has been carried out correctly.

Make connections to the recording equipment to record the variables  $[5x_1]$ ,  $[5x_2]$  and  $[10x_3]$ .

## Computer Experiment

Switch out the initial conditions used for the static check and switch in the input variables to the integrators. No initial conditions are required for the test considered here, though of course transients can be started from finite initial conditions whenever this is required.

Use the appropriate controls to impose a 10 V step in  $[10x_3]$  which is

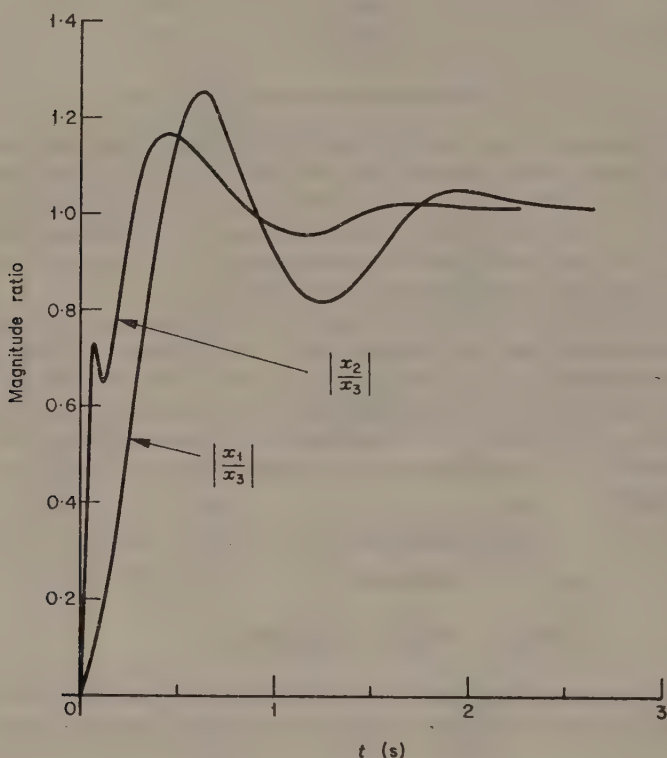


FIGURE 18.3 Step response of mechanical system.

equivalent to a 1 cm step in  $x_3$ . The computer should then solve for the transient response in  $x_1$  and  $x_2$ , producing records of  $[5x_1]$  and  $[5x_2]$  ten times slower than real time. These records should be translated into actual variables and real time so that the ratios  $|x_1/x_3|$  and  $|x_2/x_3|$  appear as in Figure 18.3.

Further tests can now be made to find the effect of changing the damping coefficient  $c$ . For  $c$  equal to 0.5 N/(cm/s), for example, it is only necessary to halve the values of attenuators 1, 2, 5 and 6. The instrument may overload, however, should the changes cause maximum transient values exceeding those assumed in setting up the program.



## Discussion

Make sure that you understand the functions of amplitude and time scaling. What is the advantage of slowing down the solution to the given problem?

Try to find out exactly what switching operations are performed by the controls provided on the available instrument. How accurately can you set the attenuator values? What lack of accuracy was revealed by the static check on the instrument? Are you satisfied that your final curves represent an acceptable solution of the mathematical problem?



## **Part II**

---

# **Stress Analysis**



## *Elastic Constants*

Before any useful calculations or experiments on stressed bodies may be performed, the stress-strain relation of the materials must be determined. Experimentally, we can measure only strain or deflection, from which the stresses may then be inferred.

For most common structural materials, the stress-strain relation is linear, or almost so, in the elastic region. This region is characterized by no permanent deformation after load is removed, i.e. complete return to original size. Two types of stress may be applied, normal or shear, and two constants at least must be determined. This experiment will determine one constant, and another will be determined in the succeeding experiment.

### **Theory**

There are four elastic constants in common use:

- (a) Young's modulus,  $E$ , defined by

$$\frac{\text{normal stress}}{\text{normal strain}}$$

- (b) Rigidity, or shear, modulus,  $G$ , defined by

$$\frac{\text{shear stress}}{\text{shear strain}}$$

- (c) Poisson's ratio,  $\nu$ , defined by

$$\frac{\text{lateral strain}}{\text{normal strain}}$$

- (d) Bulk modulus,  $K$ , defined by

$$\frac{\text{hydrostatic stress}}{\text{volume strain}}$$

The first three are all used in structural calculations. If the material under test is isotropic, i.e. its properties are the same in all directions, and homogeneous, i.e. its properties are the same throughout its volume, the four



constants will specify the behaviour completely. Two independent equations may be found relating them:

$$E = 3K(1 - 2\nu), \quad E = 2G(1 + \nu)$$

so that an isotropic, homogeneous structural material is completely specified by two elastic constants.

## Experimental Details for Young's Modulus

If a uniform bar, cross sectional area  $A$  and length  $L$  is extended by amount  $S$  due to axial load  $P$ , then

$$E = PL/AS$$

Hence

$$S = PL/AE$$

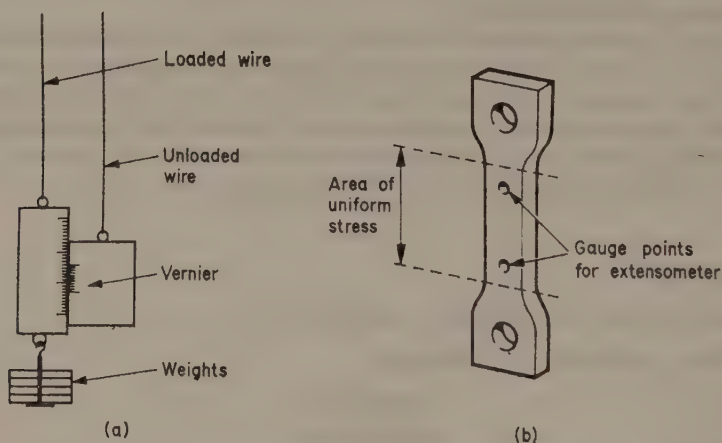


FIGURE 19.1 Measurement of Young's modulus (a) vernier method for measuring Young's modulus of wire (b) tensile apparatus for measuring Young's modulus of bar.

To make  $S$  as large as possible for accurate measurement,  $L$  must be large and  $A$  small. This is the basis of the vernier and Searle's method for determining Young's modulus, where the specimen is in the form of a long, thin wire, up to 5 m long. Variation of temperature along such a length would cause erroneous results due to a considerable thermal expansion, and so an identical wire is hung close to the specimen wire. To the ends of these wires is attached a vernier measuring device, as in Figure 19.1, and on application of the load the relative extension may be accurately measured.

If the material cannot be obtained in wire form, then measurement must be made on a machined bar. Again, the bar should be kept as long and slender as possible. The load will now have to be applied by a lever or hydraulic machine to obtain the same stress levels. Measurement of the extension is

not so simple, as the stress is not uniform at the ends of the bar where it is attached to the loading machine. In this case, the extension must be measured over a central portion of the bar by an 'extensometer'. This is a compact mechanical gauge which, when clamped to the specimen, magnifies the extension of a fixed length known as the 'gauge length'. Common types of extensometer are the Huggenberger and Demec gauges, which are available with different gauge lengths. The extension should be measured on opposite sides of the bar to provide an average value.

Plot load against extension and derive a value of Young's modulus for brass, copper, aluminium and mild steel. Repeat these measurements for the materials in bar form.

## Discussion

Compare the results for materials in wire and bar form and comment on them. Discuss the sources of error in both experiments and suggest how they may be reduced: estimate the accuracy of the results.

## ***Torsion of a Circular Shaft***

Torsion is a common type of load applied to structural members. When applied to non-circular cross-sections, the analysis is complex, so this experiment is restricted to circular shafts. The object will be to verify the torsion formulae, and to determine the rigidity modulus for several materials.

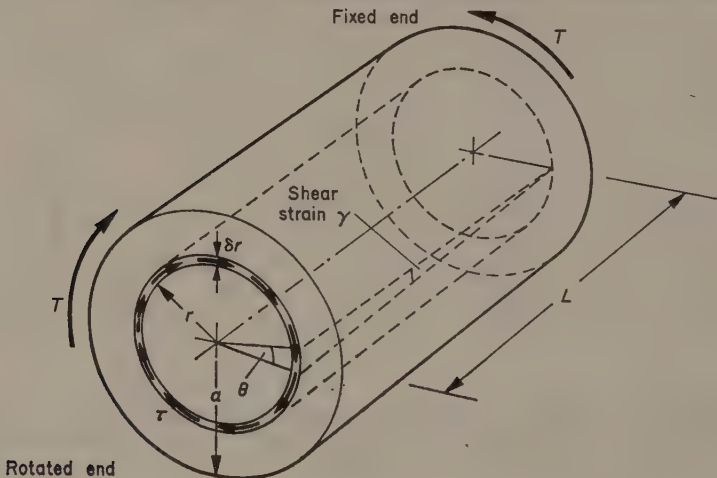


FIGURE 20.1 Torque acting on a circular shaft.

### **Theory**

For a circular shaft under pure torque  $T$ , illustrated in Figure 20.1, we make the following assumptions:

- (i) twisting is uniform along lengths of shaft,
- (ii) radii remain straight, and
- (iii) cross-sections remain plane.

The first two assumptions follow if the shaft is elastic, while the third is a consequence of the circular symmetry.

Considering an elemental tube, radius  $r$ , thickness  $\delta r$ , inside the shaft, we see that

$$\text{shear strain } \gamma = r\theta/L$$

But

$$\text{rigidity modulus } G = \tau/\gamma$$

Hence

$$\tau = Gr\theta/L$$

Now assuming constant shear stress  $\tau$  in the elemental tube, the torque on the tube is given by  $(2\pi r\delta r)\tau r = (2\pi r\delta r)\frac{Gr\theta}{L}r$

$$= 2\pi\frac{G\theta}{L}r^3\delta r$$

Hence the torque  $\tau$  on the whole shaft is given by

$$\begin{aligned} T &= \int_0^a 2\pi \frac{G\theta}{L} r^3 dr \\ &= 2\pi \frac{G\theta}{L} \left[ \frac{r^4}{4} \right]_0^a \\ &= \frac{G\theta}{L} \left[ \frac{\pi a^4}{2} \right] \end{aligned}$$

The expression in brackets is the 'polar moment of inertia of the cross-section', usually represented by  $J$ .

## Experimental Details

The circular shaft should be machined as in Figure 20.2. One end is rigidly clamped, and a radius arm is fixed to the other, so that torque may be applied by weights. To prevent any flexure, the shaft should be supported by a tail-stock at its free end.

Because of the non-uniform cross-section, the angular deflection is best measured by a torsion meter clamped to the middle of the shaft. These meters consist of two clamping rings a fixed distance apart (the gauge length), which measure the deflection by the relative movement of two levers. The length  $L$  in the equation is now the gauge length of the meter.

To allow for any initial slip in clamped parts, it is advisable to apply a small load before measurements are made. As an extra check for this type of error, readings should be taken for loading and unloading.

Plot load against deflection and derive a value for the rigidity modulus. Do this for specimens of brass, copper, aluminium and mild steel.

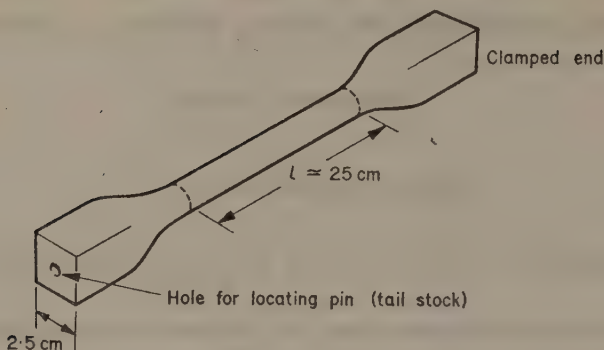


FIGURE 20.2 Specimen shape for torsion experiment.

## Discussion

Discuss the sources of error in the experiments, and estimate the accuracy of the results. Describe what would happen if the elastic limit were exceeded, and consider how well the three assumptions made in the theory have been justified.

Combine the results with the appropriate Young's modulus (obtained from Experiment 19) and plot  $E$  against  $G$ . What conclusions can you draw from this graph?

## Simple Bending

Bending of a beam is nearly always accompanied by shear forces, so that in addition to the bending stresses we have shear stresses. There is one type of loading (commonly used in testing) known as four-point loading, which produces a region of pure bending in the beam. This enables us to verify the equation for pure bending and determine the second moments of area experimentally.

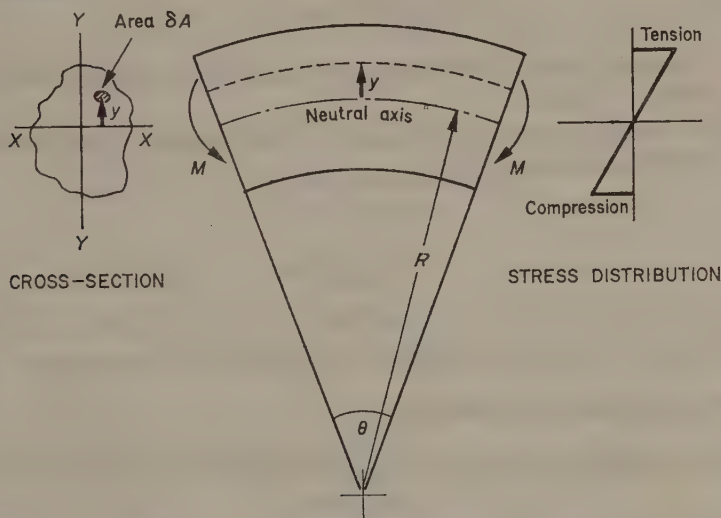


FIGURE 21.1 Element of a beam under the action of a bending moment  $M$ .

### Theory

Consider a small element of beam under a pure bending moment, as in Figure 21.1. We will assume:

- (i) Young's modulus is the same in tension and compression,
- (ii) the element was initially straight, and all filaments bend into circular arcs with a common centre of curvature, the radius of curvature  $R$  being large, and
- (iii) transverse cross-sections remain plane.



The first assumption is true enough for most elastic materials, and the second is, geometrically, a good approximation for large radii of curvature. The third assumption is not true if shear forces are present, as these distort the transverse planes; the distortion is small, however, and this derivation may be used when shear occurs. The cross-sectional shape is also distorted by the Poisson strains, caused by the varying bending stresses, and known as anticlastic curvature. This does not affect our analysis.

Assuming a *neutral axis* in the element, where the strain and stress are zero, then strain in a filament distance  $y$  from this axis is given by

$$\frac{(R + y)\theta - R\theta}{R\theta} = \frac{\sigma}{E} = \frac{y}{R}$$

From the equilibrium of forces, we have three conditions:

- (a) A small filament, cross-section  $\delta A$ , distance  $y$  from the neutral axis will be in equilibrium so the nett normal force on the total cross-section is zero, i.e.

$$\int \sigma \, dA = 0$$

or 
$$\frac{E}{R} \int y \, dA = 0$$

Thus the *neutral axis* must pass through the centroid of the cross-section.

- (b) The bending moment is balanced by the moment of normal forces about the neutral axis, i.e.

$$\begin{aligned} M &= \int \sigma y \, dA \\ &= \frac{E}{R} \int y^2 \, dA \\ &= EI/R \end{aligned}$$

where  $I$  is the second moment of area. For a rectangular beam  $I = \frac{1}{12} \times \text{breadth} \times (\text{height})^3$ .

- (c) For equilibrium about axis  $YY$  (perpendicular to the neutral axis)

$$\int \sigma x \, dA = 0$$

or 
$$\frac{E}{R} \int yx \, dA = 0$$

This integral is the product of inertia, and the axes for which it is zero are the *Principal Axes of Bending*. These axes are parallel to the sides of a rectangular cross-section. This point will be exemplified in a later experiment.

We thus have the equations of bending:

$$\frac{\sigma}{y} = \frac{E}{R} = \frac{M}{I}$$

## Experimental Details

The particular loading arrangement is shown in Figure 21.2, along with the shear force and bending moment diagrams. The bending moment is constant between the supports, so the radius of curvature is also constant over this

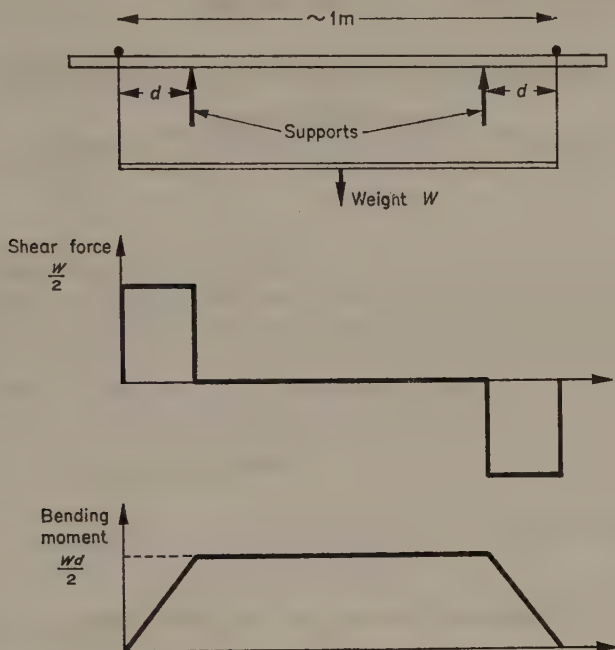


FIGURE 21.2 Loading scheme, with associated shear-force and bending-moment diagrams, for a simple beam.

length. Thus the beam traces out the arc of a circle, illustrated in Figure 21.3, and this is termed *circular bending*.

If  $\delta$  is the upward deflection of the centre point  $B$ , then from the geometry of intersecting chords

$$2R\delta = L^2$$

but

$$\frac{1}{R} = \frac{M}{EI}$$

Hence

$$\delta = \frac{ML^2}{2EI}$$

If the depth of the beam is  $2h$ , and the maximum strain at section  $B$  is  $e_{\max}$ , then

$$\sigma_{\max} = E e_{\max} = Mh/I$$

The quantity  $I/h$  is called the *section modulus* and is usually represented as  $Z$ . Therefore

$$e_{\max} = M/ZE$$

Measure the deflection and strain at point  $B$ , for increasing load, and repeat this for beams with different cross-sectional areas.

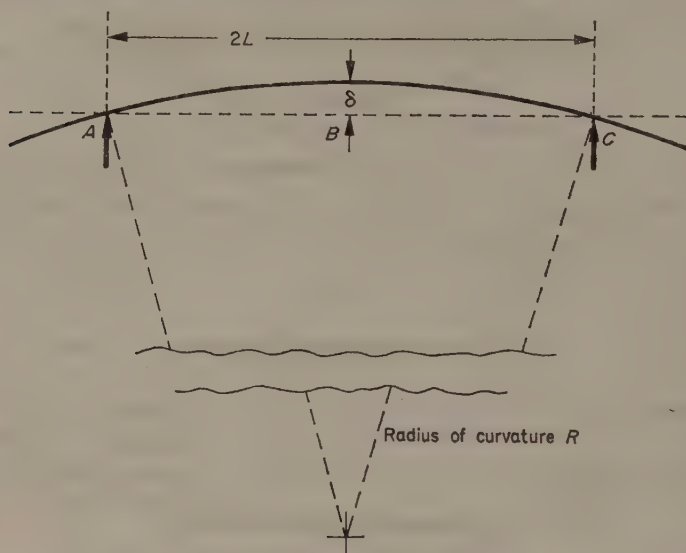


FIGURE 21.3 Deflection of the centre part of a beam under pure bending.

It is advisable to use only rectangular cross sections, having depths less than breadths.

Plot load against deflection, and load against strain, and derive values of the second moments of area. Compare these experimental values with those from direct measurements of the cross-section, giving estimates of error in each case.

Choosing a suitable value of load, plot graphs of deflection,  $\delta$ , against  $I$ , and strain,  $e_{\max}$ , against  $Z$ .

## Discussion

Derive the expression for the second moment of area of a rectangular cross-section, and comment on the values determined experimentally. Consider how well the results verify the equation of bending, and suggest which assumption is most likely to be in error.

## Bending of an L-shaped Cantilever

In the experiment on simple bending, the beam was loaded parallel to a principal axis, so the product of inertia was zero. In this experiment, the full bending theory is demonstrated by measuring the deflections of a cantilever with an L-shaped cross-section under the same load, but at different orientations to the principal axes. The positions of these axes are determined experimentally and by calculation.

### Theory

Consider the irregular cross-section in Figure 22.1, with principal axes  $Gu$  and  $Gv$ , where  $G$  is the centroid of cross-section.

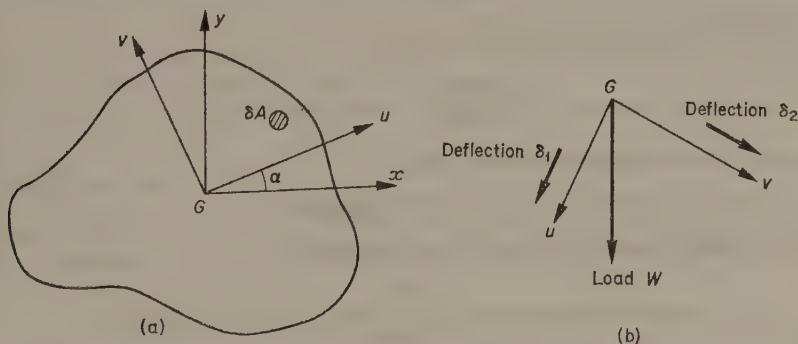


FIGURE 22.1 Principal axes and deflections of an asymmetrical beam (a) cross-section of an asymmetrical beam, (b) resolution of the deflections of an asymmetrical beam.

Let  $\delta A$  be a small element of area, the co-ordinates being  $(u, v)$  with respect to  $Gu$  and  $Gv$  and  $(x, y)$  with respect to  $Gx$  and  $Gy$ . Then

$$u = x \cos \alpha + y \sin \alpha$$

$$v = y \cos \alpha - x \sin \alpha$$

The product of inertia is defined as

$$\begin{aligned}
 I_{uv} &= \int uv \, dA \\
 &= \int (x \cos \alpha + y \sin \alpha) (y \cos \alpha - x \sin \alpha) \, dA \\
 &= \sin \alpha \cos \alpha [\int y^2 \, dA - \int x^2 \, dA] + (\cos^2 \alpha - \sin^2 \alpha) \int xy \, dA \\
 &= \frac{1}{2} \sin 2\alpha (I_{xx} - I_{yy}) + \cos 2\alpha I_{xy}
 \end{aligned}$$

For the principal axes

$$I_{uv} = 0$$

Hence 
$$\tan 2\alpha = \frac{2I_{xy}}{I_{yy} - I_{xx}}$$

Similarly it can be shown that

$$\begin{aligned}
 I_{uu} &= \int v^2 \, dA \\
 &= I_{xx} \cos^2 \alpha + I_{yy} \sin^2 \alpha - I_{yz} \sin 2\alpha \\
 I_{vv} &= \int u^2 \, dA \\
 &= I_{yy} \cos^2 \alpha + I_{xx} \sin^2 \alpha + I_{xy} \sin 2\alpha
 \end{aligned}$$

Consider a cantilever with end load  $W$ . Let  $W$  be inclined at an angle  $\phi$  to the principal plane  $Gu$ . The deflection along  $Gu$  is given by

$$\frac{W \cos \phi \cdot l^3}{3EI_{vv}} = \delta_1, \quad \text{say}$$

and the deflection along  $Gv$  is given by

$$\frac{W \sin \phi \cdot l^3}{3EI_{uu}} = \delta_2, \quad \text{say}$$

where  $l$  is the length of cantilever and

$E$  is the Young's Modulus of the material.

The deflection in the direction of load is given by

$$\delta_1 \cos \phi + \delta_2 \sin \phi = \frac{Wl^3}{3EI_{uu}I_{vv}} (I_{uu} \cos^2 \phi + I_{vv} \sin^2 \phi)$$

The deflection in the direction perpendicular to the load is given by

$$\delta_1 \sin \phi - \delta_2 \cos \phi = \frac{Wl^3 \sin 2\phi}{3EI_{uu}I_{vv}} (I_{uu} - I_{vv})$$

## Experimental Details

The L-shaped beam should be approximately 2.5 cm on its side and 1 m long. Each end should be attached rigidly to a wheel, one wheel being fixed to a

frame capable of rotation against a scale calibrated in degrees. The other wheel carries a slide from which the weight is suspended. The whole apparatus is illustrated in Figure 22.2. Two dial gauges are fixed against the load carrying wheel, in directions corresponding to zero and  $90^\circ$  of the scale.

The cantilever is rotated by fixed angular increments, say  $22.5^\circ$ , and the

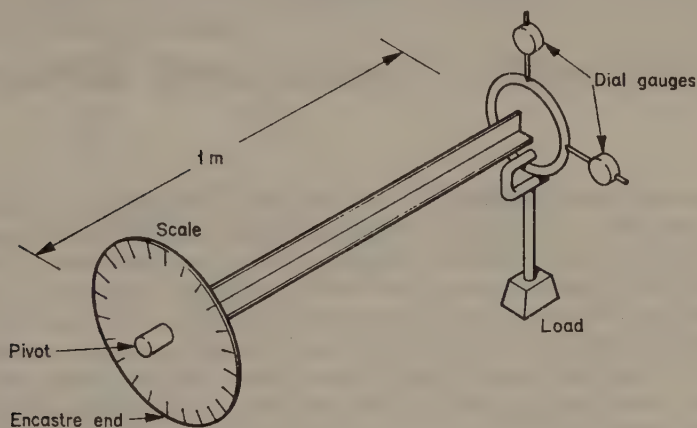


FIGURE 22.2 Cantilever scheme for an asymmetrical-beam experiment.

dial gauges read for the addition of a fixed load. It is best to apply the load each time, to allow for rigid body movements in the apparatus.

Plot graphs of the  $0^\circ$  and  $90^\circ$  deflections against angle of rotation. Determine the positions of minimum deflection, and hence determine the values of the two second moments of area. Calculate the value of these moments from the cross-section dimensions, and compare the two results.

## Discussion

Suggest what sources of error affect the experimental result, and consider what approximation the theory makes with regard to the shear force.



## Compound Stress and Strain

The states of stress and strain in a biaxial stress field may be expressed by three parameters, usually taken as two perpendicular normal components and a shear component of either stress or strain. These may then be used to calculate the principal stresses (and strains) and their directions. Provided the material is isotropic, the principal stresses and strains have the same directions, so that once the principal strains are determined, the stresses may be derived very simply using known values of the elastic constants.

Strain measuring equipment is sensitive only to extensional strain and, as shear strain cannot be measured directly, the biaxial state of strain in a particular problem must be determined from at least three measurements of extensional strain. This problem applies particularly to the surface strains of any structure, as the third principal strain is always normal to a free surface.

### Theory

*Analysis of Strain.* Suppose  $e_x$ ,  $e_y$  and  $\gamma_{xy}$  are the linear and shear strains in the plane  $Oxy$ . It is required to find an expression for  $e_\theta$ , the linear strain in a direction inclined at  $\theta$  to  $Ox$ , in terms of  $e_x$ ,  $e_y$ ,  $\gamma_{xy}$ , and  $\theta$ .

In Figure 23.1,  $OP$ , of length  $r$ , is the diagonal of a rectangle, which under the given strains distorts into the dotted parallelogram with  $P$  moving to  $P'$ . Remembering that actual strains are very small,

$$\begin{aligned} PP' &\simeq PQ \cos \theta + QR \sin \theta + RP' \cos \theta \\ &= (r \cos \theta \cdot e_x) \cos \theta + (r \sin \theta \cdot e_y) \sin \theta + (r \sin \theta \cdot \gamma_{xy}) \cos \theta \\ &= re_x \cos^2 \theta + re_y \sin^2 \theta + r\gamma_{xy} \sin \theta \cos \theta \end{aligned}$$

But

$$\begin{aligned} e &= PP'/r \\ &= \frac{1}{2}e_x(1 + \cos 2\theta) + \frac{1}{2}e_y(1 - \cos 2\theta) + \frac{1}{2}\gamma_{xy} \sin 2\theta \\ &= \frac{1}{2}(e_x + e_y) + \frac{1}{2}(e_x - e_y) \cos 2\theta + \frac{1}{2}\gamma_{xy} \sin 2\theta \end{aligned} \quad (23.1)$$

This can be compared with the similar equation for stress. The principal strains  $e_1$  and  $e_2$ , being the maximum and minimum values of strain, occur at values of  $\theta$  obtained by equating  $de_\theta/d\theta$  to zero, i.e.

$$\tan 2\theta = \gamma_{xy}/(e_x - e_y) \quad (23.2)$$

Then  $e_1$  and  $e_2$  are given by

$$\frac{1}{2}(e_x + e_y) \pm \frac{1}{2}\sqrt{\{(e_x - e_y)^2 + \gamma_{xy}^2\}} \quad (23.3)$$

In order to evaluate  $e_x$ ,  $e_y$ , and  $\gamma_{xy}$  (and hence the principal strains) it is necessary in general to know the linear strains in any three directions at a particular point. If the principal directions are known only two strains are required, since  $\gamma_{12} = 0$  and  $e_x = e_1$ ,  $e_y = e_2$ .

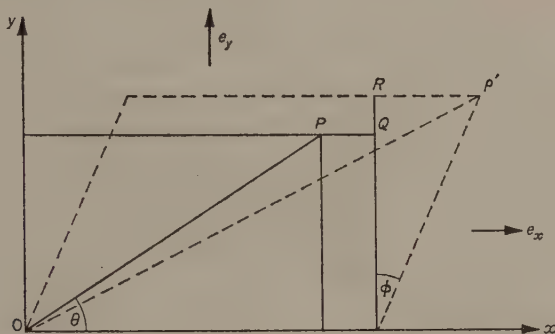


FIGURE 23.1 Deformation of a rectangular component under the action of three strain components,  $e_x$ ,  $e_y$  and  $\gamma_{xy}$ .

**Stress-Strain Relations.** A biaxial state of stress, characterized by principal stresses  $\sigma_1$  and  $\sigma_2$  will produce the following strains:

$\sigma_1$	$\sigma_2$
$\sigma_1/E$ in direction 1	$\sigma_2/E$ in direction 2
$-\nu\sigma_1/E$ in direction 2	$-\nu\sigma_2/E$ in direction 1

where  $E$  is Young's modulus and  $\nu$  is Poisson's ratio.

Assuming the strains are small, by the principle of superposition

$$\text{strain in direction 1, } e_1 = (\sigma_1 - \nu\sigma_2)/E$$

$$\text{strain in direction 2, } e_2 = (\sigma_2 - \nu\sigma_1)/E$$

## Experimental Details

The thin metal plate illustrated in Figure 23.2 should be loaded by dead weights. The particular loading arrangement, known as a 'whipple tree', ensures a uniform stress state over the centre of the plate. This area of uniform stress should be at least 25 cm square. The plate should have extensometer clips fixed parallel and perpendicular to the direction of load, and also at  $10^\circ$  intervals between these lines. A Demec gauge with 15 cm gauge length is the most convenient instrument for this experiment. To counteract any initial

curvature of the plate, extensometer measurements should be made on both sides, and the mean reading taken.

Load the plate in equal increments to just under the elastic limit, and take extensometer readings parallel and perpendicular to the load direction. Then load the plate somewhere in this range, and take extensometer measurements at  $10^\circ$  intervals.

Plot load-extension curves for the readings parallel and perpendicular to

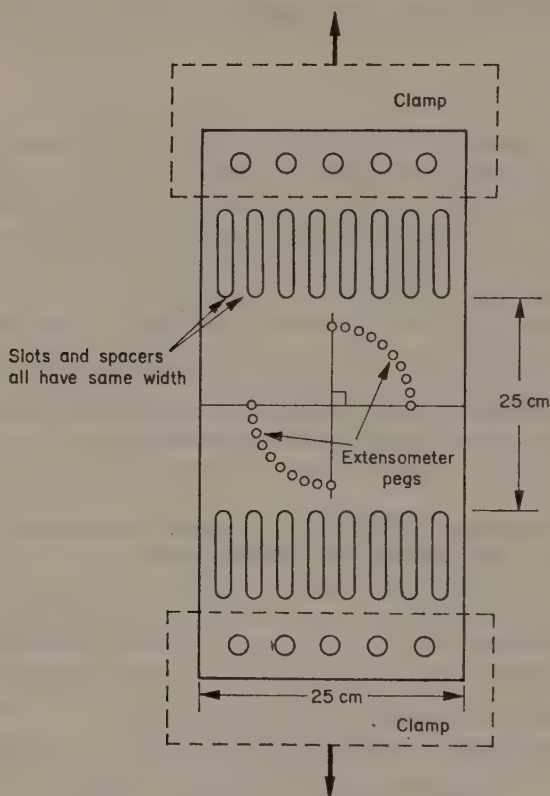


FIGURE 23.2 Plate with slots, for uniform region of strain.

the load, and determine the elastic constants. Then plot the extensometer readings against  $\cos 2\theta$ , where  $\theta$  is the angular position of the extensometer location measured from the load direction. As the load direction is a principal stress (and hence strain) direction, the shear strain  $\gamma_{xy}$  is zero, and the equation is

$$e_\theta = \frac{1}{2}(e_1 + e_2) + \frac{1}{2}(e_1 - e_2) \cos 2\theta$$

From the slope and intercept of this graph, determine  $e_1$ ,  $e_2$  and hence  $\sigma_1$ ,  $\sigma_2$ . Compare experimental and applied stresses.

## Discussion

Suggest what sources of error may effect your results and discuss how well the experiment justifies the theory. Estimate the size of strains that would produce significant errors in the approximations made in the analysis.

Suggest how the principal strains could be determined if their directions were also unknown.

## *Elastic Stability of Struts*

A thin strut that is compressed along its axis buckles at a certain critical load. It is of interest to compare the critical load as obtained experimentally with the value predicted by Euler's theory of thin struts, according to which

$$P_e = \frac{\pi^2 EI}{L^2}$$

where  $P_e$  is the critical load,  $E$  is Young's modulus,  $I$  is the geometrical moment of inertia of the cross-section of the strut, and  $L$  is its length.

Direct measurement of this Euler load is not easy. In principle, it can be measured by adding weights to the top of a vertical strut, and finding the load under which any slight lateral deflection given to the strut is maintained, as in theory this load is only infinitesimally less than the critical load. However, in practice the strut will be neither precisely straight, nor precisely vertical, and it is best to determine the Euler load in a somewhat less direct manner.

### Theory

Consider a strut with an initial radius of curvature  $R_0$  under an end load  $P$  as in Figure 24.1. From beam theory,

$$R_0 = \frac{1}{d^2 y_0 / dx^2} \quad \text{approximately}$$

and the bending moment  $M$  at distance  $x$  from the top is given by

$$M = -Py$$

Using the formula for an initially curved beam,

$$EI(1/R - 1/R_0) = M$$

then

$$EI \cdot d^2 y / dx^2 = M + EI \cdot d^2 y_0 / dx^2$$

or

$$d^2 y / dx^2 + a^2 y = d^2 y_0 / dx^2$$

where

$$a^2 = P/EI$$

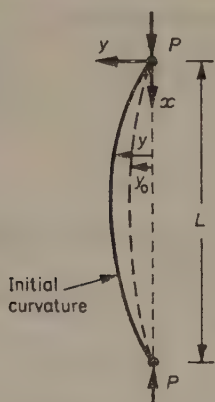


FIGURE 24.1 Deformation of an initially curved, pin-ended strut, under end-loads  $P$ .

The initial shape of the strut  $y_0$  may be assumed circular, parabolic, or sinusoidal without making much difference to the final result, but the most convenient form is

$$y_0 = c \cdot \sin(\pi x/L)$$

which satisfies the end conditions and corresponds to a maximum deflection  $c$ . Any other shape could be analysed into a Fourier series of sine terms. Then

$$d^2y/dx^2 + a^2y = -(c \cdot \pi^2/L^2) (\sin \pi x/L)$$

The complete solution is

$$y = A \sin ax + B \cos ax - \frac{c\pi^2/L^2}{(-\pi^2/L^2) + a^2} \sin \frac{\pi x}{L}$$

When  $x = 0$ ,  $y = 0$ . Therefore

$$B = 0$$

When  $x = L/2$ ,  $dy/dx = 0$ . Therefore

$$A = 0$$

Hence

$$\begin{aligned} y &= \frac{c\pi^2/L^2}{\pi^2/L^2 - a^2} \sin \frac{\pi x}{L} \\ &= \frac{cP_e}{P_e - P} \sin \frac{\pi x}{L} \end{aligned}$$

where the Euler critical load  $P_e = \pi^2 EI/L^2$ .



The deflection of the centre of the strut is

$$y_{\max} = \frac{cP_e}{P_e - P} = \Delta, \quad \text{say}$$

Rearranging,

$$\Delta = P_e \frac{\Delta}{P} - c$$

so that a plot of  $\Delta$  against  $\Delta/P$  gives a straight line of slope  $P_e$ . Such a graph is known as a Southwell plot.

Struts of the same material may be characterized by the term  $I/L^2$ , which may be simplified by expressing  $I$  as

$$I = Ak^2$$

where  $A$  is the area of cross-section and  $k$  is the radius of gyration. The term 'slenderness ratio' is now defined as

$$\text{slenderness ratio} = L/k$$

and the Euler load can be related to this expression.

## Experimental Details

The apparatus, due to J. M. Townson, is illustrated in Figure 24.2. A simple screw jack is mounted at one end of a base. At the other end is a load indicator which consists of a spring with a pointer that moves over a scale calibrated in newtons. On the base between these two items is etched a lateral deflection scale. The scale is a set of parallel lines at intervals of 1 mm. It ranges up to 4 cm on each side of the centre line, and is long enough to cover the mid-span positions of any strut. Different lengths of struts are accommodated by mounting the screw jack at different places on the base, sets of holes being bored in the base for this purpose.

The strut whose Euler load is to be determined must have, or be given, a slight curvature in the absence of any load. It has knife-edge ends, and is inserted between V-slots in pistons in the screw jack and in the load indicator.

The best struts to use are of rectangular section, with the depth much smaller than the width. Provided that the slenderness and initial curvature of the strut are such that a deflection of 2 or 3 cm is obtained at half the Euler load, satisfactory plots can be obtained.

Take rectangular struts of a material with a low Young's modulus (plastic or wood), with slenderness ratios ranging from 100 upwards. Load each strut by increments up to about half the Euler load, and measure the maximum deflection at each increment.

Draw Southwell plots for each strut. Compare the values for the Euler load of the struts of equal slenderness ratio, but different Young's modulus. If necessary, determine the Young's modulus for each strut by a simple four-point bending test, and compare calculated Euler loads with those measured. Divide the measured loads by the Young's modulus, and again compare these results.

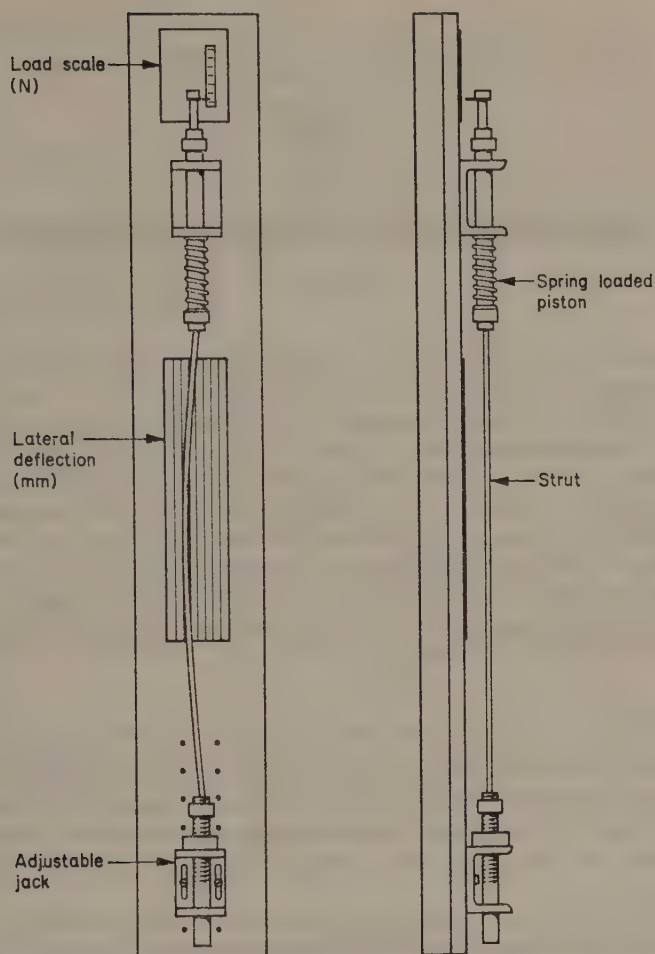


FIGURE 24.2 Townson's apparatus, showing load scale, piston, strut and adjustable jack.

Taking the struts of the same material, plot the measured and calculated Euler loads against the slenderness ratios.

## Discussion

Discuss differences between calculated and measured Euler loads for the different materials and consider how well the ratios  $P_e/E$  agree for the different materials.

Explain the significance of the graph  $P_e$  versus slenderness ratio and discuss how well this graph verifies Euler's theory, accounting for any deviations from the Euler theory.

## *Resistance Strain Gauges*

The resistance strain gauge is one of the most important developments in instrumentation for experimental stress analysis. Invented in the 1930's, it quickly replaced mechanical gauges as the standard means of measuring strains on actual structures and test models. Though other electrical gauges are available, such as the inductive extensometers, the resistance gauge has gained popularity because of its cheapness, versatility, and high sensitivity. It only provides a measure of the linear (normal) strain at one point, but a biaxial strain field may be determined by a combination of three gauges about the same point, and whole structures may be investigated using a large number of gauges to give a fairly complete stress analysis. Measurement can be carried out at one console.

### **Theory**

The electrical resistance strain gauge operates on a principle discovered in 1856 by Lord Kelvin, that when an electrical conductor is strained its resistance varies in proportion to the strain, extensional strains producing for most metals an increase in resistance, compressional strains producing a decrease.

If a conducting wire is bonded to a structure so that strains experienced by the structure are transmitted to the wire, a measure of the wire's change in resistance will give an indication of the surface strain in the direction of the wire.

As the strains experienced by most structural materials in their normal working range are very small, the changes of resistance produced in the wire will also be small, and will require extremely sensitive instrumentation in order to measure them.

The relationship between deformation and change of resistance may be obtained if we consider the case of a current-carrying wire being axially strained.

The resistance of the wire  $R$  is given by

$$R = \rho L / A$$

where  $L$  is the length of the wire,

$A = \pi r^2$  is the cross-sectional area of the wire, and  
 $\rho$  is the resistivity of the wire.

Taking logarithms,

$$\log R = \log \rho + \log L - \log A$$

where

$$\log A = \log \pi + 2 \log r$$

Differentiating,

$$\frac{dR}{R} = \frac{d\rho}{\rho} + \frac{dL}{L} - \frac{dA}{A} = \frac{d\rho}{\rho} + \frac{dL}{L} - \frac{2 dr}{r}$$

But for a cylindrical wire, a longitudinal strain  $e_l = dL/L$  produces a lateral compressive strain

$$e_r = \frac{dr}{r} = -\nu \frac{dL}{L},$$

where  $\nu$  is Poisson's ratio. Therefore

$$\left(\frac{dR}{R}\right) = \left(\frac{d\rho}{\rho}\right) + \frac{dL}{L}(1 + 2\nu)$$

and

$$\left(\frac{dR}{R} / \frac{dL}{L}\right) = (1 + 2\nu) + \left(\frac{d\rho}{\rho} / \frac{dL}{L}\right)$$

According to Bridgman (1929), for metal under hydrostatic pressure

$$d\rho/\rho = c(dV/V)$$

Obviously our stretched wire is not being subjected to hydrostatic pressure, but if we assume that Bridgman's relationship may be applied approximately then we may write

$$\begin{aligned} \frac{d\rho}{\rho} &= c \frac{dV}{V} = c \left( \frac{dL}{L} + \frac{dA}{A} \right) \\ &= c \frac{dL}{L} (1 - 2\nu) \end{aligned}$$

Hence

$$\frac{d\rho}{\rho} / \frac{dL}{L} = c(1 - 2\nu)$$

and

$$\frac{dR}{R} / \frac{dL}{L} = (1 + 2\nu) + c(1 - 2\nu)$$

The right-hand side of this equation gives us a measure of the sensitivity of a given gauge as a strain-measuring instrument and is usually replaced by  $k$ , the 'k-factor' or strain sensitivity factor for a given gauge.

Our basic equation relating change of resistance to strain is therefore

$$\frac{dR}{R} = k \frac{dL}{L} \quad \text{where strain } e_l = \frac{dL}{L}$$

For most metals  $k = 2$ , so the changes in resistance are very small. With gauges constructed from metal wire or foil it is necessary to 'fold' the wire or foil several times so that there is a large number of closely packed parallel

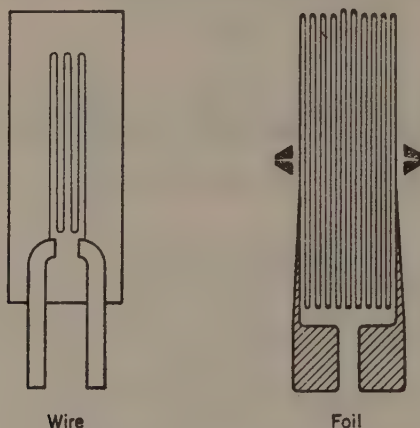


FIGURE 25.1 The standard gauge.

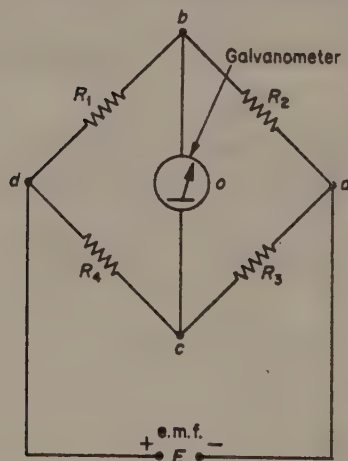


FIGURE 25.2 Wheatstone bridge for measuring resistance changes in a strain gauge.

strips along the axis of the gauge (Figure 25.1). This enables the gauge to have a reasonably high resistance.

The small changes in resistance are measured by a Wheatstone bridge, illustrated in Figure 25.2. There are many modifications to this basic circuit, but all circuits work alike when used in the 'null balance' condition. In this case, no current passes through the galvanometer, and so

$$\frac{R_1}{R_4} = \frac{R_2}{R_3}$$

If  $R_1$  is the gauge resistance, the bridge may be balanced by adjusting  $R_4$  which is usually calibrated in percentage change. Null-balance bridges are only suitable for static measurements. For dynamic work, the bridge is initially balanced, and the out-of-balance current measured.

Usually, two standard resistances ( $R_3$  and  $R_4$ ) are provided in the bridge, their resistance being the same as the strain gauges. This gives maximum sensitivity. The other two resistances are both strain gauges, one stuck on the specimen, and the other stuck to a similar piece of material nearby. This provides 'temperature compensation', an essential factor for obtaining accurate results with this method. As the resistance changes due to strain are so small, expansion or contraction of the specimen due to slight variations in temperature could be read as strain. By having two gauges stuck to the same material at the same temperature (hence putting them close together), any changes in temperature will cancel out, while actual strain in the 'active' gauge (stuck to the stressed specimen) will be over and above that of the dummy gauge (stuck to the similar piece of material).

The circuit may be balanced by a slide resistance wire, connecting the two standard gauges, and which is calibrated in percentage strain. Using this wire, the relative value of the standard resistances is changed, thus balancing the bridge. Any initial mismatch of resistance between active and dummy gauges may be compensated by adjusting the slide wire, or using small rheostats inserted in the circuit.

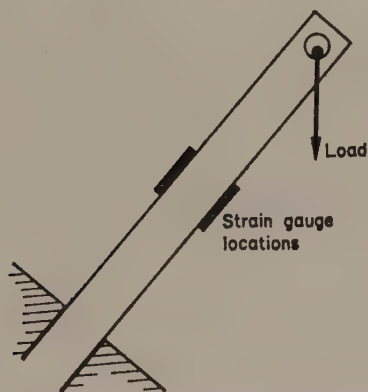


FIGURE 25.3 Tilted cantilever for producing combined bending and normal stresses.

## Experimental Details

If a commercial strain gauge bridge is not available, the student may wire up the Wheatstone bridge as above. Usually, gauges have a resistance of 120 ohm, so the standard resistors must have this value. The applied voltage



should be 2 to 6 volt d.c. A shunt should be placed across the galvanometer for protection during initial adjustments.

The gauges are supplied on a paper or thin plastic backing, with the gauge

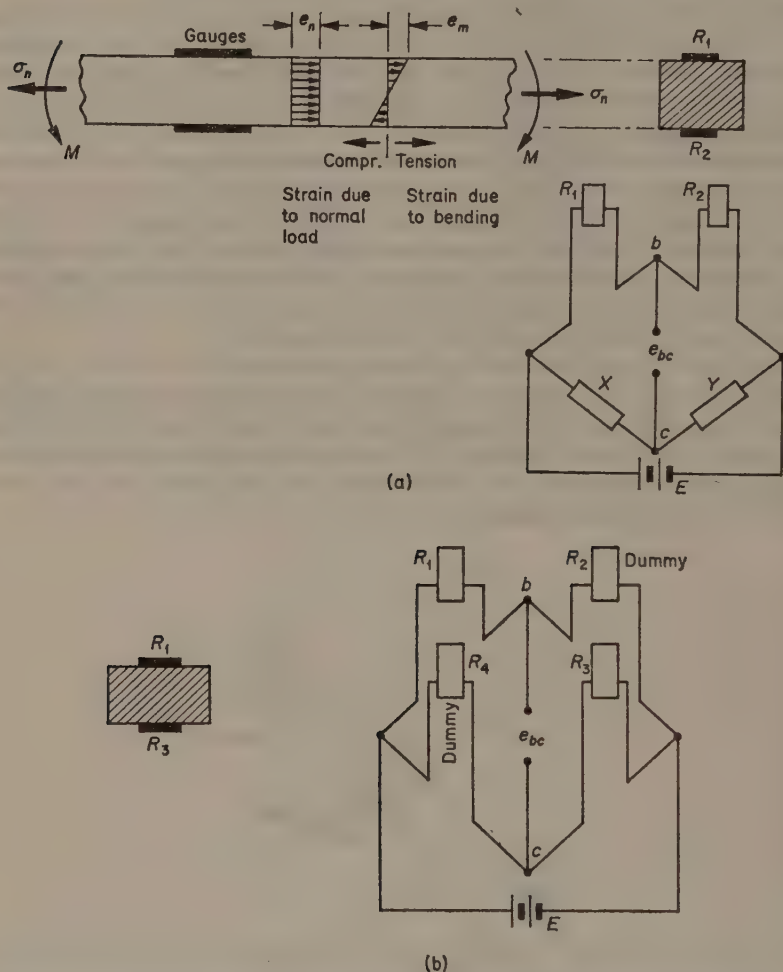


FIGURE 25.4 Wheatstone circuits for separating bending and normal strains (a) circuit for bending only, (b) circuit for normal strains only.

factor quoted by the manufacturer. One centimetre length gauges are the most commonly used, and are suitable for this experiment. Gauges may be cemented to specimens by common glues, such as Seccotine, Durofix, Araldite, etc. It is most important to obtain a very thin layer of cement, and to exclude all air bubbles.

- (i) Using a 2.5 cm wide metal tensile specimen, cement three gauges at  $45^\circ$  to each other, and another three at  $60^\circ$  to each other, making sure no gauge is aligned with the tensile axis. Cement one gauge to a similar piece of metal as dummy. Load the specimen and take the gauge readings.

Using the formula for compound strain, and Mohr's circle, determine the direction of principal strains, and their magnitudes for the  $45^\circ$  and  $60^\circ$  'rosettes' (as the gauge combinations are known). Compare these results with the known values.

- (ii) The construction of the strain gauge bridge make it possible to arrange special circuits to separate certain types of loading, while still ensuring temperature compensation. Arrange for a cantilever to be loaded as in Figure 25.3, with strain gauges cemented on both sides of the beam. The bending strain alone may be measured by attaching the gauges to the bridge as in Figure 25.4(a), and the normal strain alone by the circuit in Figure 25.4(b). In this latter case, the standard resistors must be replaced by two dummy gauges. Load the beam, and measure the changes in resistance using both circuits. Measure the angle that the load makes with the cantilever.

Calculate the normal and bending loads, and hence determine the normal and bending strains in the cantilever. Compare these with the measured strains.

## Discussion

Which type of gauge rosette makes calculation of the principal strains simplest, and which is the most suitable for analysis by Mohr's circle? Suggest a possible method for solving large numbers of rosette results, without doing the full calculation each time. Discuss the effectiveness of the dummy gauge for temperature compensation.

Explain in detail how the two circuits separate normal and bending strains, and comment on their effectiveness, suggesting what errors may arise. Suggest a circuit, involving all four arms of the bridge, for measuring pure torsion.

## *Proving Rings*

In previous experiments we have applied the loading by means of calibrated weights, so that no problem existed with regard to load measurement. When applying loads of several tons or more weights are not very convenient, even when the load is magnified by a lever system. Screw and hydraulic load systems are used nowadays in modern testing machinery to magnify the applied load, which is usually measured directly by connecting a load cell behind the jaws of the testing machine. This direct connection avoids problems due to friction etc., which occur when the load measurement is made elsewhere in the testing circuit.

Load cells are based on deflection or strain measurements using the deformation of a standard block of material, which is loaded in a simple manner so that there is a linear relation between load and deflection. The simplest device is a block of metal with strain gauges on its faces, so that change in length of the block due to applied load is monitored directly.

More sophisticated instruments magnify the deflection so that less sensitive measuring devices, such as dial gauges, can be used. An obvious solution is to use the deflection of a beam, and a proving ring is a particular example of this application. These rings are widely used in load measurements, and are particularly useful because of their compact form and high sensitivity.

### **Theory**

The deflection of a ring under diametral loading is an example of the application of Castigliano's theorem, which allows deflections to be calculated from the strain energy. The theorem states that the deflections (or rotations) of the structure at the point of application of load (or moment) and in the direction of the load equal the partial derivatives of energy with respect to load (or moment) at the points of application. If the strain energy can be calculated, it is fairly simple to find the derivatives. For beams, only the strain energy due to bending is significant, and this is given by the expression

$$\int \left[ \frac{M^2}{EI} \right] ds$$

where the integration is taken along the length of the beam. This expression

also holds for curved beams, provided that the initial radius is large compared with the dimensions of the cross-section.

The ring is illustrated in Figure 26.1(a), with the applied load  $P$  vertical. The bending moment cannot immediately be obtained in terms of  $P$  and  $R$ , but, making use of the symmetry, let  $M_0$  be the bending moment on cross-sections perpendicular to  $P$  (Figure 26.1(b)). There will also be a normal load of  $\frac{1}{2}P$  on these cross-sections.

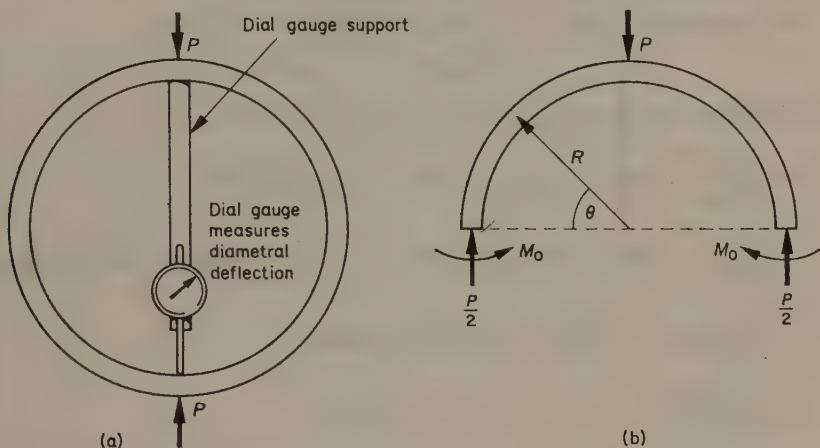


FIGURE 26.1 Loading of proving ring (a) Proving ring under diametral load, (b) Effective loading for half the ring.

At an angle  $\theta$  the bending moment  $M$  is given by

$$M = \frac{1}{2}PR(1 - \cos \theta) - M_0$$

Now

$$\begin{aligned} \text{strain energy } U &= \int \left[ \frac{M^2}{2EI} \right] ds \\ &= 4 \int_0^{\frac{1}{2}\pi} \frac{\{PR(1 - \cos \theta) - 2M_0\}^2}{8EI} R d\theta \end{aligned}$$

From Castigliano's theorem, the rotation of the horizontal cross-section is given by

$$\begin{aligned} \frac{\partial U}{\partial M_0} &= \frac{R}{2EI} \int_0^{\frac{1}{2}\pi} 2[PR(1 - \cos \theta) - 2M_0](-2) d\theta \\ &= 0 \quad \text{by symmetry.} \end{aligned}$$

Hence

$$\int_0^{\frac{1}{2}\pi} (PR - PR \cos \theta - 2M_0) d\theta = 0$$

$$PR\frac{1}{2}\pi - PR - 2M_0\frac{1}{2}\pi = 0$$

$$M_0 = PR \left[ \frac{1}{2} - \frac{1}{\pi} \right]$$

The maximum bending moment occurs when  $\theta = \pi/2$ , and is

$$M = PR/2 - M_0 = PR/\pi \approx 0.318 PR$$

The deflection of the points under the load  $P$  is given by

$$\begin{aligned} \frac{\partial U}{\partial P} &= \frac{R}{2EI} \int_0^{\frac{1}{2}\pi} 2\{PR(1 - \cos \theta) - 2M_0\}(1 - \cos \theta)R d\theta \\ &= \frac{R^2}{2EI} \int_0^{\frac{1}{2}\pi} \{2PR - 4PR \cos \theta + PR(1 + \cos 2\theta) - 4M_0 + 4M_0 \cos \theta\} d\theta \\ &= \frac{R^2}{2EI} [PR\pi - 4PR + PR\frac{1}{2}\pi - 2M_0 + 4M_0] \\ &= \frac{PR^3}{4EI} \left( \frac{8\pi^2}{\pi} \right) \end{aligned}$$

We also need to ensure that the ring is never stressed past the yield point of the material, so that maximum stress must be calculated. This can be done using the basic bending equation for a curved beam, i.e.

$$\frac{\sigma}{y} = \frac{M}{I} = E \left( \frac{1}{R} - \frac{1}{R_0} \right)$$

and substituting the value the maximum bending moment.

## Experimental Details

As the load-deflection equation involves the radius as a cubic term, the rings must be machined carefully. The material properties of the ring, e.g. Young's modulus, should also be constant throughout its length. Annealing is advisable.

Select ten steel rings, with diameters varying from 20 to 30 cm, width 2.5 cm and depth about 1 cm. Five of these rings should have the same diameter, with depths varying from 0.5 to 2.0 cm. The deflection of the rings should be measured by a dial gauge, reading to 0.0001 cm, and a suitable fitting for attaching this to the rings and applying the load, is illustrated in Figure 26.2.

Calculate the maximum permissible applied load for each ring, using a safety factor of 0.5. Load each ring in turn to its maximum (a testing machine



of several kilonewtons capacity will be necessary) and plot the load versus deflection curves. Calculate the standard deviation, or otherwise estimate

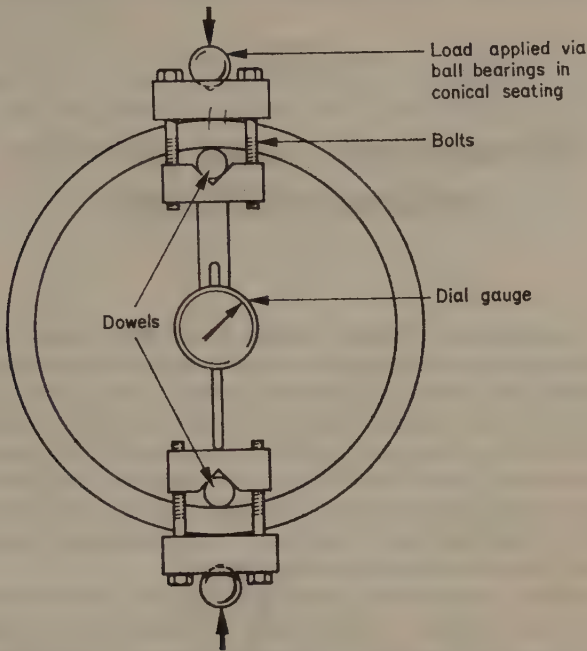


FIGURE 26.2 Attachment of dial gauge to proving ring.

the linearity of this graph. Choose a load common to all the rings of varying diameter, and plot deflection versus cube of the radius. Repeat this process for rings of common radius, but plot load against the reciprocal of the depth cubed.

## Discussion

Observe any significant non-linearities in the plotted graphs, and suggest reasons for these. Suggest any metallurgical parameters that may affect a ring's performance over a period of time. Discuss the accuracy of the load measurements and suggest a suitably precise method for quickly converting deflection to load.



---

## ***Structural Analysis by Indirect Models***

The direct determination of stresses from a model of an actual structure will depend on the various scaling factors involved between the model and structure parameters. The relations between applied forces, stress, strain, displacements, etc. can be obtained from dimensional analysis, which give the 'laws of similitude' between the model and structure. For a static problem these laws show that there are only two independent scale factors, which severely restricts the choice of model parameters. It is virtually impossible to build a model to such stringent requirements, and in practice a considerable variation from these conditions must be tolerated.

If the model is to simulate the elastic behaviour of a frame structure, then the indirect model method is most useful. In this method, only the basic geometry of the model is scaled to the structure, and the loading is applied by arbitrary deformations. The deflections of the model are proportional to its influence lines, from which the bending moments, shear forces, etc. and hence stresses may be calculated. For complicated redundant structures, this method has been used as an effective design tool, but now it can be replaced by numerical procedures of solution using digital computers.

### **Indirect Model Analysis**

Influence lines are curves that show the variation of reaction, bending moment or shear force at a point in a structure as a load moves across it. For a given load, a structure will possess any number of influence lines, depending on the section under consideration.

The experimental determination of influence lines is based on the Maxwell reciprocal theorem and the Muller-Breslau theorem. Maxwell's theorem states that the deflection of an elastic structure at point *A* due to an applied load at point *B* equals the deflection of the beam at point *B* when the same load is moved to point *A*. The directions of load and displacement must correspond for this theorem to hold, but in most applications the directions are either vertical or horizontal.

Muller-Breslau postulates that in a statically indeterminate structure the deflection of the centre line of the structural components, produced by

displacing one of the supports in the direction of a redundant reaction, defines the influence line for that reaction to some scale. This theorem also applies to rotations and shearing displacements (produced by cutting the frame) made on the frame.

The application of these theorems is best explained by reference to a simple indeterminate structure. Consider the propped cantilever in Figure 27.1(a). We wish to determine the influence line for the support reaction  $R$ ,

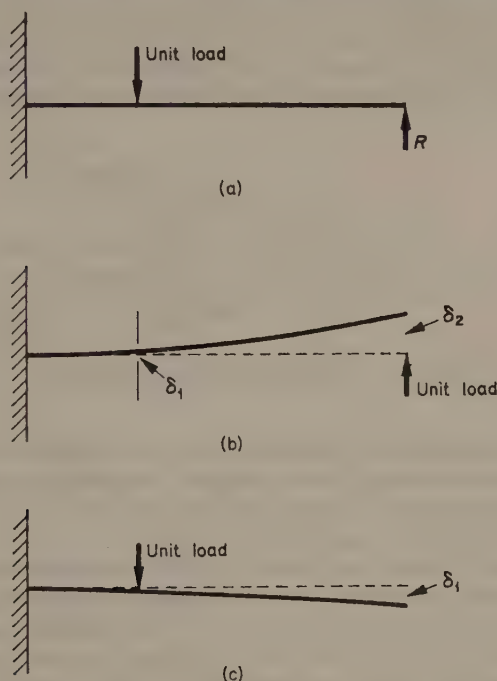


FIGURE 27.1 Application of indirect model theorems to a propped cantilever, (a) Propped cantilever with unit load in position, (b) Support removed and replaced by unit load, (c) Deflection of beam due to the unit load in its original position.

i.e. we wish to find the curve showing the variation of the reaction  $R$  when a load (taken as unity in value) is moved across the cantilever. The support is removed, and replaced by the unit load in Figure 27.1(b) and this produces a displacement  $\delta_2$  and a corresponding displacement  $\delta_1$  at the original position of the unit load, which can be taken as anywhere along the beam. From Maxwell's reciprocal theorem, the deflection  $\delta_1$  equals the deflection at the end of the beam (with the support removed) when the unit load is replaced at its original position, as in Figure 27.1(c). But this deflection is zero when the support is in position, due to the applied load  $R$ , and as a unit load produced

deflection  $\delta_2$  at this position, the reaction would produce a deflection  $R\delta_2$ . Thus the two opposing deflections cancel out, giving

$$R\delta_2 = \delta_1$$

$$R = \delta_1/\delta_2$$

By measuring the deflections of the beam along its length, and dividing by the displacement due to the unit load applied to the end of the beam, we obtain the influence line for  $R$ . Experimentally this procedure is very simple, and any number of supports can be introduced without increasing the labour.

The same principle can be applied to the determination of bending moments and shear forces, but this is more difficult in practice as arbitrary rotations and

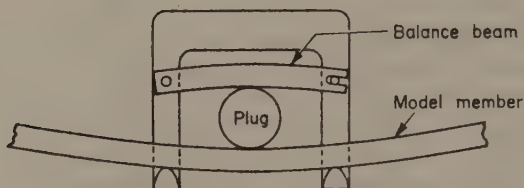


FIGURE 27.2 Bending moment deformer.

shear displacements must be introduced into the structure. Special deformers have been introduced for this purpose, for use with models using thin plastic strips which make it unnecessary to cut the structure. A bending moment deformer is illustrated in Figure 27.2.

The method is quite accurate providing (a) the structure is linearly elastic, (b) there are no stability effects, and (c) there is no gross change in geometry under load. This latter point infers that all the displacements are small, which experimentally is not convenient. For most structures, it is possible to use displacements that can be measured easily with a ruler without introducing significant errors. Plastics are the most convenient model materials because of their low modulus, but they also creep considerably at room temperature. For accurate work this can be overcome by applying the displacements through creep compensators, which are made of the same material as the model.

## Experimental Details

The propped cantilever is an ideal subject for study, as it is basically simple and several supports can be added quite easily. The beam can be a Perspex strip, at least 30 cm long, about 3 mm thick, and 1 cm wide, or a thin metal strip about 0.1 mm thick may be used if available. The strip must be clamped firmly between two metal jaws, which are mounted on a pivot and slotted into a drawing board so that the edge of the beam is against the board, as in Figure 27.3.

The first set of experiments will determine the influence lines for the support reactions as already described.

Fix the pivot rigidly in its mount, and first determine the influence line for the reaction of a single support placed at the beam's free end. The arbitrary displacement can be made by knocking panel pins into the board to support the beam. The deflected shape is best drawn on graph paper, which is pinned on the board prior to loading. The centre line of the beam should really be drawn, but as the beam is thin, its bottom or top may be used. It is also more accurate to deflect the beam by equal amounts above and below the

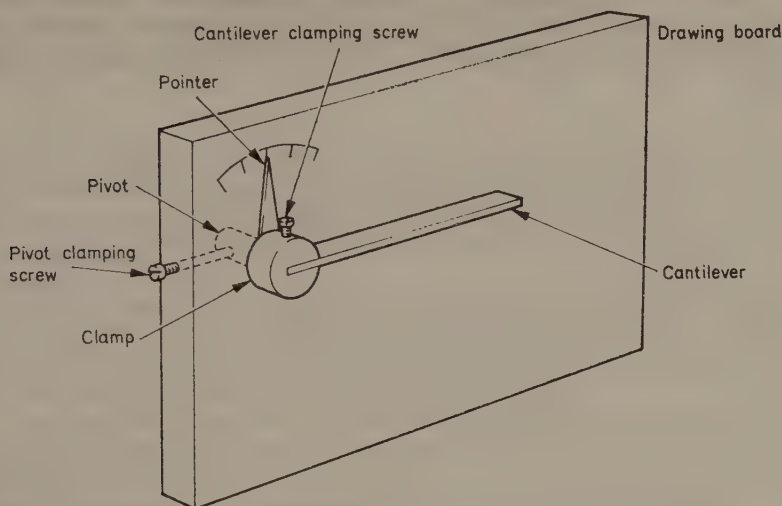


FIGURE 27.3 Arrangement of the cantilever on a drawing board.

neutral position. The displacements are then measured between the two deflected positions.

Next add a further support to the centre of the beam, and measure the influence lines for the reactions in each support whilst the other is in position. The supports may be fixed by using panel pins on either side of the beam, but make sure the fixing is firm.

Finally, determine the influence line for the bending moment at the encastre end of the beam with only a single support at the other end. In this case, the pivot clamp must be released and the clamp given an arbitrary rotation. This may be measured by fixing a long pointer to the clamp. The bending moment at the clamp due to a unit load moving along the beam is given by the ratio of beam deflection divided by clamp rotation (measured in radians).

Plot the influence lines for each of the three cases tested. The reaction and bending moment for the single support cases can be calculated fairly simply, as the deflection at this point must always be zero. Obtain the expression for the deflection of the free end due to unit load a distance  $x$  from the clamped end, and equate this to the expression for deflection due to a load  $R$  supporting

the end of the beam. This will yield  $R$  in terms of the beam constants (length, modulus, moment of inertia) and the distance  $x$ , and the influence line for  $R$  can be calculated. Use this expression to determine the bending moment influence line, and compare both calculated results with experiment, by plotting about six calculated results on the experimental graphs.

## Discussion

Discuss what sources of error may be significant in your experimental results, and why it is more accurate to measure displacements between beams deflected in opposite directions. Suggest how you would use influence lines to determine maximum stresses in your structure, and hence aid the design process.



---

## ***The Photoelastic Method of Stress Analysis***

Many transparent materials that in an unstressed state are not naturally double-refracting become so under the influence of stress. Such an effect is known as artificial or stress birefringence, and the magnitude of the optical effect produced by stress is usually a direct linear function of the stress magnitude.

The first recorded investigation of this effect was made by Sir David Brewster, who discovered that a simply loaded plate of glass exhibited the double refraction effects normally associated with a uniaxial crystal, the axis of load being equivalent to the crystal's optic axis.

The theoretical treatment of this phenomenon was developed independently by both Neumann and Maxwell, although Neumann related the optical effects to strain, whereas Maxwell expressed his equations in terms of stress. Whether, in fact, the observed phenomena are strain-based or stress-based only becomes of importance, however, when problems of a non-elastic nature are considered.

The use of photoelastic models for the stress analysis of structures by analogy was first developed into a practical technique by Coker and Filon, who in over twenty years of research at University College, London, laid the foundation of modern methods of photoelastic stress analysis. Their classic treatise on the work done during this period is still the most authoritative publication in this field.

### **The Optical Basis of the Photoelastic Effect**

It is convenient for our purposes to consider light as a transverse electromagnetic vibration. Visible light has a wavelength between approximately 4000 and 8000 Å ( $1 \text{ Å} = 10^{-8} \text{ cm}$ ).

Normal light is unpolarized in that there is no predominant plane of vibration for the electric vector of the wave. Light can be polarized however, by successive reflections or refractions at critical angles, by electrostatic or electromagnetic fields, or by passing the light through various types of



crystal. Modern practice, however, is to use 'Polaroid' sheet, a very efficient polarizing medium, which can be considered as acting on randomly vibrating light waves in the manner shown schematically in Figure 28.1. When light polarized in this way passes through a transparent substance that exhibits stress birefringence, it is split into two orthogonally polarized components, each parallel to a direction of principal stress. These components propagate

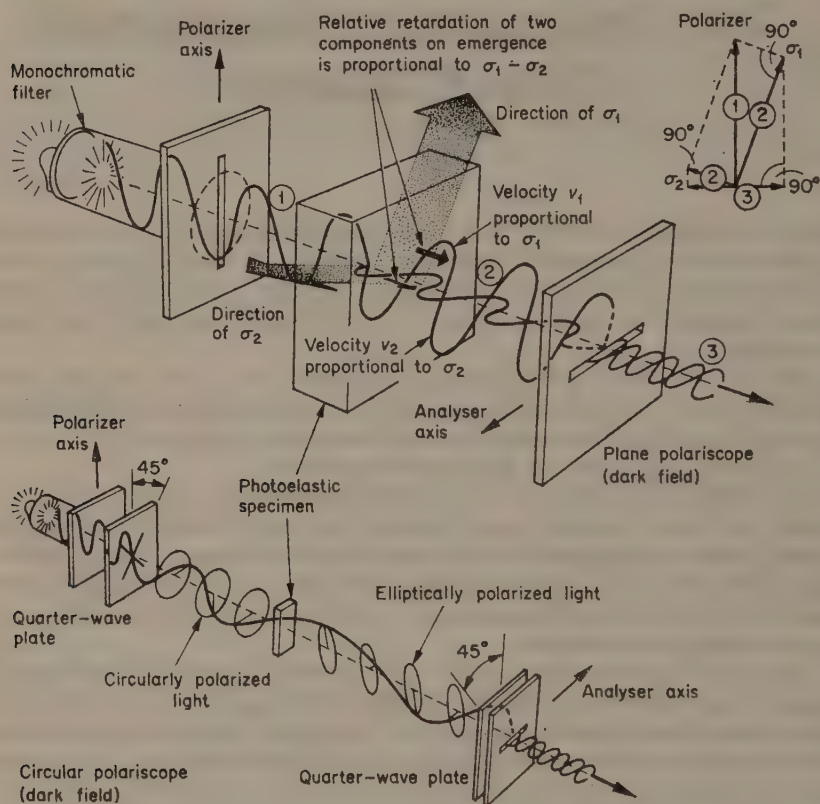


FIGURE 28.1 The photoelastic effect—plane and circularly polarized light.

through the material at different velocities. For light of a fixed wavelength (monochromatic light), the velocity of each of the components is proportional to the magnitude of the principal stress lying in its plane of vibration, i.e.

$$V_1 \propto \sigma_1; \quad V_2 \propto \sigma_2$$

Thus, on emerging from the photoelastic medium, the two components will have suffered a relative change of phase or 'relative retardation' that will be

proportional to  $(V_1 - V_2)$ . But as  $(V_1 - V_2)$  is in turn proportional to  $(\sigma_1 - \sigma_2)$  we can express the relative retardation  $\delta$  as

$$\delta = Ct(\sigma_1 - \sigma_2) \quad (28.1)$$

where  $C$  is the stress-optic coefficient and  $t$  is the thickness of the specimen.

If we view the emergent light through another sheet of Polaroid crossed with the first and called an 'Analyser' (Figure 28.1), we see only the horizontal components of these two rays. When the relative retardation is such that the two components are vibrating exactly in phase with one another, mutual extinction will occur, producing a black fringe for every point in the photoelastic structure which has a similar value of principal stress difference  $(\sigma_1 - \sigma_2)$ , assuming that  $C$  and  $t$  in equation (28.1) are constant over the structure.

A full mathematical analysis of the plane polariscope system shown in Figure 28.1 shows that, for light of a given wavelength  $\lambda$ , the transmitted intensity of light emerging from the analyser is proportional to

$$\sin^2 2a \sin^2 \frac{\pi t}{\lambda} (n_1 - n_2) \quad (28.2)$$

where  $a$  is the angle between direction of vibration of polarized light and principal stress  $\sigma_1$ ,  $t$  is the thickness of photoelastic medium,  $\lambda$  is the wavelength of monochromatic light, and  $n_1$  and  $n_2$  are the refractive indices of the two components vibrating in the directions of  $\sigma_1$  and  $\sigma_2$  respectively ( $n_1 = V/V_1$ ,  $n_2 = V/V_2$ , where  $V$  is the velocity of light in air).

Thus we can see that there are two conditions for extinction (zero intensity) of the emergent light.

- (i) Everywhere on the photoelastic structure where  $a = 0^\circ$  or  $90^\circ$  (i.e. either  $\sigma_1$  or  $\sigma_2$  aligned with polarizer axis), extinction will be produced irrespective of the particular wavelength of light being used. Thus a black fringe will be seen across the structure wherever the above conditions apply. This fringe is called an isoclinic, and it gives us the locus of points in the structure at which the principal stresses have a given direction (that of the polarizer and analyser axes). Hence by rotating the structure relative to the polarizer and analyser and so bringing the isoclinic fringe to a given point, it is possible to determine the directions of principal stresses at every point on the structure.
- (ii) Extinction of emergent light will also occur when

$$(\pi t/\lambda)(n_1 - n_2) = 0 \quad \text{or} \quad i\pi \quad i = 1, 2, 3, \dots$$

But  $t(n_1 - n_2) = \delta$

where  $\delta$  is the optical path difference or relative retardation of one component on the other. Therefore the condition for extinction is given by

$$\frac{\pi \delta}{\lambda} = 0 \quad \text{or} \quad i\pi \quad (28.3)$$

or  $\delta = 0 \quad \text{or} \quad i\lambda$

Thus when the difference in optical paths of the two components is zero or an integral number of wavelengths, extinction will occur for a given wavelength  $\lambda$ . Note that

$$\begin{aligned}\delta &= t(n_1 - n_2) \\ &= t \left( \frac{V}{V_1} - \frac{V}{V_2} \right) \\ &= Vt \left( \frac{V_2 - V_1}{V_1 V_2} \right) \\ &\simeq \frac{Vt}{V_0^2} (V_2 - V_1)\end{aligned}$$

where  $V_0$  is the velocity of the wave in the unstressed medium,  $V$  is the velocity of the wave in air, and  $V_1$  and  $V_2$  are the velocities of the wave in the planes of  $\sigma_1$  and  $\sigma_2$  as previously defined. But in equation (28.1) we have already defined relative retardation  $\delta$  as equal to  $Ct(\sigma_1 - \sigma_2)$  so we see that as  $(\sigma_1 - \sigma_2)$  and hence  $(n_1 - n_2)$  increases in magnitude from zero there will be successive extinctions at equal intervals, producing fringes of zero, first, second, third order, and so on. These fringes are called isochromatics and provide a means whereby the principal stress difference or maximum shear stress  $\frac{1}{2}(\sigma_1 - \sigma_2)$  may be determined.

If, instead of using monochromatic light, we use white light, we see that as isoclinics are independent of wavelength, they will still be seen as black fringes. Isochromatics, however, being dependent on wavelength (equation 28.3), will appear coloured in white light, the colour being given by the complementary colour observed in white light when that particular wavelength is removed by the process described in (28.2).

If we observe, in white light, a linearly increasing stress-gradient such as can be obtained with a cantilever, the colour sequence, starting with black (which we may term a 'zero-order' isochromatic), will be as shown in Figure 28.2. It will be noted that as we obtain higher order isochromatics their tint changes, as there is more than one value of  $i$  that will give extinction in a higher order spectrum. For instance, if  $\delta$  is 30 000 Å,  $\lambda (= \delta/i)$  can equal 7500, 6000, 5000, 4280, and 3750, producing five separate extinctions in the visible spectrum.

In very high orders (7 or 8) the spectrum will be interspersed at even intervals with extinction bands from one end to the other, the net effect to the human eye being indistinguishable from normal white light. Thus as fringe orders increase, the fringes become more and more pale and eventually 'wash out' completely if white light is used. If monochromatic light is used, of course, no such barrier exists to the observation of high order fringes.

To sum up, in plane-polarized white light we observe both isoclinics (black fringes) and isochromatic (coloured fringes).

If the photoelastic structure is rotated in relation to polarizer and analyser, the isoclinics will move (relative to the structure) but the isochromatics will not. The movement of the isoclinics across the structure is used as a means of

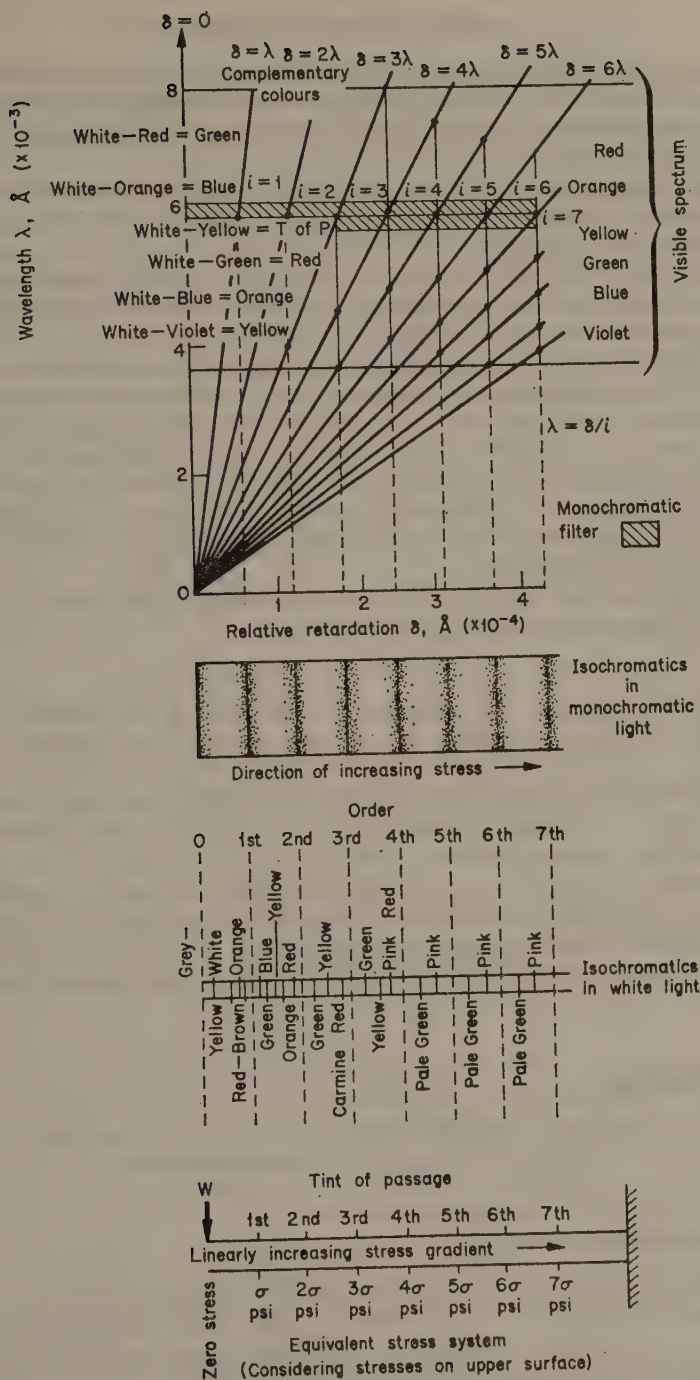


FIGURE 28.2 The use of white light in photoelasticity.



determining the direction of principal stresses at a point. The isochromatics are used to determine the magnitude of the principal stress difference or maximum shear stress at a point, as each colour observed corresponds to a certain stress magnitude (Figure 28.2).

Accurate measurements of stress magnitudes are made by means of various compensation techniques, either goniometric (Tardy or Senarmont) or by using optical compensators.

In many cases it is found more convenient to use circularly polarized light when determining stress magnitudes. A circularly polarized polariscope arrangement is shown in Figure 28.1.

Two quarter-wave plates are inserted as shown with their fast axes crossed and at  $45^\circ$  to the polarizer and analyser axes. The first  $\lambda/4$  plate splits the plane-polarized light into two orthogonal components of equal magnitude, out of phase by a quarter of a wave-length. The resulting electric vector produced by these two components thus rotates in a circle as shown schematically in Figure 28.1. On passing through the structure, the light is in general elliptically polarized as shown, and is then finally resolved by the second  $\lambda/4$  plate and analyser.

A full mathematical analysis of the system shows that the intensity of light emerging from such a system is zero when

$$t(n_1 - n_2) = 0 \quad \text{or} \quad i, i = 1, 2, 3, \dots$$

This is the condition for isochromatics and thus in the circular polariscope the isochromatic pattern can be seen without the superposition of isoclinics.

In order to return to plane-polarized light, the  $\lambda/4$  plates are simply removed from the system. It should be noted that when white light is used in conjunction with the circular polariscope, then because the quarter-wave plates correspond to  $\lambda/4$  for only one specific wavelength, the rest of the spectrum on either side of this wave-length will be elliptically polarized to a greater or lesser extent. As long as quantitative readings are taken relative to the colour corresponding to this particular wavelength, the readings will still be valid.

## Applications

The photoelastic method will be used to study a tensile specimen, a beam under four point loading, and a tensile specimen with a hole.

## Experimental Details

If a polariscope is not available, a simple instrument may be constructed from two pieces of Polaroid, two quarter-wave plates (also available from the Polaroid Corporation), a one metre V-type optical bench with four saddles, and a simple loading frame that can sit astride the bench, as shown in Figure 28.3. Two 7.5 cm diameter 15 cm focus plano-convex lenses, a projection

lens (an enlarging lens will do for this), a screen, and a 500 W projector lamp in its housing complete the equipment.

The Polaroid should be cemented to the two plano-convex lenses, which should be mounted in holders capable of rotating about the optic axis, and which are calibrated in degrees, the zero position corresponding to the polarizing axis. The lenses should be placed on either side of the loading frame, with the Polaroid facing the frame. The projector lamp is placed at the focus of one lens to produce collimated light, and the projector lens and screen are placed on the same side of the other plano-convex lens, their positions being adjusted to give a sharp image of the model in a frame of suitable size. The quarter-wave plates are inserted with their fast axis at  $45^\circ$  to the Polaroid axis (and between the Polaroid and model) and mounted on separate saddles, so that they can be easily removed.

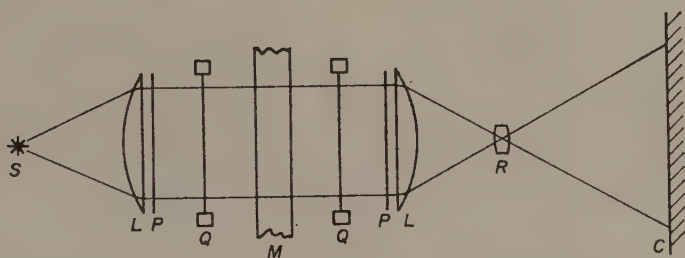


FIGURE 28.3 Optical system of polariscope: *S* is the projection lamp, *L* are plano-convex lenses, *P* is a Polaroid, *Q* are quarter-wave plates, *M* is a model, *R* the projection lens and *C* the screen.

The models may be constructed from epoxy resin or polyurethane. Cast sheets of epoxy resin may be obtained commercially. The models, which should be 6 mm thick, may be cut to the relative dimensions shown in Figure 28.4. All cutting should be done on a band-saw with a carefully filed finish to prevent residual stresses due to overheating. Similarly, all holes should be drilled under size and then reamed out.

The specimens should be about 6 mm thick and 13 mm wide (allowing extra width at the ends of the tensile specimen for attachment to loading frame). These dimensions are important, to avoid torsional effects and to obtain a reasonable number of fringes.

First examine the tensile specimen under increasing load, observing the isochromatics only. Note the relation between colour and load, and so obtain the 'fringe factor' (load necessary to produce one fringe) for the material you are using. In white light, the position of a fringe may be taken as the region between the red and blue parts of the spectrum, known as the 'tint-of-passage'.

Next observe the isochromatic fringe pattern in the region of the beam undergoing pure bending, and sketch this pattern when there is sufficient load to produce at least three (and preferably more) fringes in the field of view.



Remove the quarter-wave plates, and rotate the polarizer and analyser together to observe the positions of the black isoclinics, again restricting your observations to the region of pure bending only.

Finally observe both isochromatic and isoclinic patterns for the tensile specimen with a hole drilled in its centre. Sketch the isochromatic pattern around the hole when the load is sufficient to produce at least three fringes, and also the isoclinic pattern when the polarizer axis is parallel to the tensile axis.

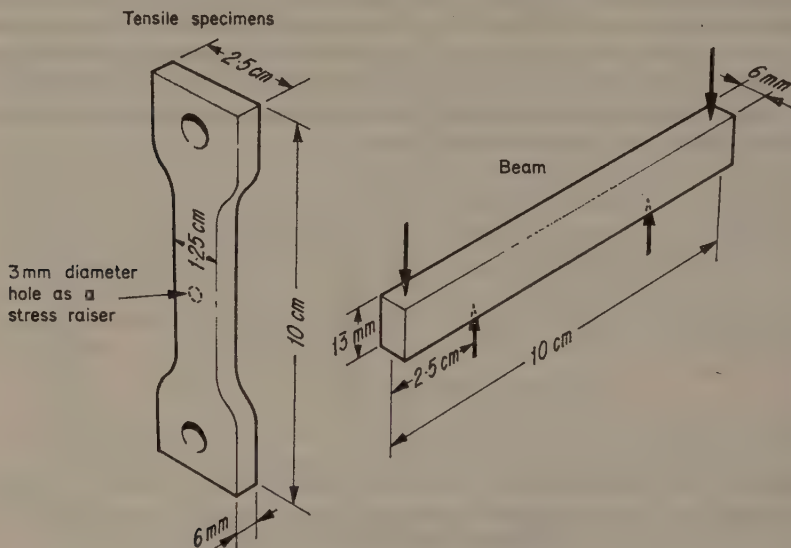


FIGURE 28.4 Dimensions of photoelastic models.

Compare the fringe patterns obtained from the tensile specimen and beam with the patterns you would expect from the stress distribution in each of them (remember that isochromatics are contours of maximum shear stress, and that isoclinics represent points where the principal stress directions are parallel to the polarizer and analyser directions).

Examine your sketches of the 'hole' specimen, and locate the position of largest maximum shear stress. Now examine the isoclinic pattern, and determine the principal stress directions at this point (these directions can also be inferred from the specimen geometry—how?) From this information determine the values of the principal stresses, and hence the stress concentration factor (i.e. the ratio of maximum principal stress around the hole to the mean tensile stress).

## Discussion

Discuss the usefulness of the photoelastic method for experimental stress analysis. Suggest one possible method for determining the values of each principal stress from photoelastic data.

## *Measuring Deflections by the Moiré Effect*

The Moiré effect is the name given to the fringe patterns observed when two straight-line grids are placed in contact, but not accurately aligned. The effect is very common in everyday objects, such as loosely woven cloth, sets of railings, television, etc.

The phenomenon has been known for a long time, but it is only in the last two decades that any attempt has been made to use it in technology. In experimental stress analysis it has been utilized to measure surface strains, flexure and deflection of plates. This experiment, which requires the minimum amount of equipment, will demonstrate the latter.

The effect is illustrated in Figure 29.1(a), where two grids of slightly different pitch are aligned with their grid lines parallel. This produces fringes parallel to the lines where the lines of one grid obstruct the spaces of the other grid. Thus the fringes represent the difference of one pitch between each grid, i.e. a fringe occurs when one grid 'catches up' on the other by one line. Measurement of the fringe spacing gives the difference between the two pitches. A similar effect occurs when two grids with identical pitches are misaligned as shown in Figure 29.1(b). A more general Moiré pattern is made up of a combination of (a) and (b).

### **Theory**

Deflections are measured by projecting a grid onto a diffuse reflecting surface, and then observing the shadow of the grid through a similar grid. This is achieved quite simply by placing a grid in close contact with the specimen and illuminating it with light at an angle  $i$  to the normal, thus projecting the grid onto the surface. If viewed normally, then any variations in the depth of the specimen beneath the grid will produce a fringe pattern, as illustrated in Figure 29.2. From this diagram, we see that the fringes represent contours of constant displacement, where the contour interval is

$$h = p/\tan i$$

where  $p$  is the grid pitch.

Using a grid of 100 lines/cm and an illuminating angle of  $20^\circ$ , the contour interval is 0.025 cm which is a useful range for beam and plate problems.

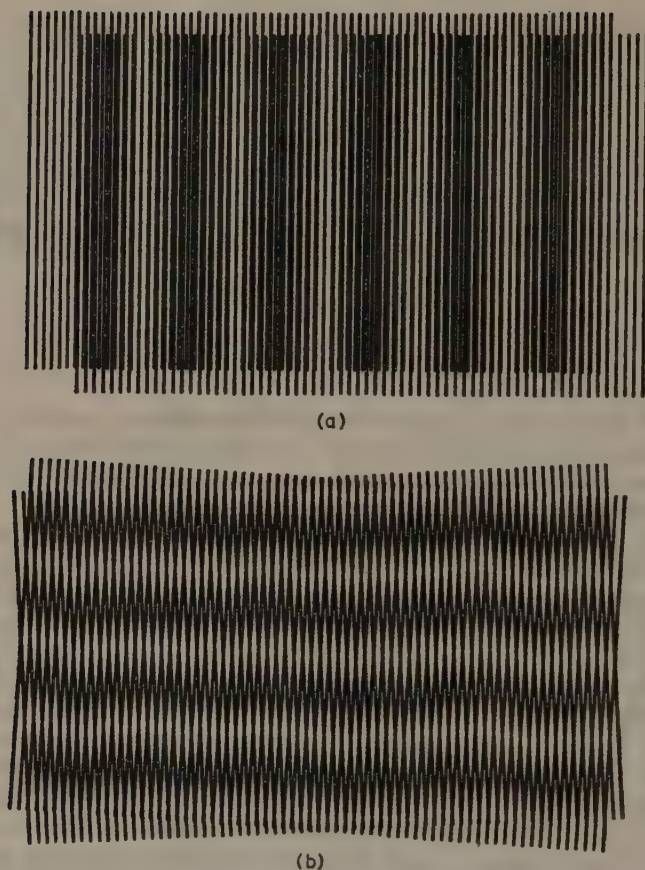


FIGURE 29.1 Examples of the Moiré effect (a) parallel grids and (b) misaligned grids.

### Applications

This technique will be used to examine the variation of the anticlastic effect for beams of different thickness. For deep beams, the lateral contraction and expansion due to the Poisson effect produces a lateral curvature that is opposite to the longitudinal curvature (Figure 29.3(a)). As the strains are related by

$$e_z = -\nu e_x \quad \text{where } \nu \text{ is Poisson's ratio}$$

then

$$\frac{1}{R_z} = -\nu \frac{1}{R_x} \quad \text{where } R \text{ is the radius of curvature.}$$

As the beam becomes thinner, the anticlastic effect is restricted to the edges of the cross-section (Figure 29.3(b)), as a uniform anticlastic curvature is not energetically possible (the beam should now be treated by plate theory). In this case, a small element at the centre of the beam must be subjected to

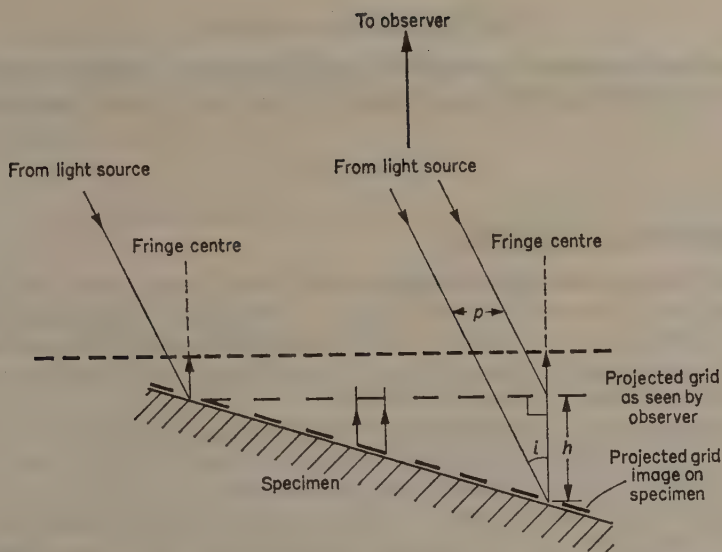


FIGURE 29.2 Principle of the Moiré 'shadow' method: each fringe position corresponds to an increase of one pitch ( $p$ ) between the light-source ray and the camera ray, so that the fringes are contours of constant depth  $h$  from the grid.

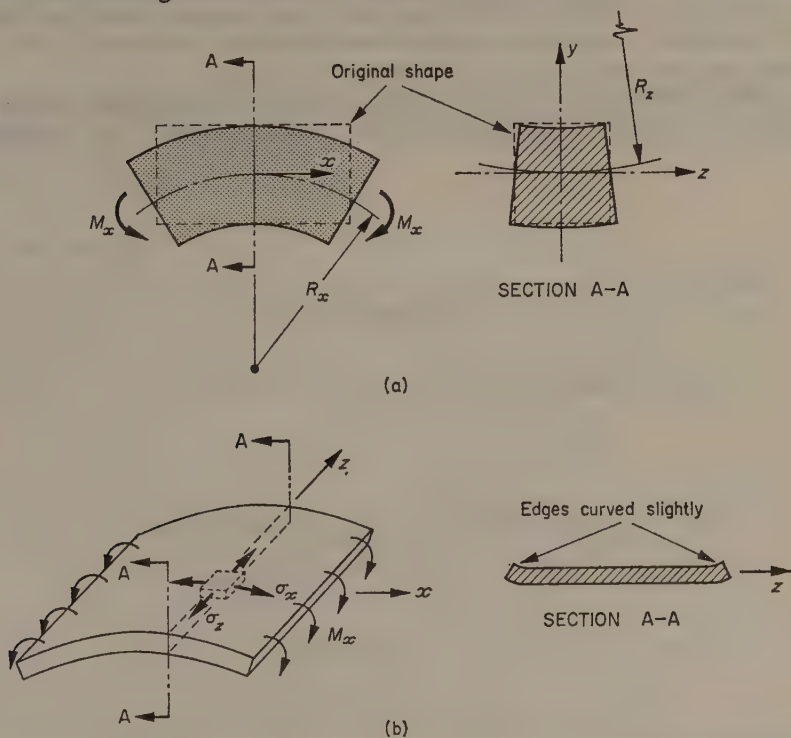


FIGURE 29.3 Anticlastic effects (a) anticlastic curvature in thick beam caused by bending, (b) bending of a thin, wide plate.

greater bending stresses to counteract the Poisson effect, and this produces an apparent increase in the beam stiffness of  $1/(1 - \nu^2)$  if simple beam theory is used.

## Experimental Details

Use six Perspex rectangular-section beams, about 20 cm wide with depths ranging from 5 cm to 1 mm. Paint the top surface with a matt white finish, and load the beams to obtain a section under pure bending. The surface of this section should be flat to within  $5 \times 10^{-3}$  cm, and if necessary these surfaces should be machined beforehand.

A Ronchi grating, with between 80–120 lines/cm should be placed on top of the beam, and illuminated with a Photoflood bulb at least 60 cm away, and about  $30^\circ$  to the specimen normal. The surface should be observed normally, either with a camera, or a cathetometer with which measurements can be made directly. It is not necessary to shut off any other lights, providing they are a considerable distance from the experiment. The lighting should be adjusted to get the best possible fringes, but try to keep the angle as large as possible.

As the angle of the illumination cannot be determined directly, an initial calibration test must be done using a beam of similar dimensions to the test pieces but machined with a 200 cm radius of curvature.

If this is placed in position with the grid on top, a reasonable number of fringes will appear and the illumination may be adjusted for maximum

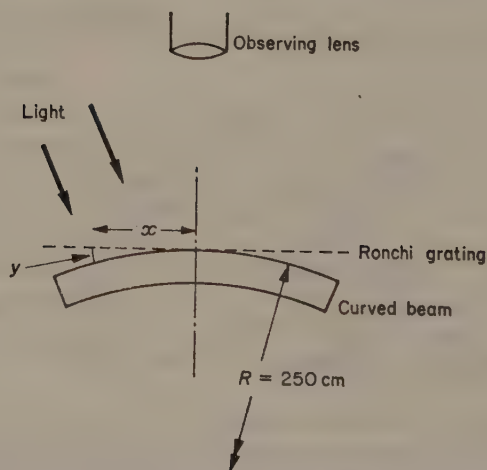


FIGURE 29.4 Geometry of a circular beam for calibrating Moiré-apparatus.



fringe contrast. The fringe separation can be measured and as the deflections lie on a circular arc, Figure 29.4, the depth at any point along the beam can be calculated from the formula

$$2Ry = x^2$$

where  $x$  is the distance along beam from uppermost part of arc, but

$$y = Nh = N \frac{p}{\tan i}$$

where  $N$  is the fringe order, or integer.

Thus by plotting  $N$  against  $x^2$ , we get a straight line graph of slope  $\tan i/2Rp$ , so that  $\tan i$  can be calculated.

The deepest beams will have to be loaded up to maximum bending stress to obtain any fringes at all. Sketch the fringe pattern for each beam, and measure the fringe positions along the centre and the two edges of each beam. The shallow beams should be loaded to obtain a reasonable number of fringes not more than twenty.

Remembering that pure bending produces a circular deflection, use the measurements along the beam to calculate  $R_x$ , and hence the value of Young's modulus for each beam, from the simple bending equation

$$E/R_x = M_x/I$$

For the deepest beams only, calculate the transverse curvature using the three measurements made on any one fringe and assuming that this transverse curvature is circular. Compare the two radii of curvature to find a value of Poisson's ratio.

## Discussion

Comment on the variation of Young's modulus that you obtain, and also on the Poisson ratio value. Do your stiffness values increase by as much as  $1/(1 - \nu^2)$ ?

What further uses do you foresee for this application of the Moiré effect?



## ***Brittle Lacquer Methods***

If a structure is coated with certain types of lacquer which harden into a very brittle thin coating, then when the structure is loaded cracks will appear in the coating in a direction perpendicular to the greater principal tensile stress. The distribution of cracks will indicate graphically the directions of the surface stresses and will show up areas of stress concentration. At this stage it is common practice to use the information obtained as a means of determining where to put strain gauges, which are then used to determine the actual strain magnitudes. However, provided that the lacquer is applied under closely controlled conditions, it is possible to determine approximate values of principal stress magnitude from the load level at which individual cracks are initiated.

There are a number of materials which can be classed as brittle lacquers and, in general, they possess the following properties:

- (a) they develop well-defined cracks at strains below the yielding strain of the structure;
- (b) the cracks, once developed, remain open when the straining load is removed;
- (c) the initial cracking response to strain is independent of the thickness of the coating within reasonable limits;
- (d) the density of the cracks at a given strain varies with the thickness of the coating—the thicker the coating, the fewer the number of cracks per centimetre for a given strain;
- (e) the coating does not flake at reasonable strain levels.

A wide variety of lacquers are suitable for this work, and even whitewash is used in some engineering works to detect any large plastic strains in structures. Unfortunately, most lacquers are very sensitive to changes in temperature and/or humidity, and this makes their quantitative use extremely difficult. They detect only tensile strains, but this problem may be overcome by pre-loading compressed specimens prior to the lacquer application, hence detecting the apparent tensile strains on unloading.

Despite these difficulties, the brittle lacquer technique is a widely used tool in machine stress analysis and, combined with resistance strain gauges, it can solve many practical stress analysis problems, particularly on curved surfaces which are difficult to analyse.

## Application

A brittle lacquer will be used to examine the effect of stress raisers, such as holes and notches, in Perspex models. Any model may be used, but useful examples are provided by stress distributions near a hole and a notch in tensile specimens. An attempt should be made to obtain quantitative measurements by spraying a Perspex cantilever with lacquer for use as a calibration bar.

## Experimental Details

A useful lacquer is made up as follows:

160 g LiOH, H <sub>2</sub> O	} to make about 800 ml solution.
480 g H <sub>3</sub> BO <sub>3</sub>	
454 g distilled water	
0.7 g Na fluoresceinate	

The result is lithium tetraborate, as developed by Hickson at the Royal Aircraft Establishment who states 'Ingredients should be the purest obtainable, and all vessels should be very clean and free from crystallization nuclei.

The lithium hydroxide is added to the water at 60 °C and stirred until most has gone into solution. Add the boric acid while stirring vigorously, continuing the agitation until complete dissolution has been effected. Dissolve the dye. Filter under vacuum through a No. 4 sintered glass filter.'

This lacquer should be applied at constant temperature and humidity, as it is very sensitive to ambient conditions. It may be sprayed or painted, and is non-toxic. It dries rapidly at room temperature.

Coat the specimens and calibration bar at the same time, ensuring the same even coating in each case. Allow to dry for one hour.

Test the coating by applying increasing load to the cantilever bar. The strain at which the first crack appears is the 'threshold strain', and should be between  $5$  and  $10 \times 10^{-3}$ . However, as the calibration bar is the same material as the specimens, it is more useful to calibrate in terms of stress. As the load is increased, more cracks appear perpendicular to the maximum principal stress direction, and will be most closely spaced in the region of highest stress, i.e. the stress raiser. Thus by counting the number of cracks/cm over a small length, perpendicular to the cracks, an estimate of the maximum principal stress can be made.

However, the most useful method of quantitative analysis is to increase the load in equal increments, and mark the position of the threshold cracks for each increment (Figure 30.1). In this way, a pattern of contours of equal tensile stress intervals can be built up, the stress level being highest at the first contour to appear.

Increase the load in equal increments for both calibration bar and specimens, and plot the contours as described.

Compare your stress maps of the calibration bar with the calculated stresses by plotting the two graphs of stress against length.

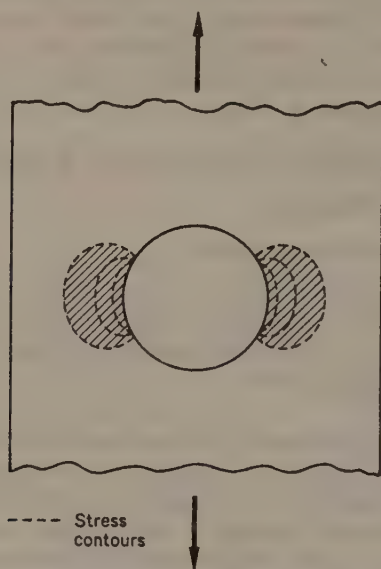


FIGURE 30.1 Stress contours from brittle lacquer cracks, by the method of equal load increments.

From the specimens, deduce the position of maximum stress, and estimate the stress-raising factor.

Remember that the brittle lacquer technique is not very reliable, and you will be lucky to be within 20% of the theoretical solution.

## Discussion

Discuss your results, and suggest possible faults in your particular technique. Comment on the usefulness of the method.

# Index

- AMPLITUDE, 46, 50
  - scaling, 93
  - ratio, 46
- Analogue computer, 91
- Angled-bevel gears, 8
- Angular momentum, 41
- Anticlastic curvature, 110, 148
- Aperiodic mode, 83
- Aperiodic motion, 32
- Attenuator, 91
  
- BACKLASH, 48
- Balancing, 24
  - of reciprocating bodies, 28
  - of rotating bodies, 24
- Band brake, 10
- Beating, 50
- Belt drive, 17
- Bending, 109
  - cantilever, 113
  - circular, 111
  - equations, 110, 132
  - moment diagram, 111
  - principal axes, 110, 113
- Birfield joint, 6
- Block diagram, 67, 82, 95
- Bridgeman, 125
- Brittle lacquers, 152
- Bulk modulus, 103
  
- CAGE, 8
- Cantilever, 37, 42, 113
  - propped, 136
- Capacitance, 64
- Carrier, 8
- Castigliano's theorem, 130
- Cathode-ray oscilloscope, 38
- Centre of mass, 13, 30, 56
- Centre of rotation, 56
- Circularly polarised light, 144
- Clutch (*see* Plate clutch)
- Coefficient of damping, 31, 45, 57
- Coefficient of friction, 17
- Compensation, 67
- Compound epicyclic gear, 9
- Compound pendulum, 13
- Computer, 91
- Connecting rod, 3, 13
- Controller, 68, 82
  - gain, 68, 82
- Coriolis acceleration, 61
- Coulomb friction, 17
- Coupled system, 50
- Crank, 3
- Crank-slider mechanism, 3, 28, 47
- Critical speed, 57
- Critically-damped response, 32
  
- DAMPED OSCILLATION, 31
- Damped system, 31
- Damping coefficient, 31, 45, 57, 82, 92
- Damping factor, 32
- Damping ratio, 46
- Dashpot, 31, 45
- Deflection, 35
  - static, 35
  - dynamic, 36
- Degrees of freedom, 30
  - one-degree-of-freedom system, 30, 45, 56
  - two-degree-of-freedom system, 50, 92
  - multi-degree-of-freedom system, 73, 76
- Demec gauge, 105, 117
- Derivative control, 69, 83
- Differential operator, 57, 63
- Displacement, 3, 31, 41, 84
- Dynamic balance, 24
  - machine, 27
- Dynamic loading, 35
- Dynamometer, 69, 84
  
- ECCENTRICITY, 56
- Eddy-current brake, 48, 69
- Elastic constants, 103

- Elastic curve, 77
- Electrically sensitive paper, 42, 48
- Electromagnetic shaker, 58, 74
- Electro-pneumatic converter, 84
- Energy, 35, 40
  - kinetic, 35, 41
  - potential, 36
  - strain, 36
  - transfer of, 53
- Epicyclic gears, 8
- Equation of motion, 13, 31, 50
- Equilibrium position, 31, 36
- Euler's theory of struts, 120
- Exponential lag, 63
- Extensometers, 105
- External load, 67, 82
  
- FEEDBACK, 68, 91
  - output-velocity feedback, 68
- Feedforward, 69
  - input-velocity feedforward, 69
- Flat belt, 18
- Fluctuation of speed, 6
- Force polygon, 26
- Forced vibration, 45
- Forcing frequency, 46
- Four-bar linkage, 3
- Four point loading, 109
- Free vibration, 13, 30, 36, 73, 77
- Frequency, 30
  - natural damped, 32
  - natural undamped, 32, 46, 56
  - ratio, 46
  - spectrum, 47
- Friction, 17
  - force, 17
- Fringe factor, 145
  
- GAIN, 68
- Gearbox, 9
- Governor, 83
- Gravitational field, 13
- Gyroscope, 60
- Gyroscopic precession, 58, 60
  
- HELICAL GEARS, 8
- Hooke's joint, 5
- Huggenbergger gauge, 105
- Hydraulic clutch, 10
- Hydrokinetic torque converter, 10
  
- IMPULSE, 40
- Impulse-momentum equation, 36, 40
- Indirect model analysis, 134
- Influence lines, 134
- Initial conditions, 51, 91
- Integral control, 83
  - time constant, 83
- Integrator, 92
- Inverter, 92
- Isochromatics, 142
- Isoclinics, 141
  
- KELVIN, LORD, 124
- Kinematic mechanisms, 3
- Kinetic energy, 35, 41
  
- LAG, 63
  - exponential, 63
  - first-order, 63
  - velocity, 68
- Laws of similitude, 134
- Linear motion, 41
- Linear system, 30
- Lissajous figures, 48
- Lithium tetraborate lacquer, 153
- Load cell, 130
  
- MAGNIFICATION RATIO, 46
- Mass moment of inertia, 12, 31, 41, 45, 67
- Maximum shear stress, 144
- Maxwell reciprocal theorem, 134, 135
- Mechanical shaker, 74
- Mode of vibration, 30
  - aperiodic, 83
  - free or natural, 30, 74
  - principal, 51, 76
- Modulus of rigidity, 31, 103, 107
  - of section, 112,
  - Young's, 103
- Moiré effect, 147
- Moment polygon, 26
- Momentum, 36, 40
  - angular, 41
  - moment of, 41
  - principle of conservation, 40
- Muller-Breslau theorem, 134, 135
  
- NATURAL FREQUENCY, 32
- Neutral axis, 110
- Newton's Second Law, 40



- Node, 77
- Noise, 83
- Non-linear system, 66
- OPERATIONAL AMPLIFIER, 91
- Output-velocity feedback, 68
- Overdamped response, 32
- PARALLEL AXES, 13
- Pendulum, 13
  - compound, 13
  - coupled, 50
- Periodic time, 13, 15
- Phase, 46
  - difference, 46, 51
- Photoelastic method, 139
- Pitch, (of gear teeth), 8
- Planet wheel, 8
- Plate clutch, 18
  - uniform pressure theory, 19
  - uniform wear theory, 19
- Poisson's ratio, 103
- Polar moment of inertia, 107
- Polariscope, 144
- Polarized light, 139
  - circularly, 144
- Polaroid, 140
- Position-control system, 67
- Potential energy, 36
- Primary force, 28
- Principal axes, of bending, 113
- Principal, strains, 116
  - stresses, 116, 140
- Principle of conservation of momentum, 40
- Process lag, 64
- Product of inertia, 110, 114
- Proportional band, 84
- Proportional control coefficient, 68, 82
- Propped cantilever, 136
- Proving rings, 130
- QUARTER WAVE PLATES, 144
- RECIPROCAL THEOREM, 134, 135
- Recorder, 48, 97
- Regulating unit, 84
- Relative retardation, 140
- Resistance strain gauges, 124
- Resonance, 47
- Resonant frequency, 26, 47
- Response, 64
  - ramp, 68
  - step, 64, 68, 83
- Restrains, 31, 35
- Rigidity modulus, 103, 107
- Ronchi grating, 150
- Rosette, 129
- Rotational motion, 41
- Rzeppa joint, 6
- SCALING, 93
  - amplitude, 93
  - time, 94
- Scotch-yolk mechanism, 48
- Searle's method, 104
- Second moment of area, 31, 109
- Secondary force, 28
- Section modulus, 112
- Self-changing gearbox, 8
- Servo motor, 68
- Shaker, 58, 74
- Shear modulus (*see* Rigidity modulus)
- Shear, strain, 107, 116
  - stress, 103, 107, 109, 144
- Similitude, 134
- Simple harmonic motion, 4, 46, 72
- Slenderness ratio, 122
- Slider, 3
- Sliding pairs, 3
- Southwell plot, 122
- Spectrum, 47
- Speed-control system, 82
- Speed ratio, 8
- Spur gears, 8
- Stability, 68, 83
- Stability of struts, 120
- Static balance, 24
- Static check, 95
- Static loading, 35
- Steady-state error, 68, 83
- Steady-state response, 46, 68
- Step response, 64, 68, 86
- Stiffness, 31, 45
- Strain energy, 36, 40, 130
  - gauge, 38, 79, 105, 117, 124
  - principal, 116
  - threshold, 153
- Stress concentration factor, 146
  - normal, 103
  - optic coefficient, 141
  - principal, 116, 140
  - strain relations, 103



- Stroboscope, 21, 58, 62
- Summing amplifier, 92
- Sun wheel, 8
- Synchro transmitter, 69
- System, 30
  - closed loop, 67, 82
  - damped, 31, 46
  - linear, 31
  - lumped, 92
  - multi-mass, 76
  - non-linear, 65
  - position-control, 67
  - proportional, 68, 82
  - speed-control, 82
  - undamped, 36, 50, 56, 73, 76
- TACHO-GENERATOR, 69, 84
- Tachometer, 20
- Threshold strain, 153
- Time constant, 46, 63
- Time scaling, 94
- Tint of passage, 145
- Torque ratio, 10
- Torque reaction, 10
- Torsion, 31, 106
  - meter, 107
  - simple theory, 31
- Townson, J. M., 122
- Transfer operator, 63, 67, 83
- Transient response, 70, 86, 98
- Transmission efficiency, 11
- Transverse vibration, 55, 72
- Trifilar suspension, 14
- Turning pairs, 3
- Two-dimensional motion, 3
- UNDAMPED OSCILLATION, 30, 36
- Undamped response, 32
- Underdamped response, 32
- V-BELT, 19
- Vector polygon, 26
- Vector quantity, 40
- Velocity lag, 68
- Velocity ratio, 6
- Vibration, 14
  - forced, 45
  - free, 14, 30, 36
  - torsional, 14, 30, 45
  - transverse, 55, 72
- Viscous friction, 17, 31
  - coefficient, 31, 45, 57, 68, 82, 92
- WHEATSTONE BRIDGE, 126
- Whirling (of shafts), 55
- Whirling speed, 26, 55
- Windage, 53
- Work-energy equation, 40
- YOUNG'S MODULUS, 56, 72, 103



620.1

WEB

1973

PAISLEY COLLEGE  
OF TECHNOLOGY  
LIBRARY

## **Experimentation for Students of Engineering**

### ***Volume II: Applied Mechanics***

Experimentation is essential in engineering. The process of learning in engineering laboratories—which is vital for good experimental practice—can be greatly enhanced by the ready availability of comment and advice on theory and practice.

It was to meet these requirements that this series was written. Although intended primarily for use by students of engineering in universities and colleges of technology, it will also serve as a more general reference to experimental practice. SI units are used throughout, supplemented in some instances by British units.

This second volume in the series describes experiments suitable for Applied Mechanics courses and these are grouped under the general headings Part I Statics and Dynamics and Part II Stress Analysis. The experiments are presented in order of increasing complexity and can be used progressively throughout a three-year course, although the order of presentation may be changed as required.

#### **Titles in the Series**

**Volume I: Experimental Method  
and Measurement**

**Volume II: Applied Mechanics**

**Volume III: Thermodynamics,  
Fluid Mechanics, and Heat Transfer**

**£1.50 net**